

HEAT TRANSFER AUGMENTATION AT A BACKWARD-FACING STEP

A DISSERTATION

*Submitted in partial fulfillment of the
requirements for the award of the degree*

of

INTEGRATED DUAL DEGREE

(Bachelor of Technology & Master of Technology)

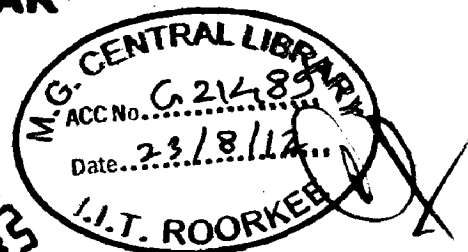
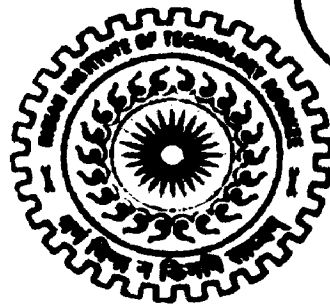
in

CHEMICAL ENGINEERING

(With Specialization in Hydrocarbon Engineering)

By

ANKIT KUMAR



DEPARTMENT OF CHEMICAL ENGINEERING
INDIAN INSTITUTE OF TECHNOLOGY ROORKEE
ROORKEE -247 667 (INDIA)
JUNE, 2012

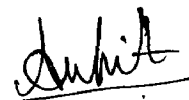
Candidate's Declaration

I hereby declare that the work, which is being presented in the dissertation entitled “**Heat Transfer Augmentation at a Backward-Facing Step**” in the partial fulfillment of the requirements of the award of the Integrated Dual Degree (Bachelor of Technology & Master of Technology) in Chemical Engineering with specialization in “Hydrocarbon Engineering”, submitted in the Department of Chemical Engineering, Indian Institute of Technology Roorkee, Roorkee, is an authentic record of my own work carried out during the period from June 2011 to June 2012 under supervision of **Dr. Amit Kumar Dhiman**, Assistant Professor, Department of Chemical Engineering, Indian Institute of Technology Roorkee, Roorkee.

I have not submitted the matter, embodied in this dissertation for the award of any other degree.

Date: June, 2012

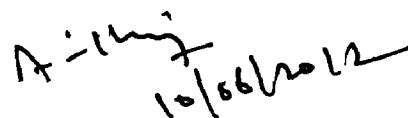
Place: Roorkee



(Ankit Kumar)

Certificate

This is to certify that the above statement made by the candidate is correct to the best of my knowledge and belief.



Dr. Amit Kumar Dhiman

Assistant Professor

Department of Chemical Engineering

Indian Institute of Technology Roorkee

Roorkee - 247667 (India)

Table of Contents

| | |
|--|------|
| Candidate`s Declaration..... | i |
| Table of Contents..... | ii |
| ACKNOWLEDGEMENTS..... | iv |
| List of Figures | v |
| List of Tables..... | viii |
| Abstract..... | ix |
| PUBLICATIONS FROM THIS WORK | x |
| Nomenclature | xii |
| SECTION – A..... | 1 |
| Forced Convection Heat Transfer Augmentation at a Backward-Facing Step | 1 |
| Chapter 1. INTRODUCTION..... | 2 |
| Chapter 2. Previous Work on Forced Convection in the Backward-Facing Step Geometry | 3 |
| Chapter 3. Problem Statement and Mathematical Formulation | 6 |
| Chapter 4. Numerical Solution Procedure | 10 |
| Chapter 5. Results and Discussions..... | 15 |
| 5.1 Validation of results | 15 |
| 5.2 Flow patterns..... | 17 |
| 5.3 Thermal Patterns..... | 21 |
| 5.4 Drag Coefficient | 24 |
| 5.5 Local Nusselt Number | 26 |
| 5.6 Average and Peak Nusselt Number..... | 28 |
| 5.7 Pressure Drop..... | 32 |
| 5.8. Further Scope for Experimental Analysis..... | 33 |
| Chapter 6. Conclusions | 35 |
| SECTION – B..... | 36 |
| Natural Convection Heat Transfer Augmentation at a Backward-Facing Step | 36 |
| Chapter 7. An Introduction to the Phenomenon of Natural Convection | 37 |
| 7.1 Physical Mechanism of Natural Convection | 37 |
| 7.2. Equation of Motion..... | 40 |

| | |
|---|----|
| 7.3. The Grashof Number | 45 |
| 7.4. NATURAL CONVECTION OVER SURFACES | 46 |
| 7.4.1. Vertical Plates ($T_s = \text{constant}$) | 48 |
| 7.4.2. Vertical Cylinders | 48 |
| 7.4.3. Inclined Plates..... | 49 |
| 7.4.4. Horizontal Plates | 51 |
| 7.4.5. Horizontal Cylinders and Spheres..... | 51 |
| 7.5. NATURAL CONVECTION INSIDE ENCLOSURES..... | 52 |
| 7.5.1. Horizontal Rectangular Enclosures | 54 |
| 7.5.2. Inclined Rectangular Enclosures..... | 55 |
| 7.5.3. Vertical Rectangular Enclosures | 56 |
| Chapter 8. Literature Review on Natural Convection in Enclosures | 57 |
| Chapter 9. Problem Statement, Governing Equations and Boundary Conditions | 64 |
| Chapter 10. Numerical Methodology..... | 66 |
| Chapter 11. Results and Discussions..... | 70 |
| 11.1. Validation of Results | 72 |
| 11.2. Flow and Thermal Patterns | 73 |
| 11.3. Average Nusselt Values..... | 77 |
| 11.4. Drag Coefficients..... | 81 |
| Chapter 12. Conclusions | 82 |
| References..... | 83 |

ACKNOWLEDGEMENTS

I express my deep sense of gratitude to my guide **Dr. Amit Kumar Dhiman**, Assistant Professor, Department of Chemical Engineering, Indian Institute of Technology Roorkee, Roorkee, for his keen interest, constant guidance and encouragement throughout the course of this work, his experience, assiduity and deep insight of the subject held this work always on a smooth and steady course.

Thanks are due to **Dr. Vijay Kumar Agarwal**, Professor and Head, Department of Chemical Engineering, Indian Institute of Technology Roorkee, for providing various facilities during this dissertation.

Above all, I want to express my heartiest gratitude to The Almighty, my parents (Mrs. Babita Singh and Mr. Hridya Nand Singh), for their love, faith and support for me, which has always been a constant source of inspiration.


ANKIT KUMAR

List of Figures

Fig. 1. Schematic diagram and boundary conditions of the BFS problem with adiabatic circular cylinder.

Fig. 2. Non-uniform grid structure for the unobstructed BFS flow: (a) complete and (b) magnified views.

Fig. 3. Non-uniform grid structure for the BFS flow obstructed with a circular cylinder: (a) complete and (b) magnified views.

Fig. 4. Validation of the Nusselt number distribution with those of Kondoh et al.

Fig. 5. Streamline profiles for $Re = 1$: a) Unobstructed case; b) $y_c = 0.5$; c) $y_c = 1.0$ and d) $y_c = 1.5$

Fig. 6. Streamline profiles for $Re = 100$: a) Unobstructed case; b) $y_c = 0.5$; c) $y_c = 1.0$ and d) $y_c = 1.5$

Fig. 7. Streamline profiles for $Re = 200$: a) Unobstructed case; b) $y_c = 0.5$; c) $y_c = 1.0$ and d) $y_c = 1.5$

Fig. 8. Isotherm profiles for $Re = 1$: a) Unobstructed case; b) $y_c = 0.5$; c) $y_c = 1.0$ and d) $y_c = 1.5$

Fig. 9. Isotherm profiles for $Re = 100$: a) Unobstructed case; b) $y_c = 0.5$; c) $y_c = 1.0$ and d) $y_c = 1.5$

Fig. 10. Isotherm profiles for $Re = 200$: a) Unobstructed case; b) $y_c = 0.5$; c) $y_c = 1.0$ and d) $y_c = 1.5$

Fig. 11. Variation of overall drag coefficient (C_D) with Reynolds number and y_c .

Fig. 12. Effect of Reynolds number on the variation of the local Nusselt number distribution (Nu vs. X): a) Unobstructed case; b) $y_c = 0.5$; c) $y_c = 1.0$; and d) $y_c = 1.5$

Fig. 13. Variation of heat transfer characteristics with Reynolds number: (a) Maximum Nusselt number (Nu_{max}); and (b) Average Nusselt number (Nu_{avg}).

Fig. 14. Variation of the point of maximum heat transfer (X_{max}) with Reynolds number and y_c .

Fig. 15. Variation of $Nu_{max} / Nu_{unobstructed}$ with the Reynolds number and y_c .

Fig. 16. Variation of the dimensionless pressure drop (dP) between inlet and outlet with Reynolds number (Re) and y_c .

Fig. 17. Schematic detail of proposed test section and apparatus for experimental analysis.

Fig. 18: Schematic diagram of an example depicting natural convection.

Fig. 19: Isotherms in natural convection over a hot plate in air. (a) Laminar flow (b) Turbulent flow.

Fig. 20: Typical velocity and temperature profiles for natural convection flow over a hot vertical plate at temperature T_s inserted in a fluid at temperature T_∞ .

Fig. 21: Forces acting on a differential control volume in the natural convection boundary layer over a vertical flat plate.

Fig. 22: The Grashof number Gr is a measure of the relative magnitudes of the buoyancy force and the opposing viscous force acting on the fluid.

Fig. 23: Natural convection heat transfer correlations are usually expressed in terms of the Rayleigh number raised to a constant n multiplied by another constant C , both of which are determined experimentally.

Fig. 24: Natural convection flows on the upper and lower surfaces of an inclined hot plate.

Fig. 25: Natural convection flows on the upper and lower surfaces of a hot horizontal plate.

Fig. 26: Natural convection flow over a horizontal hot cylinder.

Fig. 27: Convective currents in a vertical rectangular enclosure.

Fig. 28: Convective currents in a horizontal enclosure with (a) hot plate at the top and (b) hot plate at the bottom.

Fig. 29: A Nusselt number of 3 for an enclosure indicate that heat transfer through the enclosure by natural convection is three times that by pure conduction

Fig. 30: A horizontal rectangular enclosure with isothermal surfaces.

Fig. 31: An inclined rectangular enclosure with isothermal surfaces.

Fig. 32: A vertical rectangular enclosure with isothermal surfaces.

Fig. 33. Schematic diagram of physical system.

Fig. 34 .GRID 1

Fig. 35.GRID 2

Fig. 36.GRID 3

Fig. 37.GRID 4

Fig. 38. Streamline patterns for different positions of the adiabatic circular cylinder.

Fig. 39. Isotherm patterns for different positions of the adiabatic circular cylinder.

Fig. 40. Streamlines for a) $Ra = 10^3, \alpha = 0$ b) $Ra = 10^3, \alpha = 1$ c) $Ra = 10^3, \alpha = 4$ d) $Ra = 10^4, \alpha = 0$ e) $Ra = 10^4, \alpha = 1$ f) $Ra = 10^4, \alpha = 4$ g) $Ra = 10^5, \alpha = 0$ h) $Ra = 10^5, \alpha = 1$ i) $Ra = 10^5, \alpha = 4$

Fig. 41. Isotherm patterns for $Pr = 1$ and for a) $Ra = 10^3, \alpha = 0$ b) $Ra = 10^3, \alpha = 1$ c) $Ra = 10^3, \alpha = 4$ d) $Ra = 10^4, \alpha = 0$ e) $Ra = 10^4, \alpha = 1$ f) $Ra = 10^4, \alpha = 4$ g) $Ra = 10^5, \alpha = 0$ h) $Ra = 10^5, \alpha = 1$ i) $Ra = 10^5, \alpha = 4$

Fig. 42. Isotherm patterns for $Pr = 10$ and for a) $Ra = 10^3, \alpha = 0$ b) $Ra = 10^3, \alpha = 1$ c) $Ra = 10^3, \alpha = 4$ d) $Ra = 10^4, \alpha = 0$ e) $Ra = 10^4, \alpha = 1$ f) $Ra = 10^4, \alpha = 4$ g) $Ra = 10^5, \alpha = 0$ h) $Ra = 10^5, \alpha = 1$ i) $Ra = 10^5, \alpha = 4$

Fig. 43. Isotherm patterns for $Pr = 50$ and for a) $Ra = 10^3, \alpha = 0$ b) $Ra = 10^3, \alpha = 1$ c) $Ra = 10^3, \alpha = 4$ d) $Ra = 10^4, \alpha = 0$ e) $Ra = 10^4, \alpha = 1$ f) $Ra = 10^4, \alpha = 4$ g) $Ra = 10^5, \alpha = 0$ h) $Ra = 10^5, \alpha = 1$ i) $Ra = 10^5, \alpha = 4$

Fig. 44. Nusselt number variations with angular speed at the heated step for $Ra = 10^3$.

Fig. 45. Nusselt number variations with angular speed at the heated step for $Ra = 10^4$.

Fig. 46. Nusselt number variations with angular speed at the heated step for $Ra = 10^5$.

Fig. 47. Drag variations with angular speed at the circular cylinder for $Ra = 10^3$.

List of Tables

Table 1: Sensitivity analysis for flow across the backward-facing step obstructed by an adiabatic circular cylinder. (Here N_{cells} represents total number of cells in the grid; N_c is the number of points on the surface of cylinder, Δ_{cylinder} is the minimum grid spacing in the vicinity of the cylinder and Δ_{wall} is the minimum grid spacing in the vicinity of the wall.)

Table 2: Validation of the value of the reattachment length X_R ($Re = 100$, $ER = 2$).

Table 3: Coefficients of the exponential fit to the variation of the maximum Nusselt number (Nu_{max}) with Reynolds number (Re) for $Pr = 0.71$ (air) and $1 \leq Re \leq 200$:

Table 4. Comparison of predicted Nusselt numbers with those of de Vahl Davis [68] under various Rayleigh numbers.

Table 5. Enhancement factors for various cases of rotation of the circular cylinder with respect to the stationary case.

Abstract

The current study investigates the augmentation in the laminar forced and natural convection characteristics of the backward-facing step flow in a two-dimensional channel by means of introducing an adiabatic circular cylinder in the domain. The effects of various cross stream positions (i.e., $y_c = 0 - 1.5$) of the circular cylinder on the flow and heat transfer characteristics of the backward-facing step flow has been numerically explored. For forced convection the Reynolds number range 1 – 200 and Prandtl number of 0.71 (air) were explored. For natural convection a Rayleigh number range of $10^3 - 10^5$, Prandtl number range of 1 – 50 and an angular circular cylinder rotation of 0 – 4 rad.s^{-1} were explored. The governing continuity, Navier-Stokes and energy equations along with appropriate boundary conditions are solved by using FLUENT. The flow and thermal fields have been explained by stream-line and isotherm profiles, respectively. The engineering parameters like wake/recirculation length, total drag coefficient and average Nusselt number, etc. are calculated for the above range of conditions. The present results show an enhancement in the peak Nusselt value of up to 155 % for the case of forced convection and a 20 times increase for the case of natural convection using a circular cylinder as compared to the unobstructed case (i.e., without cylinder). Finally, simple correlations for total drag coefficient and peak Nusselt number are obtained for the above range of conditions.

PUBLICATIONS FROM THIS WORK

PUBLISHED

- Ankit Kumar, Amit K. Dhiman, Effect of a circular cylinder on separated forced convection at a backward-facing step.

International Journal of Thermal Sciences - 52(2012)176 – 185

UNDER REVIEW

- Ankit Kumar, A.K.Dhiman, Forced convection heat transfer of an incompressible Newtonian fluid downstream of a backward-facing step: Effect of expansion ratio, Reynolds number and Prandtl number.

Chemical Engineering & Technology – Under Review

COMMUNICATED

- Ankit Kumar, A.K.Dhiman, Natural convection heat transfer augmentation in a backward-facing step enclosure by using a rotating circular cylinder

International Journal of Thermal Sciences

CONFERENCES

- Ankit Kumar, A. K. Dhiman, Numerical Simulation of Laminar Flow over a backward facing step using the finite volume method.

Proceedings of the **International Conference on Emerging Trends in Mechanical Engineering**, Thapar University (Patiala), 2011

- Ankit Kumar, A. K. Dhiman, 'Low Re flow of an incompressible Newtonian fluid downstream of a backward facing step: A Benchmark problem.'

Proceedings of the **4th International Conference on Fluid Mechanics and Fluid Power**, IIT Madras, 2010

Nomenclature

| | |
|-------------|---|
| ER | Channel expansion ratio, $H/(H - S)$ |
| S | Step height, m |
| H | Downstream channel height, m |
| L | Downstream channel length, m |
| d | Diameter of the cylinder, m |
| u | Longitudinal velocity, m/s |
| \bar{u}_e | Average inlet velocity, m/s |
| v | Transverse velocity, m/s |
| h | Heat transfer coefficient |
| k | Thermal conductivity |
| C_p | Specific heat of the fluid, J/kg K |
| U | Dimensionless longitudinal velocity, u/\bar{u}_e |
| V | Dimensionless transverse velocity, v/\bar{u}_e |
| Nu | Local Nusselt number on heat transfer surface (i.e., lower wall downstream of step) |
| Nu_{avg} | Mean of Nusselt number on heat transfer surface (i.e., lower wall downstream of step) |
| Nu_{max} | Maximum value of Nusselt number |
| f | Shedding frequency of the Karman Vortex, s^{-1} |
| C_D | Total drag coefficient ($= \frac{2F_D}{\rho U_{avg}^2}$) |
| C_{DF} | Friction drag coefficient ($= \frac{2F_{DF}}{\rho U_{avg}^2}$) |
| C_{DP} | Pressure drag coefficient ($= \frac{2F_{DP}}{\rho U_{avg}^2}$) |

| | |
|-----------|---|
| P | Pressure, $P^*/(\rho \bar{u}_e^2)$ |
| Pr | Prandtl number, $\mu C_P/k$ |
| Ra | Rayleigh number, $Ra_L = Gr_L Pr = \left[\frac{g\beta (T_s - T_\infty) L_c^3}{\nu^2} \right] Pr$ |
| Re | Reynolds number based on inlet flow velocity, $(\bar{u}_e S)/(\nu)$ |
| St | Strouhal number based on inlet flow velocity, $(fd)/(\bar{u}_e)$ |
| T | Dimensionless temperature, $(T^* - T_1)/(T_w - T_1)$ |
| t | Time, s |
| T_1 | Temperature at inlet boundary, K |
| T_w | Temperature of heat transfer surface (lower wall downstream of step), K |
| x | Coordinate in mainstream direction with $x = 0$ at step location, m |
| y | Coordinate perpendicular to mainstream direction with $y = 0$ at bottom step corner, m |
| X, Y | Dimensionless stream-wise and transverse coordinates, $X = x/S$; $Y = y/S$ |
| X_R | Dimensionless x -coordinate where flow reattaches (for flow reattachment point) |
| X_{max} | Dimensionless x -coordinate of the point of peak Nusselt number |
| x_c | Dimensionless stream-wise position of the circular cylinder, $x_c = x_c^*/S$ |
| y_c | Dimensionless cross stream position of the circular cylinder, $y_c = y_c^*/S$ |
| F_D | Total drag force per unit length of the cylinder, N/m |
| F_{DF} | Frictional component of total drag force per unit length of cylinder, N/m |
| F_{DP} | Pressure component of total drag force per unit length of cylinder, N/m |

Greek symbols

| | |
|----------|---|
| ν | Kinematic viscosity, $m^2 \cdot s^{-1}$ |
| μ | Viscosity of fluid, Pa.s |
| ρ | Density, $kg \cdot m^{-3}$ |
| α | Angular Speed, $rad \cdot s^{-1}$ |

Subscripts

avg Average value

max Maximum value

W Wall

R Value at reattachment point

c Cylinder position

Superscript

* Dimensional variable

SECTION - A

Forced Convection Heat Transfer Augmentation at a Backward-Facing Step

Chapter 1. INTRODUCTION

Flow separation and subsequent reattachment exert an important influence on the mechanism of heat transfer. In some cases, they have a harmful effect such as uneven heat loading in thermal equipment, but in others, they produce a beneficial effect like heat transfer enhancement around the flow reattachment point. Thus, in engineering practice, it is quite essential to understand the basic mechanism of heat transfer in separating and reattaching flows. A backward-facing step is one of the most fundamental geometries where the flow separation and reattachment occur. Flow past a backward-facing step has a variety of engineering applications such as energy system equipment, electronic cooling, cooling of nuclear reactors, cooling of turbine blades, combustion chambers, environmental control systems, and many other devices. Innumerable studies have been conducted in relation to this geometry, however most of them were concerned only with the flow and our understanding of heat transfer seems still immature. Backward-facing step flows under laminar conditions have been investigated both experimentally [1-3] and numerically [4-8] to obtain the basic information of the flow separation and reattachment phenomena in laminar flow regime. This work sets out to examine the heat transfer enhancement of backward-facing step flows in horizontal channels by using an adiabatic circular cylinder installation in the channel over a wide range of Reynolds number in the steady two-dimensional flow regime. However, before undertaking a detailed presentation and discussion of this problem, it is useful to recount briefly the current status of the relevant literature.

Chapter 2. Previous Work on Forced Convection in the Backward-Facing Step Geometry

Most of the currently available literature on the incompressible fluid flow over a backward-facing step relates to the high Reynolds number region where the main thrust has been to investigate the wake phenomena. In contrast, much less attention has been devoted to heat transfer characteristics. Armaly et al.[1] studied the relationship between the Reynolds number and the reattachment length by a numerical simulation method and an experimental method. The results were presented for laminar, transitional and turbulent flow of air for Reynolds number = 70 – 8000 (Reynolds number, Re is based on twice the upstream channel height). Their results indicated that the wake length increases with increasing Reynolds number for $Re < 1200$; wake length decreases with the Reynolds number when the Reynolds number varies between 1200 and 5500; wake length reaches a fixed value for $Re > 5500$. Chiang and Sheu[9] conducted steady three-dimensional flow analysis in the channel for the range $100 < Re < 1000$ using the backward-facing step geometry and the flow conditions reported by Armaly et al.[1]. They found that the flow at the plane of symmetry develops into a 2-D like profile only when the channel width is increased up to 100 times of the upstream step height for $Re = 800$. Kaiktsis et al. [5] performed 3-D simulations employing periodic boundary condition in the span-wise direction. However, their numerical results still show noticeable discrepancy from the experimental results. Three-dimensional numerical simulation was performed by Iwai et al.[10] for the flow over a backward-facing step at low Reynolds number in order to investigate the effects of the duct aspect ratio. They found that the downstream of the step remained 2-D only at $Re = 200$ and 300. An aspect ratio of 16 was needed to obtain a 2-D region near the centreline at $Re = 250$. This 2-D region became wider for a lower Reynolds number. Biswas et al.[11] investigated the flow over a backward-facing step for various expansion ratios of 1.9423, 2.5 and 3.0 for the Reynolds number range 10^{-4} to 800. They reported that the flow shows strong 2-D behaviour for $Re < 400$. Erturk[12] examined the 2-D steady incompressible backward-facing step flow for Reynolds number = 100 to 3000 (based on height of the channel) for the expansion ratio of 2. The results showed that, for the backward-facing step flow an inlet channel that is at least five step heights long is required for accuracy. It was shown that the location of the exit boundary and the outflow

boundary condition has an effect both on the accuracy and on the largest Reynolds number that could be computed numerically. Also, the size of the recirculating region was shown to grow almost linearly as the Reynolds number increases. Lan et al.[13] have reported results from 3-D simulations of turbulent forced convection adjacent to backward-facing step in a rectangular duct by using FLUENT at very high Reynolds number range of 20,000 - 50,000.

In addition to the fluid flow solution, Dyne and Heinrich[14]and Choudhury[15] solved the energy equation for the constant heat flux boundary condition. They have investigated the Nusselt number distribution along the wall. It approaches fully developed value in the downstream direction. Mixed convective heat transfer in an inclined duct with backward-step geometry results are presented by Hong et al.[16]. The effects of inclination angle and the Prandtl number in the range($0.07 \leq Pr \leq 100$) on the flow and heat transfer characteristics are reported. They found that the increase in inclination angle increases the reattachment length but decreases the wall friction coefficient. Kondoh et al. [17]studied the laminar heat transfer characteristics of backward-facing step problem. They reported local Nusselt number, peak Nusselt number and its location and thermal front. They found that the peak Nusselt number is not necessarily located at or very near to the reattachment location.

The heat flux in thermal devices has become more and more vast due to the increasing compactness requirements for the respective systems. It should be important to search for ways to effectively augment the heat transfer characteristics of backward-facing step flow in channels. AbuHijleh[18] numerically investigated the effects of the addition of a porous floor segment on the heat transfer performance of a two-dimensional laminar boundary-layer flow over a backward-facing step. Martin et al. [19] presented the results of heat transfer enhancement of backward-facing step flow by using a porous medium inserted into the channel. Results indicated that, in general, the porous inserts reduce or eliminate the lower wall recirculation zone. However, the recirculation zone is lengthened if the inserts are short and extremely porous.

Thus it can be summarized here that limited studies are available that have dealt with how to alter the flow structure and temperature distribution, and then to attain the high heat transfer performance of backward-facing step flow in channels. Moreover, no previous results are available on the problem of heat transfer augmentation in the BFS geometry using an

adiabatic circular cylinder for the laminar range. Therefore, the main objective of this study is to examine the heat transfer enhancement of backward-facing step flows in horizontal channels by using an adiabatic circular cylinder installation in the channel over a wide range of Reynolds number in the steady two-dimensional flow regime.

Chapter 3. Problem Statement and Mathematical Formulation

The physical flow system for the backward-facing step with a built-in circular cylinder is shown in Fig. 1. The backward-facing step with step height “S”, also the non-dimensionalizing length scale, is exposed to a uniform velocity field ($U=1$) and at a uniform temperature, at the channel inlet. The non-dimensional downstream distance between the edge of the step and the exit plane of the domain is taken as 40 and the non-dimensional upstream distance between the inlet plane and the step edge is taken as 10. In order to explore the influence of the assumed finite domain, especially for the largest Reynolds number, computations have been carried out for $Re = 200$ and downstream lengths of 35, 40 and 45 for the unobstructed step geometry (i.e., without cylinder). The corresponding relative change in the reattachment length is found to be about 0.3%. Hence a length of 40 is selected for further simulations. Similarly, the variation in the reattachment length for the upstream lengths of 10, 15 and 20 at $Re = 200$ is found to be less than 0.5%. Thus, an upstream length of 10 has been used in all the subsequent numerical calculations to simulate the upstream inlet domain.

The downstream bottom surface of the backward-facing step is maintained at a uniform temperature ($T = 1$). Besides, the rest portions of the geometry including the upper wall are well insulated. It is well known that the flow separation and recirculation cause very poor heat transfer characteristics in the region near the step. To alter the hydrodynamic and thermal characteristics, an adiabatic circular cylinder (diameter, $d = 0.4$) is introduced in the geometry immediately downstream of the step. The diameter of the cylinder is so chosen as to keep the H/d ratio in the appropriate range so as to ensure the steady nature of the flow in the downstream channel as has been previously described by Singha and Sinhamahapatra[20] for channel flow. The stream-wise downstream position of the circular cylinder is maintained constant at $x_c = 0.6$ in this study. This cylinder position is chosen as the dimensionless wake length varies from 0 – 8 for the range of physical parameters considered in this work and so it was ensured that the entire flow pattern downstream of the step is influenced by the cylinder's presence. It is expected that the circular cylinder would strongly affect the velocity and temperature distributions of the backward-facing step flow resulting in possible heat transfer enhancement. As such, the

influences of different positions of the cylinder in the domain on the flow and heat transfer have been experimented in detail.

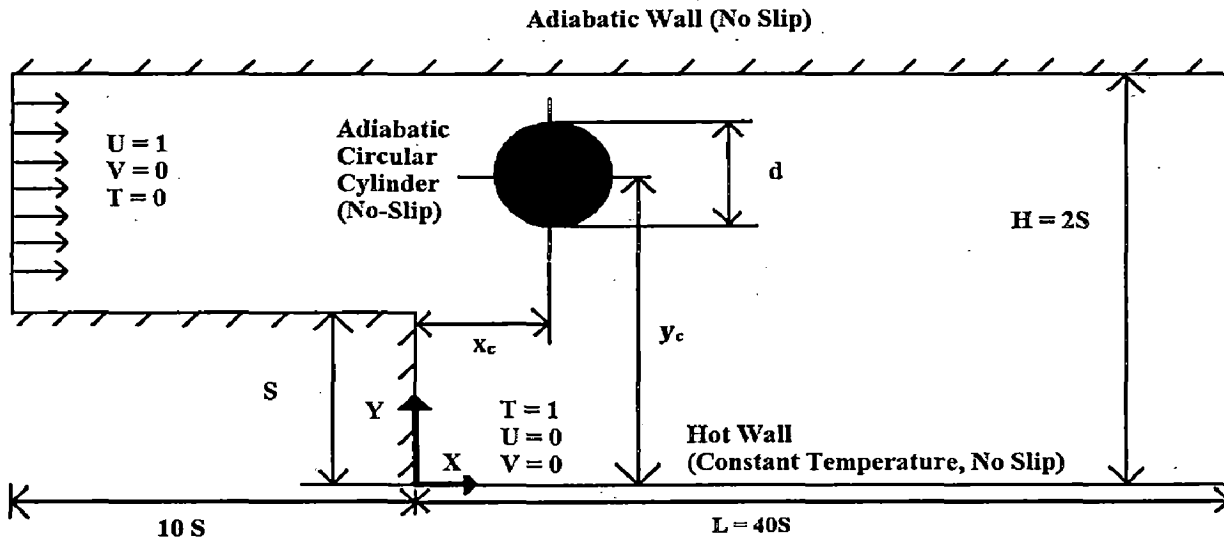


Fig. 1. Schematic diagram and boundary conditions of the BFS problem with adiabatic circular cylinder.

The flow and temperature fields are governed by continuity, Navier-Stokes and energy equations. The fluid properties are assumed to be constant and the viscous dissipation in the energy equation is also neglected. Therefore, the present results are applicable to situations where the temperature difference is not too large and for moderate viscosity. In this study, the temperature difference between the incoming fluid and the bottom wall, i.e., $(T_w - T_1)$ is assumed to be small (1 K) with $T_w = 300$ K and $T_1 = 299$ K so that the variation of physical properties (e.g., density, viscosity, thermal conductivity, etc.) of the working fluid (air) with temperature could be neglected. As such, the effect of temperature induced buoyancy in the fluid domain has been neglected and also the resulting momentum and energy equations have been solved by treating them as decoupled.

The governing equations (in their dimensionless forms) are the continuity, the x- and y-components of Navier-Stokes and thermal energy equations, as given below

Continuity equation:

$$\frac{\partial U}{\partial X} + \frac{\partial V}{\partial Y} = 0 \quad (1)$$

X – momentum

$$\frac{\partial U}{\partial t} + \frac{\partial UU}{\partial X} + \frac{\partial VU}{\partial Y} = -\frac{\partial P}{\partial X} + \frac{1}{Re} \left(\frac{\partial^2 U}{\partial X^2} + \frac{\partial^2 U}{\partial Y^2} \right) \quad (2)$$

Y – momentum

$$\frac{\partial V}{\partial t} + \frac{\partial UV}{\partial X} + \frac{\partial VV}{\partial Y} = -\frac{\partial P}{\partial Y} + \frac{1}{Re} \left(\frac{\partial^2 V}{\partial X^2} + \frac{\partial^2 V}{\partial Y^2} \right) \quad (3)$$

Energy equation

$$\frac{\partial T}{\partial t} + \frac{\partial(UT)}{\partial X} + \frac{\partial(VT)}{\partial Y} = \frac{1}{RePr} \left(\frac{\partial^2 T}{\partial X^2} + \frac{\partial^2 T}{\partial Y^2} \right) \quad (4)$$

The dimensionless boundary conditions may be written as follows:

- At inlet boundary $U = 1$, $V = 0$, $T = 0$.
- At upper and lower boundaries and all solid surfaces $U = 0, V = 0, \frac{\partial T}{\partial n} = 0$ (insulated boundary condition, with “n” representing the normal direction).
- At the bottom surface immediately downstream of the backward-facing step $T = 1$.
- At the exit plane $\frac{\partial U}{\partial X} = 0, \frac{\partial V}{\partial X} = 0$ and $\frac{\partial T}{\partial X} = 0$ (fully developed flow assumption).

Equations (1)–(4) together with the above-noted boundary conditions are solved to obtain $U(X, Y)$, $V(X, Y)$, $P(X, Y)$ and $T(X, Y)$, which in turn can be post-processed to obtain the

values of the integral quantities and of the derived variables like stream function and vorticity, etc. At this point, it is appropriate to introduce some definitions:

- The local Nusselt number along the surface of the hot bottom plate is of interest to the thermal system designer and is defined as:

$$Nu(X) = -\left(\frac{\partial T}{\partial Y}\right) = \frac{hS}{k} \quad (5)$$

- Such local values are further averaged over the bottom surface of the step to obtain the surface averaged Nusselt number as follows:

$$Nu_{avg} = \frac{1}{L} \int_0^L Nu(X) dX \quad (6)$$

Here L has been taken as the length of the bottom surface.

- The total drag coefficient on the circular cylinder is given by:

$$C_D = \frac{2F_D}{\rho \bar{u}_e^2 S} \quad (7)$$

where F_D represents the total drag force per unit length of the cylinder and is a combination of friction and pressure drag as given by:

$$F_D = F_{DP} + F_{DF} = \frac{1}{2} C_{DP} \rho \bar{u}_e^2 S + \frac{1}{2} C_{DF} \rho \bar{u}_e^2 S \quad (8)$$

Chapter 4. Numerical Solution Procedure

Figure 2 presents the computational grid structure adopted for solving the case of unobstructed backward facing flow problem (i.e., without cylinder). The grid is generated by using GAMBIT, a pre-processor of FLUENT and shows the non-uniform orthogonal grid structure for the whole of the computational domain (Fig. 2a) along with the magnified view (Fig. 2b). It consists of both uniform and non-uniform grid distributions having a close clustering of grid points in the regions of large gradients and coarser grids in the regions of low gradients. The surface limiting the height of the channel is a critical zone where considerable gradients in velocity components and temperature will occur. For handling this situation, a very fine grid is proposed in this zone as well as near the bottom wall of the channel. The result is a mirror non-uniform grid progressively increasing in the direction normal to the solid surface and to the line of symmetry, such that the smallest control volumes are in the vicinity of the bottom wall and the step height and the largest control volumes are midway between these two reference surfaces.

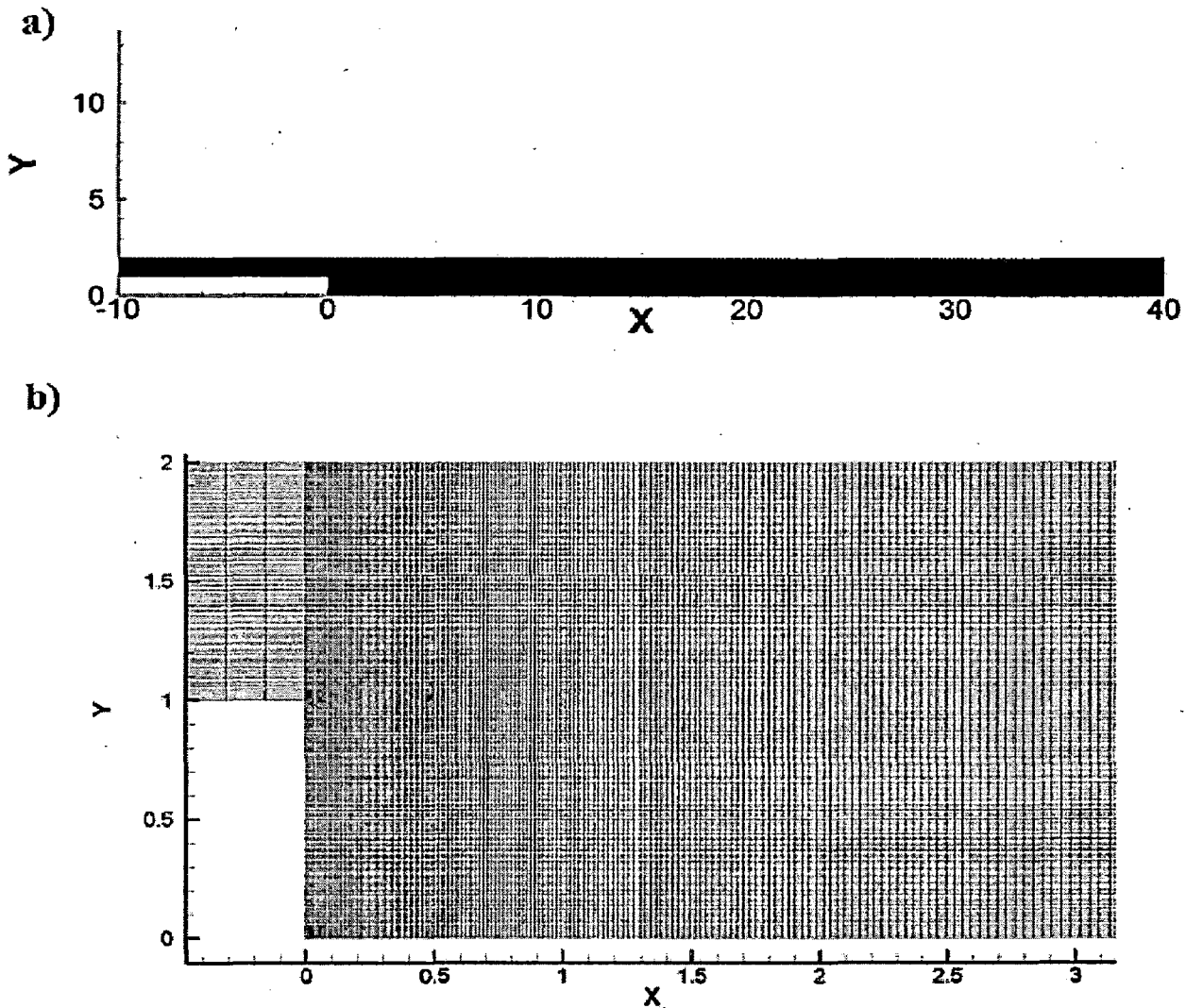


Fig. 2. Non-uniform grid structure for the unobstructed BFS flow: (a) complete and (b) magnified views.

A thorough analysis of the sensitivity of the simulation results with regard to the number of elements, mesh size and grid fineness for each case is carried out using 3 different grids of varying fineness and the results have been presented in Table 1. After the sensitivity analysis a computational grid consisting of 90,701 cells with the minimum grid spacing in the vicinity of the wall being $0.003S$ and the maximum grid spacing being $0.19S$ is found to be sufficiently fine to resolve the flow and heat transfer phenomena in the unobstructed backward-facing step case and is used in all subsequent calculations.

Table 1: Sensitivity analysis for flow across the backward-facing step obstructed by an adiabatic circular cylinder. (Here N_{cells} represents total number of cells in the grid, N_c is the number of points on the surface of cylinder, Δ_{cylinder} is the minimum grid spacing in the vicinity of the cylinder and Δ_{wall} is the minimum grid spacing in the vicinity of the wall.)

| Case | Grid Details | | | | C_D | | |
|-------------|--------------|--------------------|-------|----------------------------|----------|----------|----------|
| | Grid | N_{cells} | N_c | Δ_{cylinder} | Re = 10 | Re = 100 | Re = 200 |
| $y_c = 0.5$ | G1 | 45070 | 200 | 0.0063 | 0.415998 | -0.05693 | -0.02608 |
| | G2 | 82810 | 400 | 0.0032 | 0.410823 | -0.05749 | -0.02623 |
| | G3 | 149570 | 600 | 0.0021 | 0.407287 | -0.05937 | -0.02631 |
| $y_c = 1.0$ | G1 | 45070 | 200 | 0.0063 | 2.534756 | 0.390306 | 0.273059 |
| | G2 | 82810 | 400 | 0.0032 | 2.530499 | 0.388285 | 0.271648 |
| | G3 | 149570 | 600 | 0.0021 | 2.532636 | 0.38756 | 0.270923 |
| $y_c = 1.5$ | G1 | 45070 | 200 | 0.0063 | 4.249154 | 1.079197 | 0.825561 |
| | G2 | 82810 | 400 | 0.0032 | 4.303255 | 1.173836 | 0.824055 |
| | G3 | 149570 | 600 | 0.0021 | 4.346411 | 1.110178 | 0.828922 |

| Case | Grid Details | | | Nu_{max} | | |
|--------------|--------------|--------------------|------------------------|-------------------|----------|----------|
| | Grid | N_{cells} | Δ_{wall} | Re = 10 | Re = 100 | Re = 200 |
| Unobstructed | G1 | 46801 | 0.006 | 1.04562 | 1.88462 | 2.46631 |
| | G2 | 90701 | 0.003 | 1.04898 | 1.89436 | 2.44642 |
| | G3 | 151471 | 0.002 | 1.04962 | 1.90365 | 2.45563 |

Similarly, the grid structure adopted for simulating the case of the adiabatic circular cylinder in the backward-facing step domain is shown in Fig.3. The complete computational grid is shown in Fig. 3a along with the magnified view (Fig. 3b). In order to capture the physics of the boundary layer separation around the circular cylinder a very fine grid has been constructed in a square region immediately surrounding the cylinder. For a sensitivity analysis, the surface of the cylinder has been approximated with 3 different densities of 50, 100 and 150 grid points in each quadrant (a total of 200, 400 and 600 grid points on the entire cylinder's circumference) respectively. The rest of the domain is similar to that of the unobstructed case. The minimum grid spacing surrounding the cylinder for the three grids is 0.0063, 0.0032 and 0.0021

respectively. The percentage relative change in the values of the total drag coefficient for the above three grids is found to be less than 1% for $Re = 200$. Hence, the grid size of 82,810 cells is used in this work.

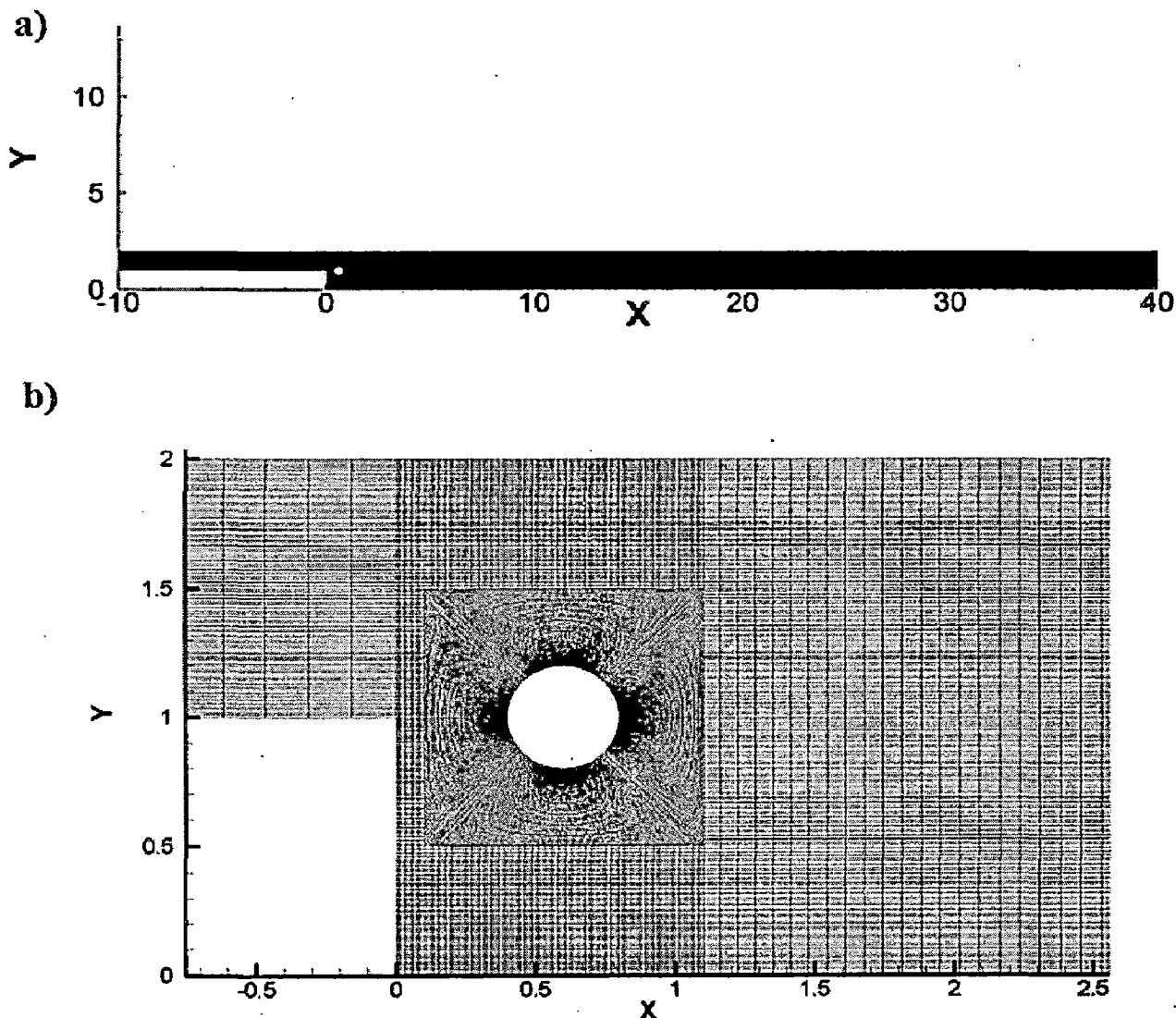


Fig. 3. Non-uniform grid structure for the BFS flow obstructed with a circular cylinder: (a) complete and (b) magnified views.

This numerical study has been carried out using FLUENT (version 6.3). The two-dimensional laminar, segregated solver is used to solve the incompressible flow on the collocated grid arrangement. The 'constant density' and 'Newtonian' viscosity models are used. The QUICK scheme has been used to discretize the convective terms in the momentum and thermal energy equations. The semi-implicit method for the pressure linked equations (SIMPLE) scheme

is used for solving the pressure-velocity decoupling. FLUENT solves the system of algebraic equations using the Gauss–Siedel (G–S) point-by-point iterative method in conjunction with the algebraic multi-grid (AMG) method solver. The use of AMG scheme can greatly reduce the number of iterations (and thus, CPU time) required to obtain a converged solution, particularly when the model contains a large number of control volumes. The relative convergence criteria of 10^{-10} for the continuity and x- and y-components of the velocity and 10^{-20} for temperature is prescribed in this work.

Chapter 5. Results and Discussions

Inspection of the foregoing analysis indicates that the flow and heat transfer characteristics in the present system depends on eight parameters. These are the Reynolds number Re , the Prandtl number Pr , the dimensionless height of the backward-facing step S , the dimensionless diameter of the circular cylinder d , the stream-wise dimensionless distance between the backward-facing step and the circular cylinder x_c , the cross-stream dimensionless distance between the hot bottom surface of the backward-facing step and the circular cylinder y_c , the dimensionless length of the hot section of bottom plate L and the expansion ratio of the system ER . Since a vast number of the governing dimensionless parameters is required to characterize the system, a comprehensive analysis of all combinations of problems is not practical. While computations can be performed for any combination of these parameters, the objective here is to present a sample of results that would illustrate the effects of Re , and y_c on the convective heat transfer. In particular, air ($Pr = 0.71$) flowing through the channel with $ER = 2$ and $L = 40S$ is considered. The results are presented for the cases with Re varying from 1 to 200 and y_c from 0 to 1.5.

5.1 Validation of results

The numerical solution procedure used here has been benchmarked with standard results for the incompressible flow over a backward-facing step reported elsewhere[17]. The validation of the local Nusselt number variation for the case of $S = 0.5$ and $Re = 100$ has been presented in Fig. 4. Further, the present value of the reattachment length for the benchmark backward-facing step problem ($ER = 2$, $Re = 100$) has been compared with a large number of other sources [21-24] and has been presented in Table 2. The minimum percentage deviation of the values obtained in this study as compared with those available in the literature is found to be about 0.3%(Acharya et al.[21]) while the maximum deviation is around 6% (Cochran et al.[23]).

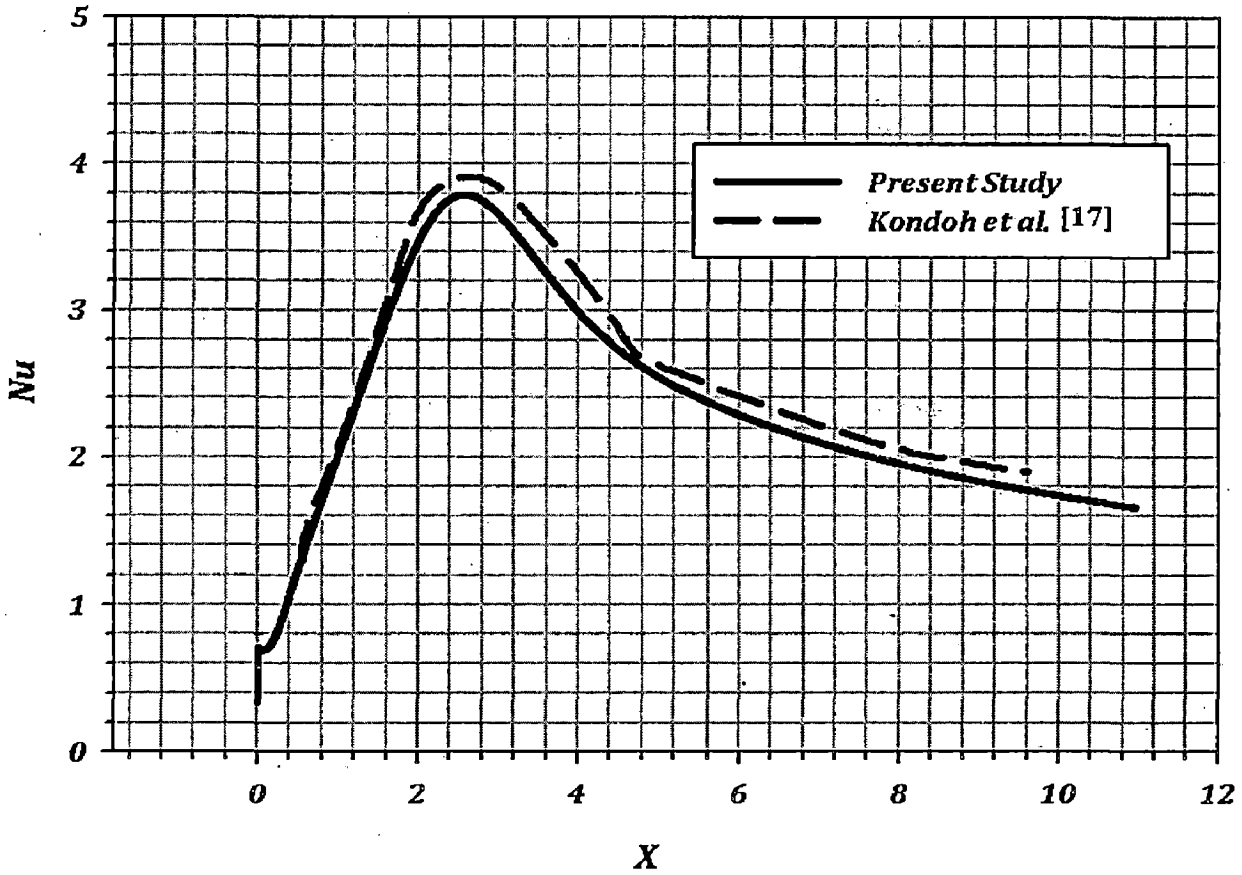


Fig. 4. Validation of the Nusselt number distribution with those of Kondoh et al. [17]

Table 2: Validation of the value of the reattachment length X_R ($Re = 100$, $ER = 2$).

| Source | Solution method | X_R/S |
|---------------------------|-------------------|---------|
| Acharya et al., [21] | Finite Difference | 4.975 |
| Choudhury and Woolfe [22] | Finite Volume | 5.02 |
| Cochran et al., [23] | Finite Volume | 5.325 |
| Hong et al., [24] | Finite Difference | 4.94 |
| Present work | Finite Volume | 4.9898 |

In addition to the above benchmarking, the general validity of the code used here has been checked for a few other flow problems: namely, the flow in a lid driven square cavity; the results obtained in this work are in perfect agreement with the results available in the literature [25]. This further confirms the accuracy and the reliability of the present numerical solution procedure.

5.2 Flow patterns

Figures 5, 6 and 7 present representative flow patterns for the current system by way of streamlines for $Re = 1$, 100 and 200 respectively. To ensure a comparative study of the effect of the cross-stream position of the circular cylinder on the flow characteristics, all the four cases (unobstructed flow, $y_c = 0.5$, $y_c = 1.0$ and $y_c = 1.5$) have been presented over the entire range of Reynolds number considered. For the limiting case without the installation of the circular cylinder, as the Reynolds number is gradually increased ($1 \leq Re \leq 200$), the flow separates at the edge of the step and a closed primary recirculation region is observed behind the step. The size of these recirculation zones increases with an increase in the Reynolds number for a fixed value of the expansion ratio of 2. Further downstream of the reattachment points, the flow regains its fully developed flow behavior. At $Re = 200$, the appearance of a secondary recirculation region on the upper wall can also be observed (Fig. 7a).

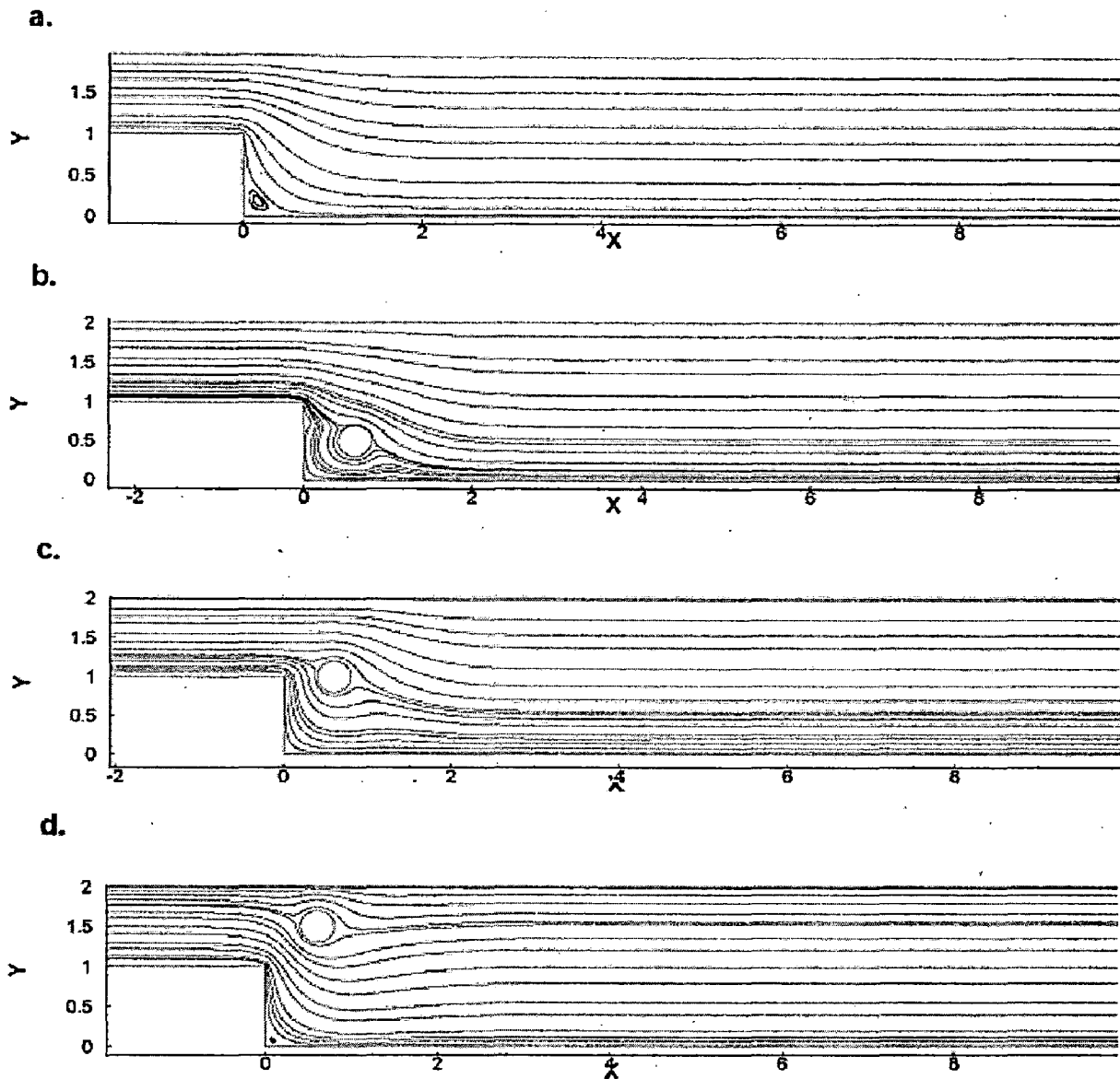


Fig. 5. Streamline profiles for $Re = 1$: a) Unobstructed case; b) $y_c = 0.5$; c) $y_c = 1.0$ and d) $y_c = 1.5$

In the case of $y_c = 0.5$ when the cylinder was mounted at the lowest position, the top surface of the cylinder is positioned below the top surface of the step. Thus as can be seen in Figs. 5(b), 6(b) and 7(b), the flow coming from upstream of the step is not seriously obstructed by the cylinder and dividing shear layer between the main flow and the recirculating flow region is not noticeably affected by the presence of the cylinder. Therefore, the separation streamlines from the top corner of the step resemble in behaviour the counterparts for the unobstructed case.

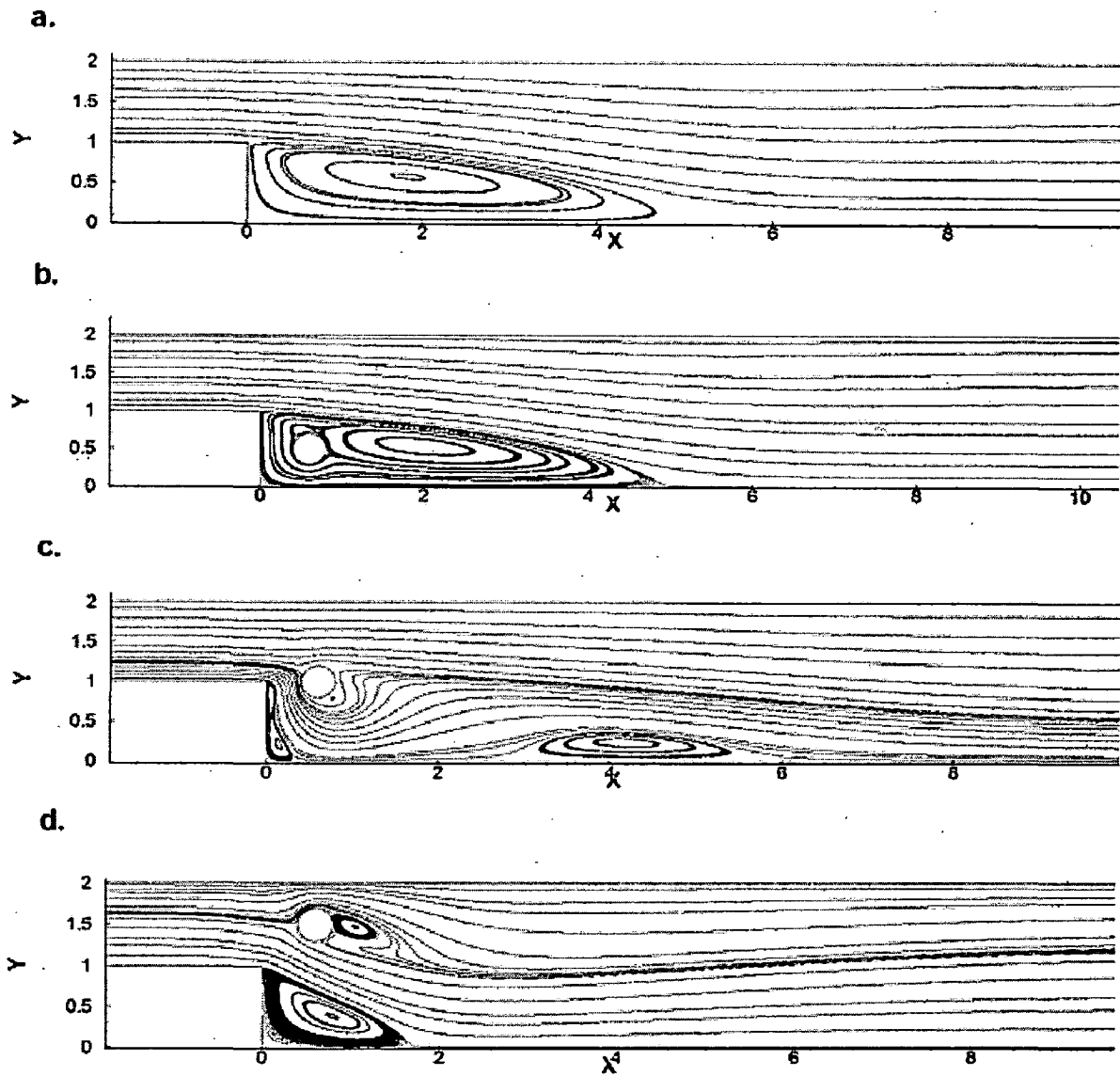


Fig. 6. Streamline profiles for $Re = 100$: a) Unobstructed case; b) $y_c = 0.5$; c) $y_c = 1.0$ and d) $y_c = 1.5$

In the case $y_c = 1.0$, on the other hand, the top half of the cylinder is located above the top surface (mid-plane) of the step. In this case firstly, the motion of fluid flowing over the cylinder is seem to be affected to some extent. Related to this effect as can be clearly observed from Figs. 6(c) and 7(c), the reattachment of discrete vortices in the primary recirculation zone adjacent to the step occurs at a position clearly upstream of the corresponding positions observed in the cases of unobstructed flow and the flow at $y_c = 0.5$. Secondly, some portion of the fluid passing over the top of the step creeps into the region underneath the cylinder through the gap between

the step and the cylinder. As can be seen in Fig.7(c), the stream line representing this fluid motion moves down and once reattaches the bottom surface. But it separates soon from the bottom surface and is entrained into the wake of the cylinder. Therefore, a secondary separation bubble appears downstream of the primary reattachment point. This case also presents a significant compression of the stream lines deflected beneath the circular cylinder.

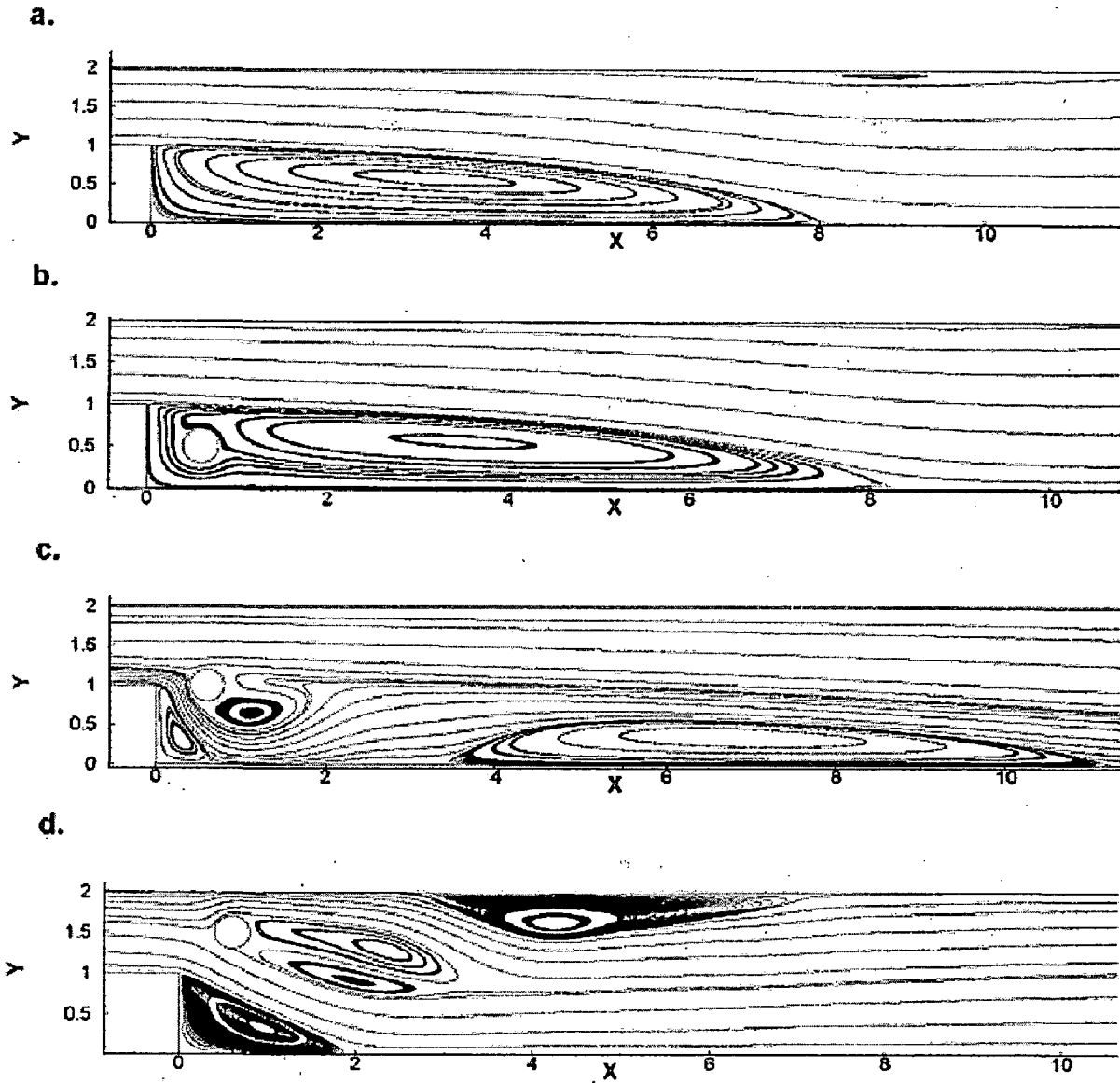


Fig. 7. Streamline profiles for $Re = 200$: a) Unobstructed case; b) $y_c = 0.5$; c) $y_c = 1.0$ and d) $y_c = 1.5$

In the last case, $y_c = 1.5$, a larger amount of fluid moves through the gap between the cylinder and the top corner of the step. The characteristic fluid flow patterns for $Re = 1, 100$ and 200 are shown in Figs. 5(d), 6(d) and 7(d), respectively. Although there is not any significant flow pattern eminent for the case of $Re = 1$, however an increase in Reynolds number brings forth similar trends as seen for $y_c = 1.0$ and the unobstructed case. Firstly, there is a reduction in the size of the primary recirculation zone formed behind the step (as compared to its other counterpart for the same Re in the unobstructed case) but no appearance of a secondary recirculation zone. Secondly, as the Reynolds number is gradually increased, flow separates from the rear portion of the circular obstacle and forms two vortices behind the circular cylinder that are slightly directed downwards. The size of these vortices increases with increasing value of the Reynolds number for $1 < Re \leq 200$. Further, it is observed that at the highest value of Reynolds number of 200 , there is the formation of a secondary separation bubble on the upper wall of the step geometry (Fig. 7d). Investigations into the time varying nature of these vortices revealed them to be of steady state nature. The solution of time-dependent equations and the drag coefficient with time is monitored for the flow to reach the fully periodic regime. A first order implicit scheme for time discretization of the equations is used with a time-step size of 0.01 s. Simulations are continued until the time varying variations in the drag coefficient cancel out and a steady value is reached. Further, the Strouhal number for each case is monitored and is found to be zero indicating steady state nature of the vortices in the range considered here.

5.3 Thermal Patterns

The representative steady isotherm profiles for the present system for Prandtl number, $Pr = 0.71$ and Reynolds numbers, $Re = 1, 100$ and 200 are illustrated in Figs. 8, 9 and 10, respectively. As shown in Figs. 9(a) and 10(a), under the influence of the reattaching flow, the temperature contours for the case of unobstructed flow undergo local compression around the flow-reattachment point. The thermal boundary layer is compressed by the reattaching wall-ward flow. As a result, a layer with steep temperature gradient is formed above the wall around the flow reattachment point, which leads to heat transfer enhancement there.

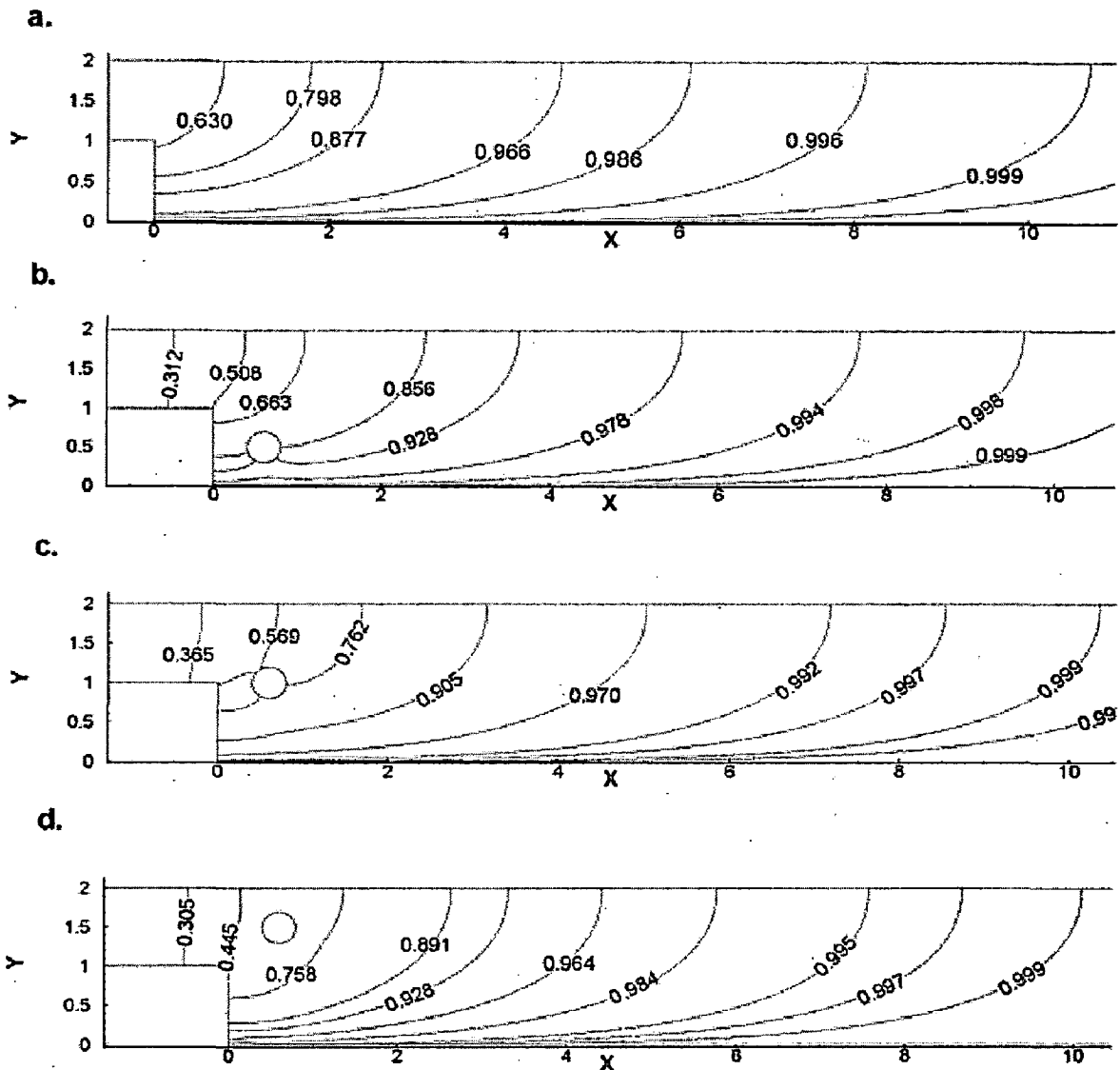


Fig. 8. Isotherm profiles for $Re = 1$: a) Unobstructed case; b) $y_c = 0.5$; c) $y_c = 1.0$ and d) $y_c = 1.5$

Comparing isotherms for the case of $y_c = 0.5$ (Figs. 8b, 9b and 10b) with those for the unobstructed flow, it is found that there is not any significant variation except for the slight distortion of the isotherms in the vicinity of the circular cylinder. This is complemented by the similarity in flow patterns for the two cases. The isotherms for the cylinder position of $y_c = 1.0$ (Figs. 8c, 9c and 10c) depict a marked compression and crowding of the isotherms below the cylinder and close to the reattachment point of the primary recirculation zone. The isotherms further get compressed at another point downstream that lies close to the reattachment point of the secondary separation bubble. The effects are more pronounced at higher values of the flow

Reynolds number. Further, there is excessive congestion of isotherm lines on that side of the cylinder that directly obstructs the flow compared to its rear side. Similar to the case of $y_c = 1.0$, there is compression of the isotherms noticed for $y_c = 1.5$ (Figs. 8d, 9d and 10d). However, there is only one point of compression corresponding to the reattachment point of the primary recirculation zone and lies significantly upstream compared to its other counterparts.

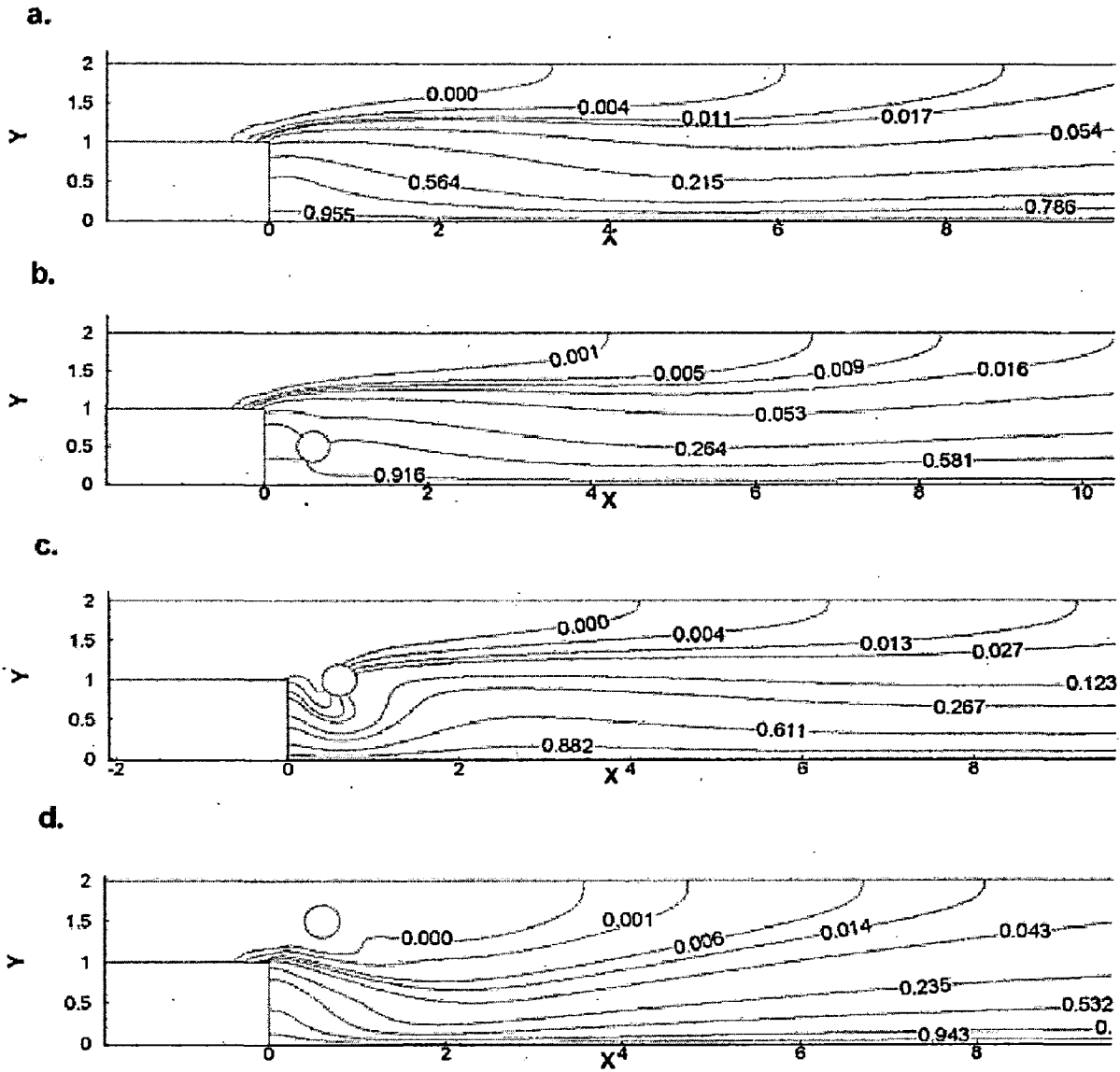


Fig. 9. Isotherm profiles for $Re = 100$: a) Unobstructed case; b) $y_c = 0.5$; c) $y_c = 1.0$ and d) $y_c = 1.5$

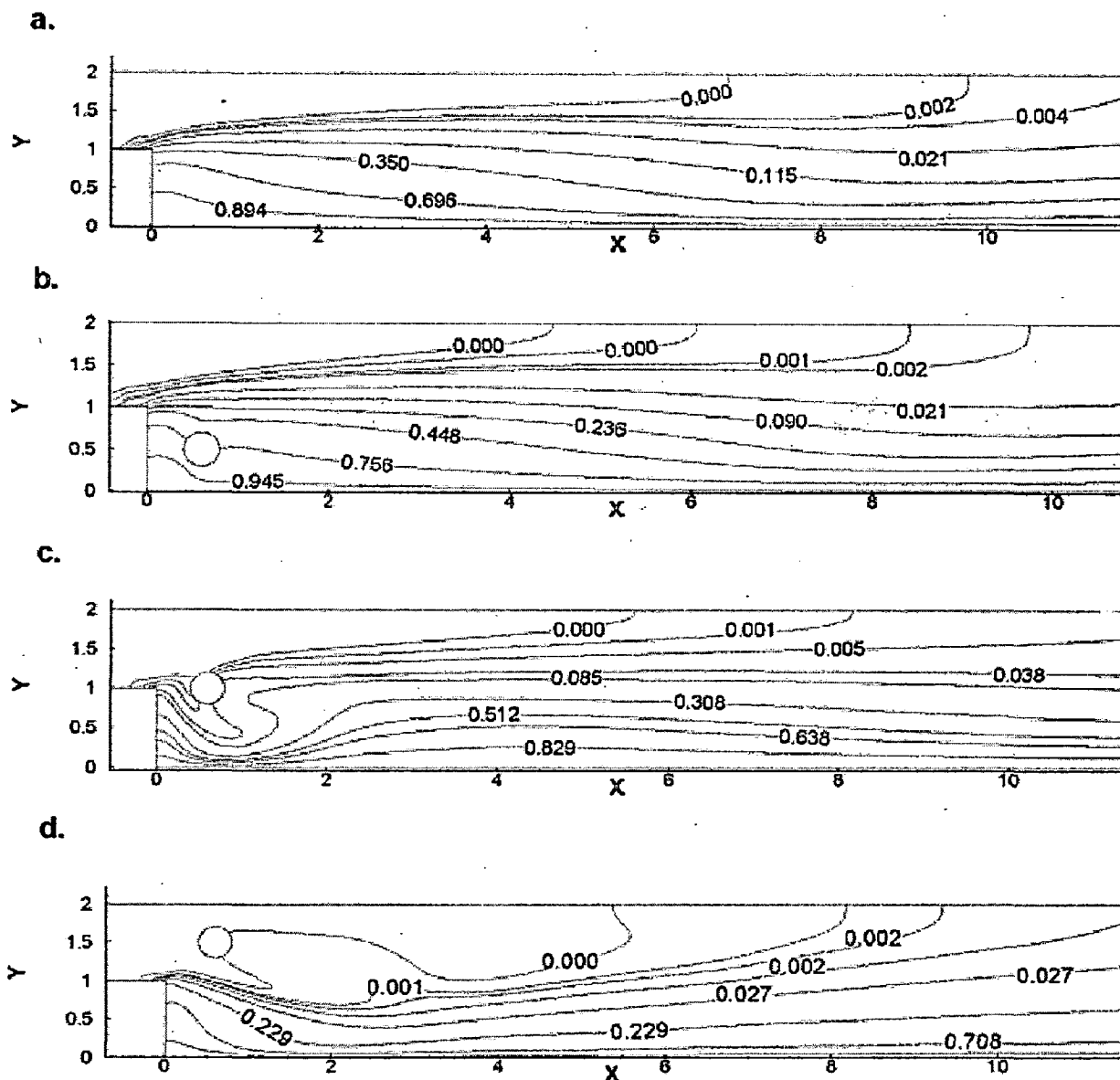


Fig. 10. Isotherm profiles for $Re = 200$: a) Unobstructed case; b) $y_c = 0.5$; c) $y_c = 1.0$ and d) $y_c = 1.5$

5.4 Drag Coefficient

The drag is the force exerted by the fluid on the bluff body in the direction on the flow. There are two components that contribute to drag: friction drag coefficient and pressure drag coefficient. Therefore, the sum of two components is the total drag coefficient, as defined in Eq. (7). Figure 11 presents the variation of the overall drag coefficient of the circular cylinder used in

this system with Reynolds number for the various cases considered. It is observed that the value of the overall drag coefficient decreases with increasing value of the Reynolds number. At low Reynolds numbers, drag is strongly dependent on the Reynolds number because the viscous forces play a dominant role in the steady flow regime. From this figure (Fig. 11), it can be observed that the values of the overall drag coefficient for the case of $y_c = 1.5$ are higher than that of the other two cases. This can be directly explained on the fact that for $y_c = 1.5$, the cylinder faces the fluid flow directly as against $y_c = 1.0$ and $y_c = 0.5$ where there is only partial obstruction of the flow.

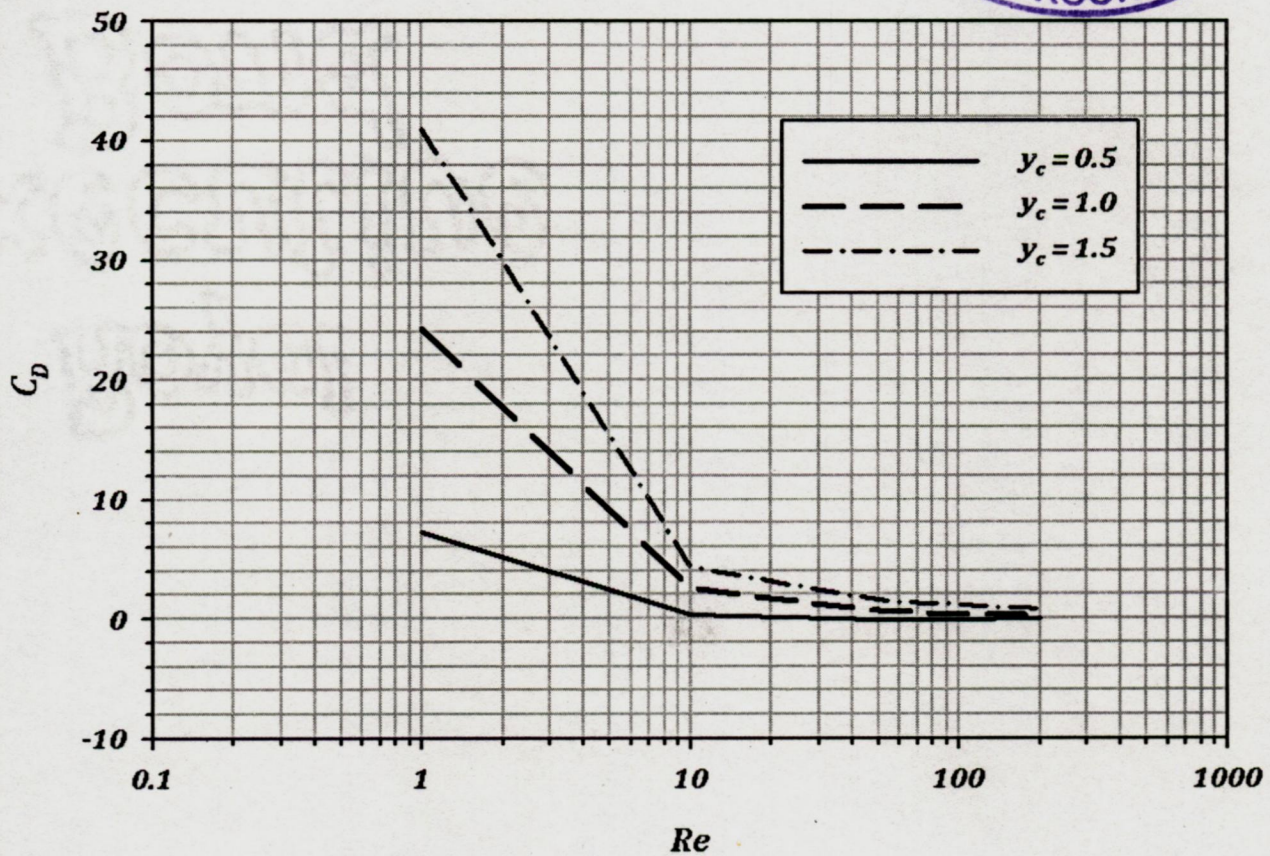
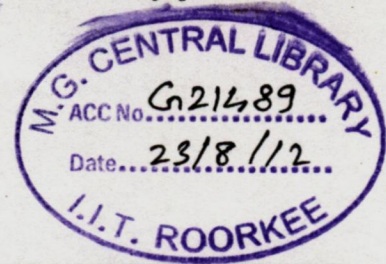


Fig. 11. Variation of overall drag coefficient (C_D) with Reynolds number and y_c .

A simple drag correlation is obtained for the range of conditions studied here. The total drag coefficient for the intermediate values of the Reynolds number can be calculated by using Eqs. (8) and (9) for the range $1 < Re \leq 200$.

For $y_c = 1.0$:

$$C_D = 24.11(Re)^{-1.006} + 0.1551 \quad (9)$$

For $y_c = 1.5$:

$$C_D = 40.24(Re)^{-1.051} + 0.7595 \quad (10)$$

The above expressions have a maximum error of less than 0.54% and about 5.0% respectively with the computed results. Fitting a similar expression for the case of $y_c = 0.5$ yields a greater value of error and hence has not been presented here.

5.5 Local Nusselt Number

Figure 12 shows the lengthwise distribution of the local Nusselt number (Eq. 5) along the bottom wall for the four different flow configurations considered here and for flows involving different Reynolds number. The abscissa is the distance from the step normalized by the step height. From these figures it can be generalized that at distances sufficiently away from the step (beyond the peak Nusselt number location) the local Nusselt numbers increase with an increase in the Reynolds number. However, the individual plots for the various configurations show ample features to be studied individually.

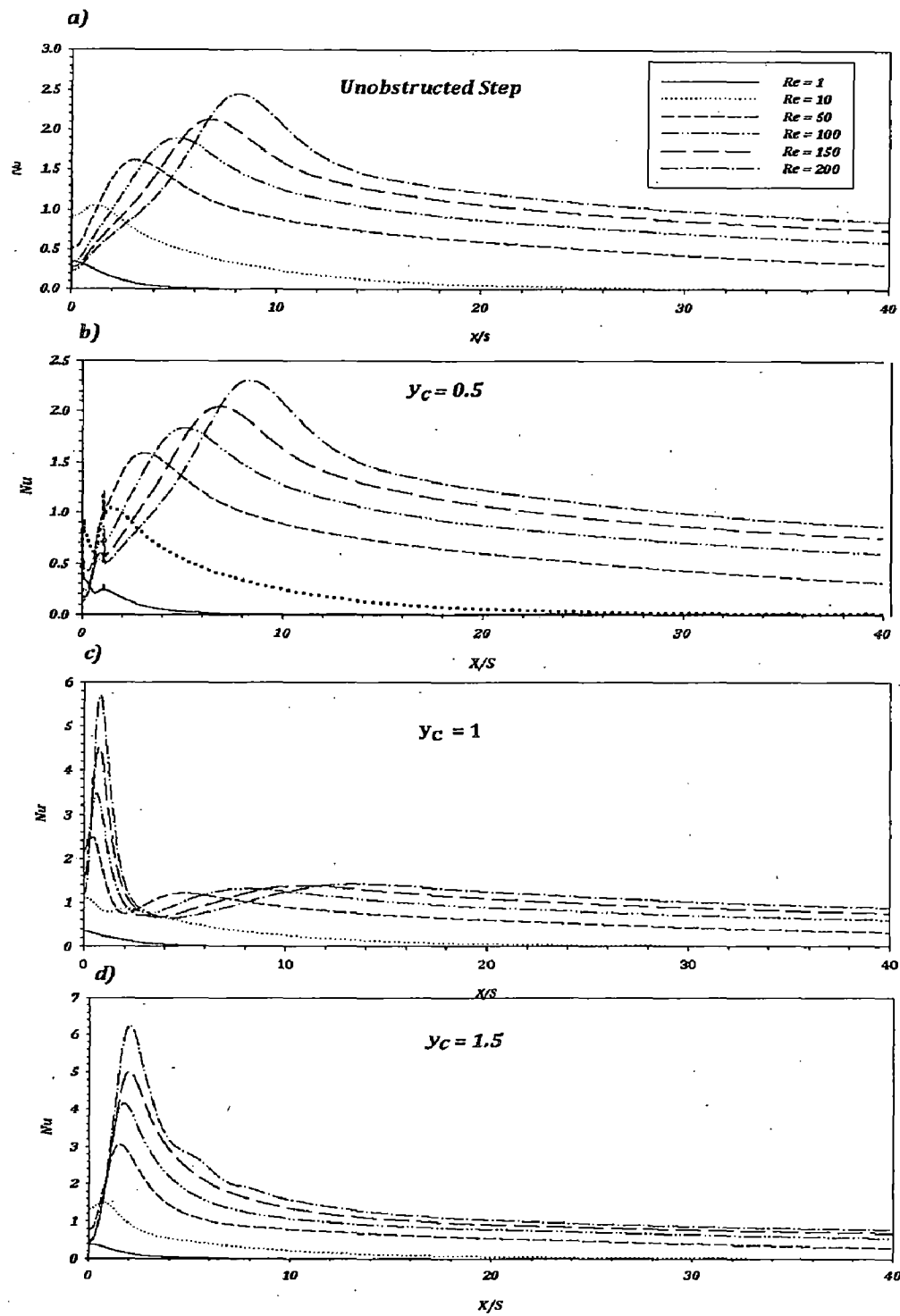


Fig. 12. Effect of Reynolds number on the variation of the local Nusselt number distribution (Nu vs.X): a) Unobstructed case; b) $y_c = 0.5$; c) $y_c = 1.0$; and d) $y_c = 1.5$

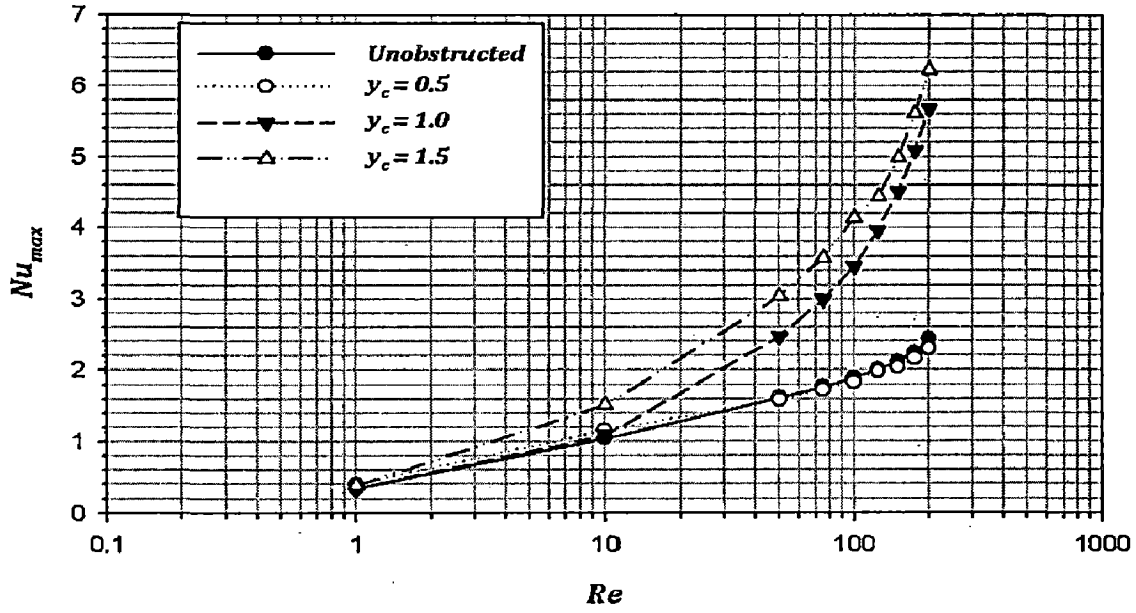
Figure 12(a) shows the local Nusselt variation for the unobstructed flow, and as can be seen from the graph that there exists a peak in the Nusselt number that corresponds to a point close to the flow reattachment point (where significant compression of the thermal boundary layer occurs). The case of $y_c = 0.5$ (as depicted in Fig.12 b) does not show any significant variation in the nature of the local Nusselt plots compared to the unobstructed flow. However there is a slight distortion in the initial parts of the plot owing to the presence of the circular cylinder in the flow separation zone.

The local Nusselt variation for the case of $y_c = 1.0$ (Fig.12 c) and $y_c = 1.5$ (Fig.12 d) illustrate a drastic enhancement in the peak Nusselt values as compared to the other cases. This is attributed to the enhanced compression of the thermal boundary layer by the adiabatic circular cylinder in the backward-facing step geometry. Further Fig.12 (c) shows the presence of two peaks in the local Nusselt variation. The first higher peak corresponding to the reattachment point of the primary recirculation zone and the second lower peak corresponding to the reattachment of the secondary separation bubble. However, the case of $y_c = 1.5$ (Fig.12 d) shows only one peak in the Nusselt number value on account of the lone recirculation zone in this geometry (as illustrated in Fig.6d and Fig. 7d).

5.6 Average and Peak Nusselt Number

In this study, the average Nusselt number is obtained by averaging the local Nusselt number over the bottom surface of the backward-facing step (Eq. 6). The variation of the average and the peak value of the Nusselt number with Reynolds number for the values of the Reynolds number from 1 to 200 and the various flow configurations are presented in Fig. 13. It can be generalized that the peak value of the Nusselt number increases monotonically with Re (Fig. 13a). Similarly, all the cases considered here show a monotonic increase in the Nu_{avg} value with increase in the Reynolds number as is shown in Fig 13(b).

a)



b)

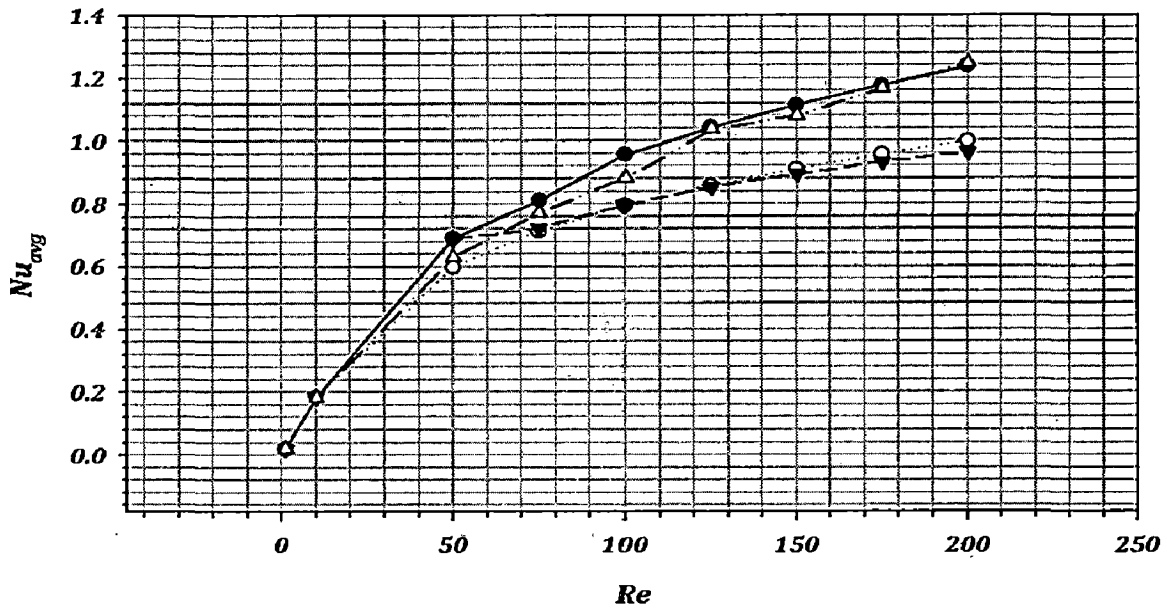


Fig. 13. Variation of heat transfer characteristics with Reynolds number: (a) Maximum Nusselt number (Nu_{max}); and (b) Average Nusselt number (Nu_{avg}).

From an application standpoint, it is convenient to correlate the present heat transfer results by simple expressions. Simple dimensional considerations suggest the Nusselt number to be a function of the Reynolds number, Prandtl number, and the nature of the thermal boundary condition. In order to correlate Nu_{max} with Re and for the fixed Pr of 0.71, the data obtained is modelled to an exponential equation of the form:

$$Nu_{max} = a * (Re)^b + c \quad (11)$$

The fitted expressions for individual cases of cylinder position have been shown in Table 3 also indicating the average error in each case.

Table 3: Coefficients of the exponential fit to the variation of the maximum Nusselt number (Nu_{max}) with Reynolds number (Re) for $Pr = 0.71$ (air) and $1 \leq Re \leq 200$:

| Cylinder position | a | b | c | Average error (%) |
|-------------------|--------|--------|---------|-------------------|
| Unobstructed Flow | 0.9816 | 0.2073 | -0.6072 | 0.5502 |
| $y_c = 0.5$ | 1.582 | 0.1418 | -1.144 | 0.4654 |
| $y_c = 1.0$ | 0.1406 | 0.6824 | 0.3045 | 1.9927 |
| $y_c = 1.5$ | 0.3318 | 0.5402 | 0.1784 | 2.444 |

Further, the variation of the point of maximum heat transfer with the Reynolds number has been illustrated in Fig. 14 and shows that the point moves further downstream with increasing Re . Also it may be noted from the graph that for a given Reynolds number, the point of maximum heat transfer lies very close to the step for the cases of $y_c = 1.0$ and $y_c = 1.5$ as compared to the unobstructed case and $y_c = 0.5$.

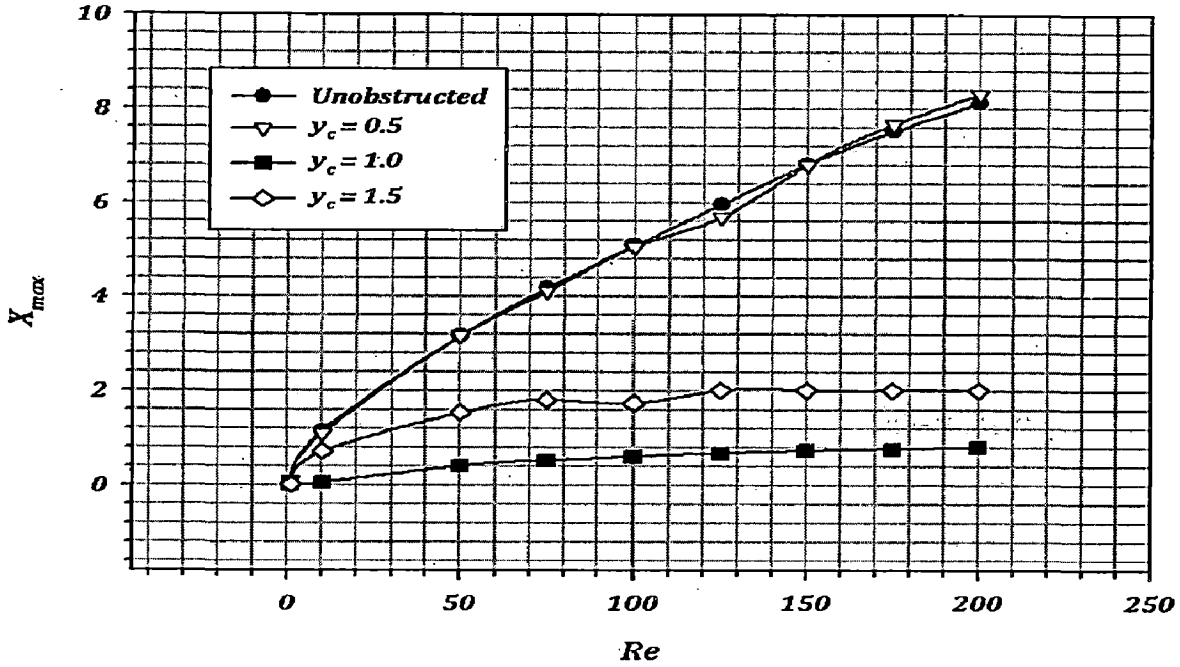


Fig. 14. Variation of the point of maximum heat transfer (X_{max}) with Reynolds number and y_c .

Finally, the enhancement of the heat transfer performance through the circular cylinder installation is investigated. Figure 15 shows the variation of $Nu_{max} / Nu_{unobstructed}$ versus Re for the three cross-stream positions of the cylinder. Nu_{max} and $Nu_{unobstructed}$ represent the maximum Nusselt numbers for the obstructed step and the unobstructed case of the bottom plate, respectively. It is seen that $Nu_{max} / Nu_{unobstructed}$ rises with the increase in Re for $y_c = 1.0$ and 1.5 and declines for $y_c = 0.5$. In addition, the maximum value of $Nu_{max} / Nu_{unobstructed}$ is found to be about 2.55. This means that, with an adiabatic circular cylinder installed on the upper part at $y_c = 1.5$, the enhancement of heat transfer coefficient for the hot lower wall is 155% of that without a cylinder at $Re = 200$.

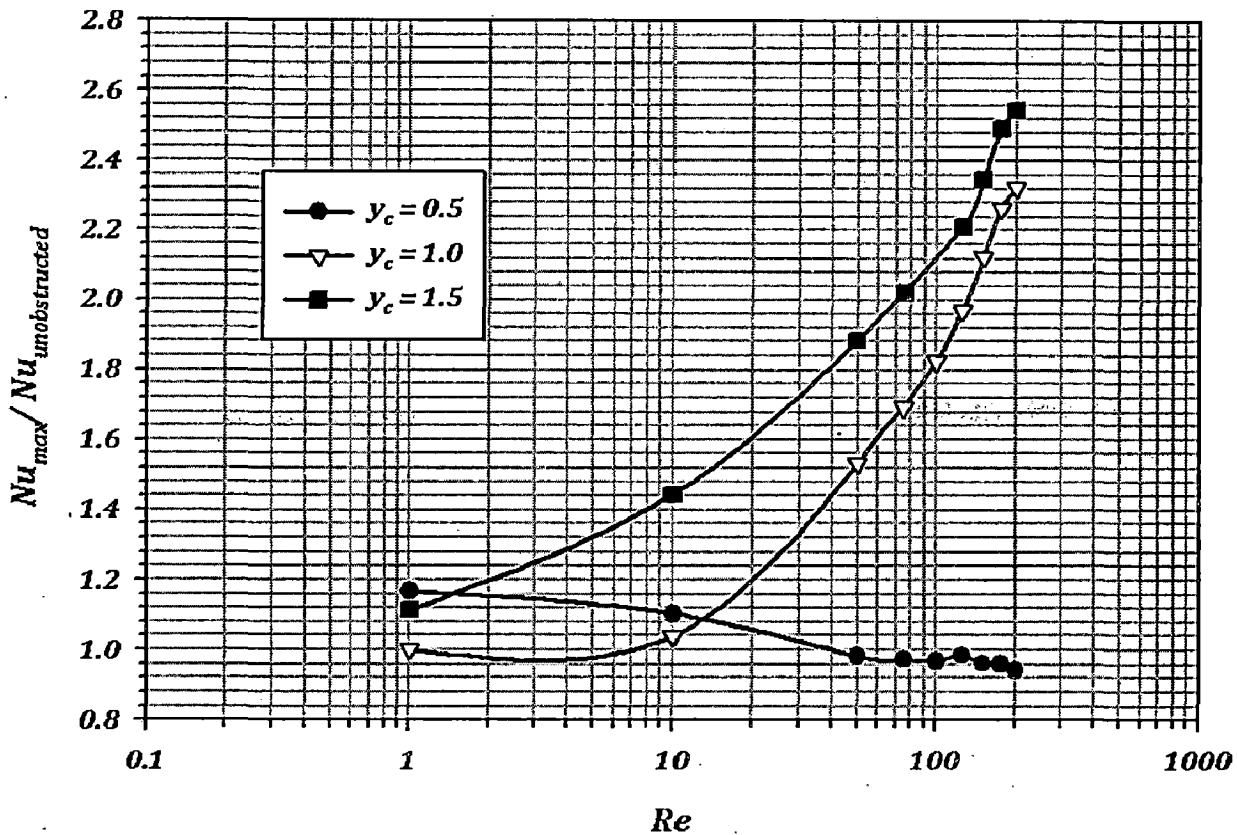


Fig. 15. Variation of $Nu_{max} / Nu_{unobstructed}$ with the Reynolds number and y_c .

5.7 Pressure Drop

A heat transfer increment is generally accompanied by a pressure penalty. Figure 16 shows the variation of the dimensionless pressure drop (dP) between the inlet and the outlet sections of the backward-facing step for different transverse positions of the circular cylinder in the domain as compared with that for the unobstructed case. As expected, the pressure drop is slightly larger for the case of $y_c = 1.5$ where the fluid is directly obstructed by the cylinder. The other cases for $y_c = 0.5$ and $y_c = 1.0$ also show a very meagre increase in the pressure drop. The maximum increment in the pressure drop as compared with that for the unobstructed case is found to be of around 37% for $y_c = 1.5$ at $Re = 200$ which correlates very economically with an augmentation of 155%

in the heat transfer characteristics for the same.

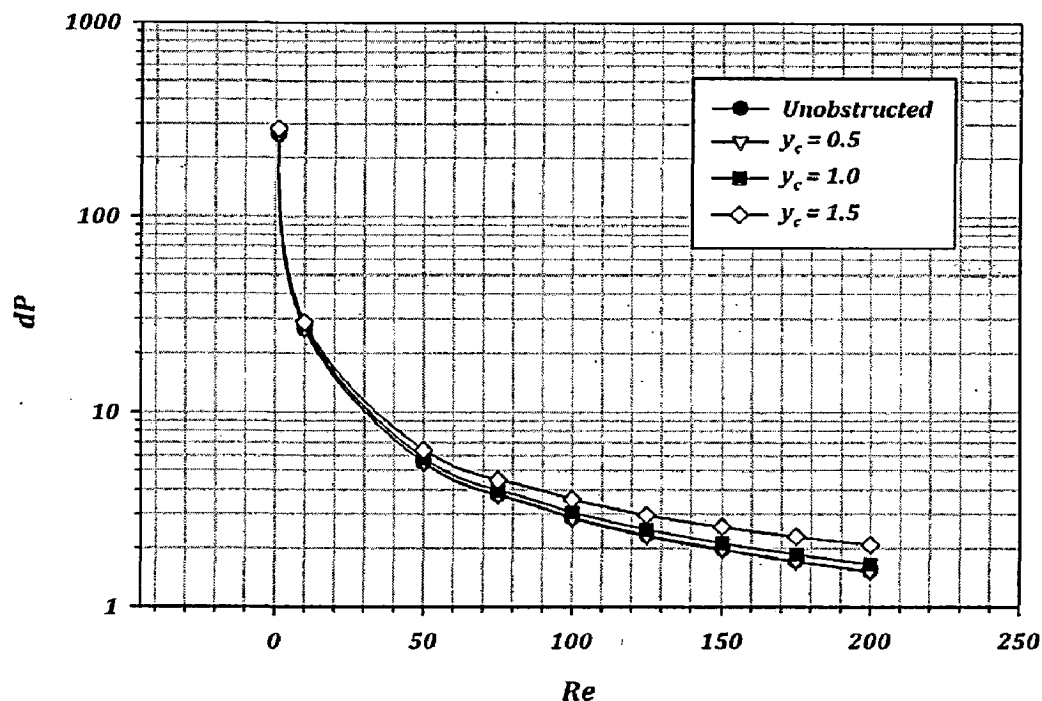


Fig. 16. Variation of the dimensionless pressure drop (dP) between inlet and outlet with Reynolds number (Re) and y_c .

5.8. Further Scope for Experimental Analysis

Although, the current work involves a numerical investigation into the problem of heat transfer augmentation in the backward-facing step geometry by means of an adiabatic circular cylinder in the laminar range, subsequent experimentation of the same is necessary. A similar experimental study on the heat transfer augmentation in a turbulent channel flow obstructed with an inserted square rod has been carried out by Yao et al. [26]. Their analysis involved flow visualization and heat transfer measurements in the geometry. Intermittent dye injection method was introduced to visualize the Karman vortex shed from the rod and to track its motion. Hydrogen bubble method was combined to visualize the near-wall flow. A similar experimental apparatus as shown in Fig. 17 is proposed to visualize the flow and heat transfer results as have been presented in the

current study. The fluid flow characteristics and also the heat transfer augmentation may be visualized by using one or the other commercial fluid flow measurement techniques available viz. Laser Doppler Velocimetry, Particle Image Velocimetry (PIV) etc.

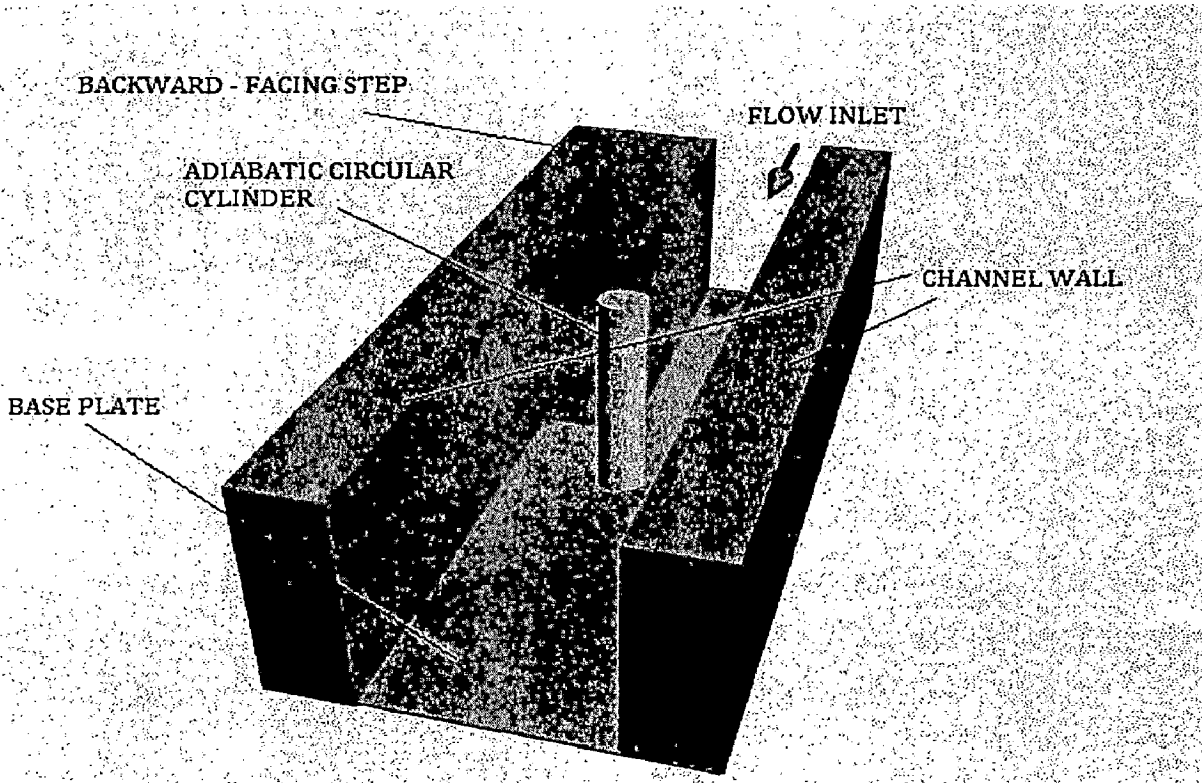


Fig. 17. Schematic detail of proposed test section and apparatus for experimental analysis.

Chapter 6. Conclusions

In the present work, the heat transfer in a separating and reattaching flow is numerically studied by simulating the flow and heat transfer downstream of the backward-facing step for $Re = 1 - 200$, $y_c = 0 - 1.5$ and $Pr = 0.71$. The heat transfer enhancements of backward-facing step flow in a two-dimensional channel through the introduction of an adiabatic circular cylinder in the channel have been explored in detail. Attention is particularly focused on the effect of the relative cross-stream position of the circular cylinder on the flow structure, temperature distribution and Nusselt number variation for the system at various Reynolds numbers. It has been demonstrated that the insertion of a circular cylinder is effective for altering the velocity field of the backward-facing flow if the cylinder is positioned at the appropriate position. This change in the flow characteristics results in a heat transfer enhancement across the bottom surface of the step. The results showed that for the Reynolds number range considered here, the maximum enhancement in the Nusselt number value is around 155% for the constant wall temperature case. Further, it is also found that the peak and average value of the Nusselt number increases monotonically with the Reynolds number. Finally, simple correlations of total drag coefficient and peak Nusselt number are obtained for the range of conditions studied here.

SECTION – B

Natural Convection Heat Transfer Augmentation at a Backward-Facing Step

Chapter 7. An Introduction to the Phenomenon of Natural Convection

7.1 Physical Mechanism of Natural Convection

Many familiar heat transfer applications involve natural convection as the primary mechanism of heat transfer. Some examples are cooling of electronic equipment such as power transistors, TVs, and VCRs; heat transfer from electric baseboard heaters or steam radiators; heat transfer from the refrigeration coils and power transmission lines; and heat transfer from the bodies of animals and human beings. Natural convection in gases is usually accompanied by radiation of comparable magnitude except for low-emissivity surfaces.

We know that a hot boiled egg (or a hot baked potato) on a plate eventually cools to the surrounding air temperature (Fig. 18). The egg is cooled by transferring heat by convection to the air and by radiation to the surrounding surfaces. Disregarding heat transfer by radiation, the physical mechanism of cooling a hot egg (or any hot object) in a cooler environment can be explained as follows:

As soon as the hot egg is exposed to cooler air, the temperature of the outer surface of the egg shell will drop somewhat, and the temperature of the air adjacent to the shell will rise as a result of heat conduction from the shell to the air. Consequently, the egg will soon be surrounded by a thin layer of warmer air, and heat will then be transferred from this warmer layer to the outer layers of air. The cooling process in this case would be rather slow since the egg would always be blanketed by warm air, and it would have no direct contact with the cooler air farther away. We may not notice any air motion in the vicinity of the egg, but careful measurements indicate otherwise. The temperature of the air adjacent to the egg is higher, and thus its density is lower, since at constant pressure the density of a gas is inversely proportional to its temperature. Thus, we have a situation in which some low-density or "light" gas is surrounded by a high-density or "heavy" gas, and the natural laws dictate that the light gas rise.

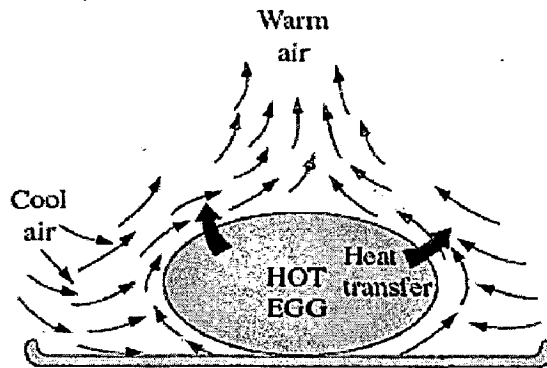


Figure 18: Schematic diagram of an example depicting natural convection. [27]

The space vacated by the warmer air in the vicinity of the egg is replaced by the cooler air nearby, and the presence of cooler air in the vicinity of the egg speeds up the cooling process. The rise of warmer air and the flow of cooler air into its place continue until the egg is cooled to the temperature of the surrounding air. The motion that results from the continual replacement of the heated air in the vicinity of the egg by the cooler air nearby is called a natural convection current, and the heat transfer that is enhanced as a result of this natural convection current is called **natural convection heat transfer**.

In heat transfer studies, the primary variable is temperature, and it is desirable to express the net buoyancy force in terms of temperature differences. But this requires expressing the density difference in terms of a temperature difference, which requires knowledge of a property that represents the variation of the density of a fluid with temperature at constant pressure.

The magnitude of the natural convection heat transfer between a surface and a fluid is directly related to the flow rate of the fluid. The higher the flow rate, the higher the heat transfer rate. In fact, it is the very high flow rates that increase the heat transfer coefficient by orders of magnitude when forced convection is used. In natural convection, no blowers are used, and therefore the flow rate cannot be controlled externally. The flow rate in this case is established by the dynamic balance of buoyancy and friction. The buoyancy force is

caused by the density difference between the heated (or cooled) fluid adjacent to the surface and the fluid surrounding it, and is proportional to this density difference and the volume occupied by the warmer fluid. It is also well known that whenever two bodies in contact (solid–solid, solid–fluid, or fluid–fluid) move relative to each other, a friction force develops at the contact surface in the direction opposite to that of the motion. This opposing force slows down the fluid and thus reduces the flow rate of the fluid. Under steady conditions, the air flow rate driven by buoyancy is established at the point where these two effects balance each other.

The friction force increases as more and more solid surfaces are introduced, seriously disrupting the fluid flow and heat transfer. For that reason, heat sinks with closely spaced fins are not suitable for natural convection cooling. Most heat transfer correlations in natural convection are based on experimental measurements. The instrument often used in natural convection experiments is the Mach–Zehnder interferometer, which gives a plot of isotherms in the fluid in the vicinity of a surface. The operation principle of interferometers is based on the fact that at low pressure, the lines of constant temperature for a gas correspond to the lines of constant density, and that the index of refraction of a gas is a function of its density. Therefore, the degree of refraction of light at some point in a gas is a measure of the temperature gradient at that point. An interferometer produces a map of interference fringes, which can be interpreted as lines of constant temperature as shown in Figure 19. The smooth and parallel lines in (a) indicate that the flow is laminar, whereas the eddies and irregularities in (b) indicate that the flow is turbulent.

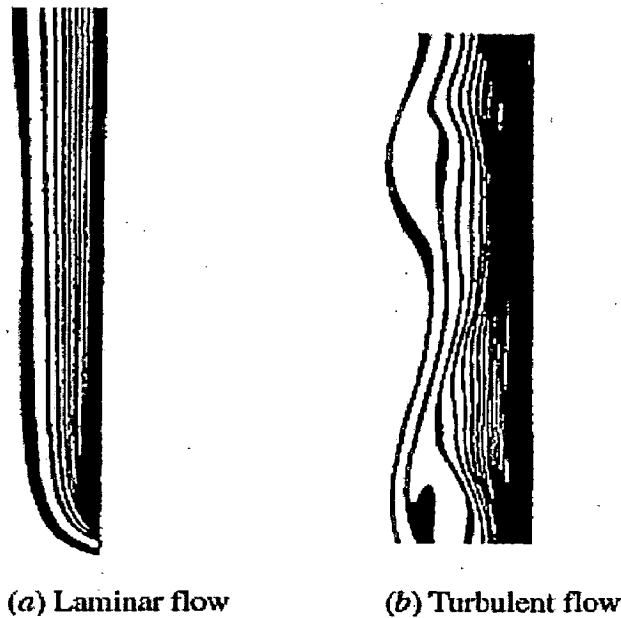


Figure 19: Isotherms in natural convection over a hot plate in air. (a) Laminar flow (b) Turbulent flow. [27]

7.2. Equation of Motion

In this section we derive the equation of motion that governs the natural convection flow in laminar boundary layer. The conservation of mass and energy equations for forced convection are also applicable for natural convection, but the momentum equation needs to be modified to incorporate buoyancy.

Consider a vertical hot flat plate immersed in a quiescent fluid body. We assume the natural convection flow to be steady, laminar, and two-dimensional, and the fluid to be Newtonian with constant properties, including density, with one exception: the density difference $\rho - \rho_\infty$ is to be considered since it is this density difference between the inside and the outside of the boundary layer that gives rise to buoyancy force and sustains flow. (This is known as the Boussinesq approximation.) We take the upward direction along the plate to be x , and the direction normal to surface to be y , as shown in Figure 20.

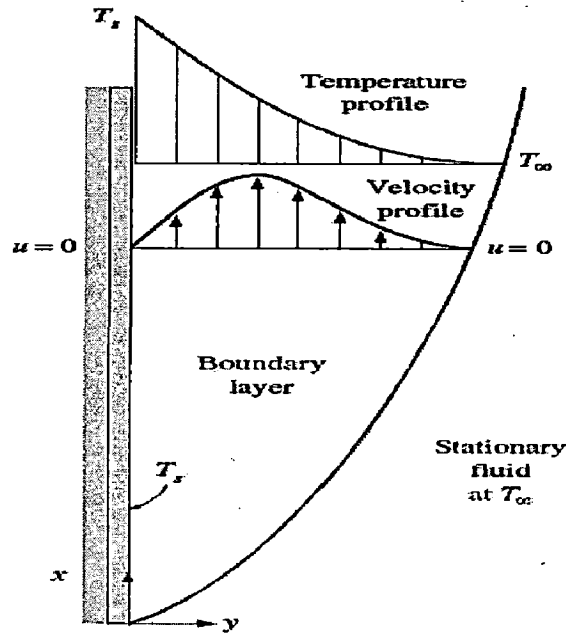


Figure 20: Typical velocity and temperature profiles for natural convection flow over a hot vertical plate at temperature T_s , inserted in a fluid at temperature T_∞ [27]

Therefore, gravity acts in the $-x$ -direction. Noting that the flow is steady and two-dimensional, the x - and y -components of velocity within boundary layer are $u = u(x, y)$ and $v = v(x, y)$, respectively.

The velocity and temperature profiles for natural convection over a vertical hot plate are also shown in Figure 20. As in forced convection, the thickness of the boundary layer increases in the flow direction. Unlike forced convection, however, the fluid velocity is zero at the outer edge of the velocity boundary layer as well as at the surface of the plate. This is expected since the fluid beyond the boundary layer is motionless. Thus, the fluid velocity increases with distance from the surface, reaches a maximum, and gradually decreases to zero at a distance sufficiently far from the surface. At the surface, the fluid temperature is equal to the plate temperature, and gradually decreases to the temperature of the surrounding fluid at a distance sufficiently far from the surface, as shown in the figure. In the case of cold surfaces, the shape of the velocity and temperature profiles remains the same but their direction is reversed.

Consider a differential volume element of height dx , length dy , and unit depth in the z -direction (normal to the paper) for analysis. The forces acting on this volume element are shown in Figure 21. Newton's second law of motion for this control volume can be expressed as

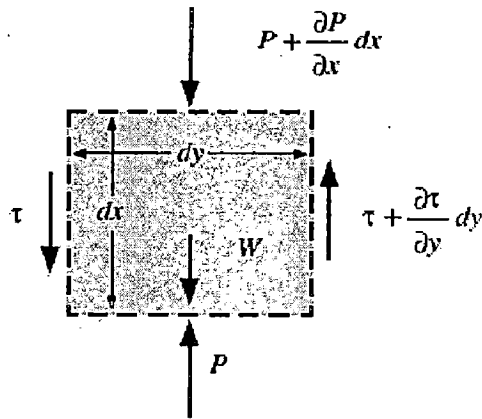


Figure 21: Forces acting on a differential control volume in the natural convection boundary layer over a vertical flat plate.[27]

$$\delta m \cdot a_x = F_x \quad (12)$$

where $\delta m = \rho(dx \cdot dy \cdot 1)$ is the mass of the fluid element within the control volume. The acceleration in the x -direction is obtained by taking the total differential of $u(x, y)$, which is $du = (\partial u/\partial x)dx + (\partial u/\partial y)dy$, and dividing it by dt .

We get

$$a_x = \frac{du}{dt} = \frac{\partial u}{\partial x} \frac{dx}{dt} + \frac{\partial u}{\partial y} \frac{dy}{dt} = u \frac{\partial u}{\partial x} + v \frac{\partial u}{\partial y} \quad (13)$$

The forces acting on the differential volume element in the vertical direction are the pressure forces acting on the top and bottom surfaces, the shear stresses acting on the side surfaces (the normal stresses acting on the top and bottom surfaces are small and are

disregarded), and the force of gravity acting on the entire volume element. Then the net surface force acting in the x-direction becomes

$$\begin{aligned}
 F_x &= \left(\frac{\partial \tau}{\partial y} dy \right) (dx \cdot 1) - \left(\frac{\partial P}{\partial x} dx \right) (dy \cdot 1) - \rho g (dx \cdot dy \cdot 1) \\
 &= \left(\mu \frac{\partial^2 u}{\partial y^2} - \frac{\partial P}{\partial x} - \rho g \right) (dx \cdot dy \cdot 1) \quad (14)
 \end{aligned}$$

since $\tau = (\partial u / \partial y)$. Substituting Eqs. 13 and 14 into Eq. 12 and dividing by $\rho \cdot dx \cdot dy \cdot 1$ gives the conservation of momentum in the x-direction as:

$$\rho \left(u \frac{\partial u}{\partial x} + v \frac{\partial u}{\partial y} \right) = \mu \frac{\partial^2 u}{\partial y^2} - \frac{\partial P}{\partial x} - \rho g \quad (15)$$

The x-momentum equation in the quiescent fluid outside the boundary layer can be obtained from the relation above as a special case by setting $u = 0$. It gives

$$\frac{\partial P_\infty}{\partial x} = -\rho_\infty g \quad (16)$$

which is simply the relation for the variation of hydrostatic pressure in a quiescent fluid with height, as expected. Also, noting that $v \ll u$ in the boundary layer and thus $\partial v / \partial x \approx \partial v / \partial y \approx 0$, and that there are no body forces (including gravity) in the y-direction, the force balance in that direction gives $\partial P / \partial y = 0$. That is, the variation of pressure in the direction normal to the surface is negligible, and for a given x the pressure in the boundary layer is equal to the pressure in the quiescent fluid. Therefore, $P = P(x) = P_\infty(x)$ and $\partial P / \partial x = \partial P_\infty / \partial x = -\rho_\infty g$.

Substituting into Eq. 15,

$$\rho \left(u \frac{\partial u}{\partial x} + v \frac{\partial u}{\partial y} \right) = \mu \frac{\partial^2 u}{\partial y^2} + (\rho_\infty - \rho)g \quad (17)$$

The last term represents the net upward force per unit volume of the fluid (the difference between the buoyant force and the fluid weight). This is the force that initiates and sustains convection currents.

From the definition of the volumetric expansion coefficient β , we have

$$(\rho_\infty - \rho) = \rho\beta (T - T_\infty) \quad (18)$$

Substituting it into the last equation and dividing both sides by ρ gives the desired form of the x-momentum equation,

$$\left(u \frac{\partial u}{\partial x} + v \frac{\partial u}{\partial y} \right) = \nu \frac{\partial^2 u}{\partial y^2} + (T - T_\infty)g\beta \quad (19)$$

This is the equation that governs the fluid motion in the boundary layer due to the effect of buoyancy. Note that the momentum equation involves the temperature, and thus the momentum and energy equations must be solved simultaneously.

The set of three partial differential equations (the continuity, momentum, and the energy equations) that govern natural convection flow over vertical isothermal plates can be reduced to a set of two ordinary nonlinear differential equations by the introduction of a similarity variable. But the resulting equations must still be solved numerically.

7.3. The Grashof Number

The governing equations of natural convection and the boundary conditions can be non-dimensionalized by dividing all dependent and independent variables by suitable constant quantities: all lengths by a characteristic length L_c , all velocities by an arbitrary reference velocity (which, from the definition of Reynolds number, is taken to be $U = Re_L v / L_c$), and temperature by a suitable temperature difference (which is taken to be $T_s - T_\infty$) as where asterisks are used to denote non-dimensional variables. Substituting them into the momentum equation and simplifying gives

$$u^* \frac{\partial u^*}{\partial x^*} + u^* \frac{\partial u^*}{\partial x^*} = \left[\frac{g\beta (T_s - T_\infty)L_c^3}{\nu^2} \right] \frac{T^*}{Re_L^2} + \frac{1}{Re_L} \frac{\partial^2 u^*}{\partial y^{*2}} \quad (20)$$

The dimensionless parameter in the brackets represents the natural convection effects, and is called the Grashof number Gr ,

$$Gr_L = \left[\frac{g\beta (T_s - T_\infty)L_c^3}{\nu^2} \right] \quad (21)$$

the flow regime in forced convection is governed by the dimensionless Reynolds number, which represents the ratio of inertial forces to viscous forces acting on the fluid. The flow regime in natural convection is governed by the dimensionless Grashof number, which represents the ratio of the buoyancy force to the viscous force acting on the fluid (Fig. 22).

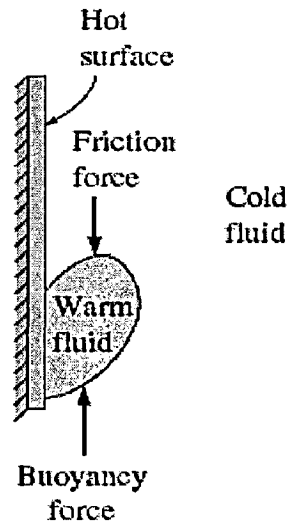


Figure 22: The Grashof number Gr is a measure of the relative magnitudes of the buoyancy force and the opposing viscous force acting on the fluid.[27]

The role played by the Reynolds number in forced convection is played by the Grashof number in natural convection. As such, the Grashof number provides the main criterion in determining whether the fluid flow is laminar or turbulent in natural convection. For vertical plates, for example, the critical Grashof number is observed to be about 10^9 . Therefore, the flow regime on a vertical plate becomes turbulent at Grashof numbers greater than 10^9 .

7.4. NATURAL CONVECTION OVER SURFACES

Natural convection heat transfer on a surface depends on the geometry of the surface as well as its orientation. It also depends on the variation of temperature on the surface and the thermophysical properties of the fluid involved.

Although we understand the mechanism of natural convection well, the complexities of fluid motion make it very difficult to obtain simple analytical relations for heat transfer by solving the governing equations of motion and energy. Some analytical solutions exist for natural convection, but such solutions lack generality since they are obtained for simple

geometries under some simplifying assumptions. Therefore, with the exception of some simple cases, heat transfer relations in natural convection are based on experimental studies.

Of the numerous such correlations of varying complexity and claimed accuracy available in the literature for any given geometry, we present here the ones that are best known and widely used. The simple empirical correlations for the average Nusselt number Nu in natural convection are of the form

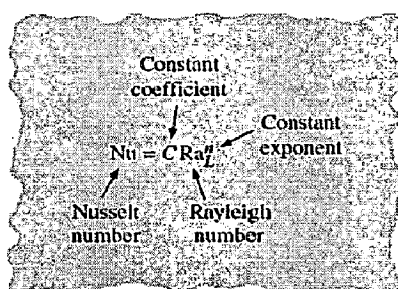


Figure 23: Natural convection heat transfer correlations are usually expressed in terms of the Rayleigh number raised to a constant n multiplied by another constant C , both of which are determined experimentally.[27]

where Ra_L is the **Rayleigh number**, which is the product of the Grashof and Prandtl numbers:

$$Ra_L = Gr_L Pr = \left[\frac{g\beta(T_s - T_\infty)L_c^3}{\nu^2} \right] Pr \quad (22)$$

The values of the constants C and n depend on the geometry of the surface and the flow regime, which is characterized by the range of the Rayleigh number. The value of n is usually $1/4$ for laminar flow and $1/3$ for turbulent flow. The value of the constant C is normally less than 1. Simple relations for the average Nusselt number for various geometries are given in Table 4, together with sketches of the geometries. Also given in this table are the characteristic lengths of the geometries and the ranges of Rayleigh number in

which the relation is applicable. All fluid properties are to be evaluated at the film temperature.

When the average Nusselt number and thus the average convection coefficient is known, the rate of heat transfer by natural convection from a solid surface at a uniform temperature T_S to the surrounding fluid is expressed by Newton's law of cooling as:

$$Q_{conv} = hA_S(T_S - T_\infty) \quad (23)$$

where A_S is the heat transfer surface area and h is the average heat transfer coefficient on the surface.

7.4.1. Vertical Plates ($T_S = \text{constant}$)

For a vertical flat plate, the characteristic length is the plate height L . In Table 4 we give three relations for the average Nusselt number for an isothermal vertical plate. The first two relations are very simple. Despite its complexity, we suggest using the third one recommended by Churchill and Chu (1975)[28] since it is applicable over the entire range of Rayleigh number. This relation is most accurate in the range of $10^{-1} < Ra_L < 10^9$.

7.4.2 Vertical Cylinders

An outer surface of a vertical cylinder can be treated as a vertical plate when the diameter of the cylinder is sufficiently large so that the curvature effects are negligible. This condition is satisfied if

$$D \geq \frac{35L}{Gr_L^{1/4}} \quad (24)$$

When this criterion is met, the relations for vertical plates can also be used for vertical cylinders. Nusselt number relations for slender cylinders that do not meet this criterion are available in the literature.

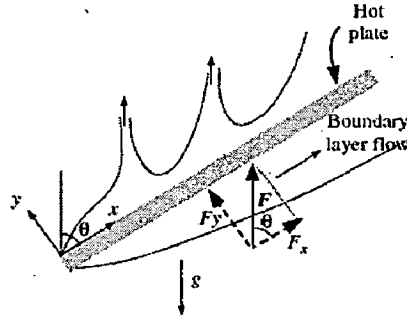


Figure 24: Natural convection flows on the upper and lower surfaces of an inclined hot plate.

7.4.3 Inclined Plates

Consider an inclined hot plate that makes an angle θ from the vertical, as shown in Figure 24, in a cooler environment. The net force $F = (\rho_{\infty} - \rho)g$ (the difference between the buoyancy and gravity) acting on a unit volume of the fluid in the boundary layer is always in the vertical direction. In the case of inclined plate, this force can be resolved into two components: $F_y = F \cos \theta$ parallel to the plate that drives the flow along the plate, and $F_x = F \sin \theta$ normal to the plate. Noting that the force that drives the motion is reduced, we expect the convection currents to be weaker, and the rate of heat transfer to be lower relative to the vertical plate case.

The experiments confirm what we suspect for the lower surface of a hot plate, but the opposite is observed on the upper surface. The reason for this curious behavior for the upper surface is that the force component F_y initiates upward motion in addition to the parallel motion along the plate, and thus the boundary layer breaks up and forms plumes, as shown in the figure. As a result, the thickness of the boundary layer and thus the resistance to heat transfer decreases, and the rate of heat transfer increases relative to the vertical orientation.

In the case of a cold plate in a warmer environment, the opposite occurs as expected: The boundary layer on the upper surface remains intact with weaker boundary layer flow and thus lower rate of heat transfer, and the boundary layer on the lower surface breaks apart (the colder fluid falls down) and thus enhances heat transfer.

When the boundary layer remains intact (the lower surface of a hot plate or the upper surface of a cold plate), the Nusselt number can be determined from the vertical plate relations provided that g in the Rayleigh number relation is replaced by $g \cos \theta$ for $\theta < 60^\circ$. Nusselt number relations for the other two surfaces (the upper surface of a hot plate or the lower surface of a cold plate) are available in the literature [e.g., Fujii and Imura (1972)[29]].

7.4.4. Horizontal Plates

The rate of heat transfer to or from a horizontal surface depends on whether the surface is facing upward or downward. For a hot surface in a cooler environment, the net force acts upward, forcing the heated fluid to rise. If the hot surface is facing upward, the heated fluid rises freely, inducing strong natural convection currents and thus effective heat transfer, as shown in Figure 25. But if the hot surface is facing downward, the plate will block the heated fluid that tends to rise (except near the edges), impeding heat transfer. The opposite is true for a cold plate in a warmer environment since the net force (weight minus buoyancy force) in this case acts downward, and the cooled fluid near the plate tends to descend.

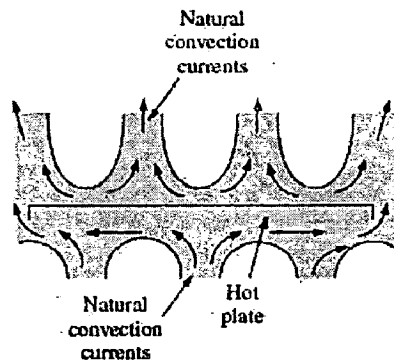


Figure 25: Natural convection flows on the upper and lower surfaces of a hot horizontal plate.[27]

7.4.5 Horizontal Cylinders and Spheres

The boundary layer over a hot horizontal cylinder starts to develop at the bottom, increasing in thickness along the circumference, and forming a rising plume at the top, as shown in Figure 26. Therefore, the local Nusselt number is highest at the bottom and lowest at the top of the cylinder when the boundary layer flow remains laminar. The opposite is true in the case of a cold horizontal cylinder in a warmer medium, and the boundary layer in this case starts to develop at the top of the cylinder and ending with a descending plume at the bottom.

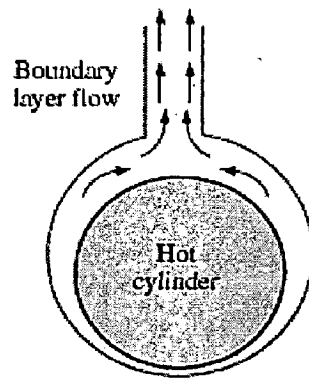


Figure 26: Natural convection flow over a horizontal hot cylinder.[27]

7.5. NATURAL CONVECTION INSIDE ENCLOSURES

A considerable portion of heat loss from a typical residence occurs through the windows. We certainly would insulate the windows, if we could, in order to conserve energy. The problem is finding an insulating material that is transparent. An examination of the thermal conductivities of the insulating materials reveals that *air is a better insulator* than most common insulating materials. Besides, it is transparent. Therefore, it makes sense to insulate the windows with a layer of air. Of course, we need to use another sheet of glass to trap the air. The result is an *enclosure*, which is known as a *double-pane window* in this case. Other examples of enclosures include wall cavities, solar collectors, and cryogenic chambers involving concentric cylinders or spheres. Enclosures are frequently encountered in practice, and heat transfer through them is of practical interest. Heat transfer in enclosed spaces is complicated by the fact that the fluid in the enclosure, in general, does not remain stationary. In a vertical enclosure, the fluid adjacent to the hotter surface rises and the fluid adjacent to the cooler one falls, setting off a rotary motion within the enclosure that enhances heat transfer through the enclosure. Typical flow patterns in vertical and horizontal rectangular enclosures are shown in Figures 27 and 28.

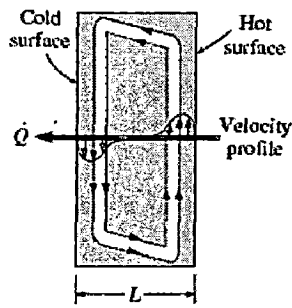


Figure 27: Convective currents in a vertical rectangular enclosure.[27]

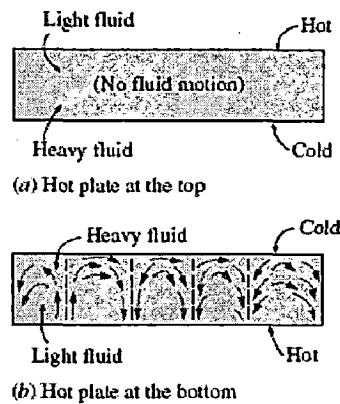


Figure 28: Convective currents in a horizontal enclosure with (a) hot plate at the top and (b) hot plate at the bottom.[27]

The characteristics of heat transfer through a horizontal enclosure depend on whether the hotter plate is at the top or at the bottom, as shown in Figure 28. When the hotter plate is at the *top*, no convection currents will develop in the enclosure, since the lighter fluid will always be on top of the heavier fluid. Heat transfer in this case will be by *pure conduction*, and we will have $Nu = 1$. When the hotter plate is at the *bottom*, the heavier fluid will be on top of the lighter fluid, and there will be a tendency for the lighter fluid to topple the heavier fluid and rise to the top, where it will come in contact with the cooler plate and

cool down. Until that happens, however, the heat transfer is still by *pure conduction* and $Nu = 1$. When $Ra > 1708$, the buoyant force overcomes the fluid resistance and initiates natural convection currents, which are observed to be in the form of hexagonal cells called *Bénard cells*. For $Ra > 3 \cdot 10^5$, the cells break down and the fluid motion becomes turbulent.

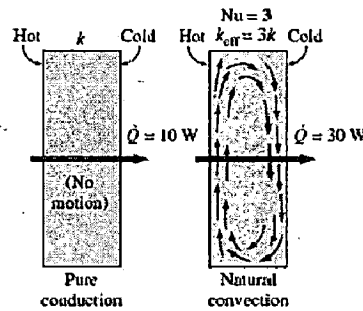


Figure 29: A Nusselt number of 3 for an enclosure indicate that heat transfer through the enclosure by natural convection is three times that by pure conduction [27]

7.5.1. Horizontal Rectangular Enclosures

We need no Nusselt number relations for the case of the hotter plate being at the top, since there will be no convection currents in this case and heat transfer will be downward by conduction ($Nu = 1$). When the hotter plate is at the bottom, however, significant convection currents set in for $Ra_L > 1708$, and the rate of heat transfer increases (Fig. 30). For horizontal enclosures that contain air, Jakob (1949)[30] recommends the following simple correlations

$$Nu = 0.195Ra_L^{\frac{1}{4}} \quad 10^4 < Ra_L < 4 \cdot 10^5 \quad (25)$$

$$Nu = 0.068Ra_L^{\frac{1}{3}} \quad 4 \cdot 10^5 < Ra_L < 10^7 \quad (26)$$

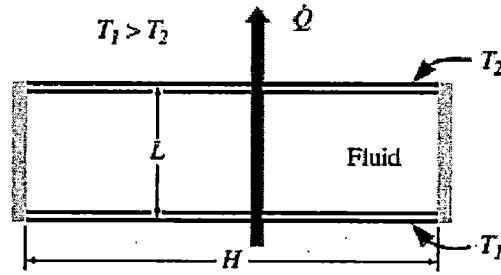


Figure 30: A horizontal rectangular enclosure with isothermal surfaces.

These relations can also be used for other gases with $0.5 < Pr < 2$. Using water, silicone oil, and mercury in their experiments, Globe and Dropkin (1959) obtained this correlation for horizontal enclosures heated from below,

$$Nu = 0.069 Ra_L^{\frac{1}{3}} Pr^{0.074} \quad 3 * 10^5 < Ra_L < 7 * 10^9 \quad (27)$$

Based on experiments with air, Hollands et al (1976)[31] recommend this correlation for horizontal enclosures,

$$Nu = 1 + 1.44 \left[1 - \frac{1708}{Ra_L} \right] + \left[\frac{Ra_L^{\frac{1}{3}}}{18} - 1 \right] \quad Ra_L < 10^8 \quad (28)$$

7.5.2. Inclined Rectangular Enclosures

Air spaces between two inclined parallel plates are commonly encountered in flat-plate solar collectors (between the glass cover and the absorber plate) and the double-pane skylights on inclined roofs. Heat transfer through an inclined enclosure depends on the **aspect ratio** H/L as well as the tilt angle from the horizontal (Fig. 31). For large aspect ratios ($H/L \geq 12$), this equation [Hollands et al., (1976)[31]] correlates experimental data extremely well for tilt angles up to 70° ,

$$Nu = 1 + 1.44 \left[1 - \frac{1708}{Ra_L \cos \theta} \right] \left(1 - \frac{1708(\sin 1.8\theta)^{1.6}}{Ra_L \cos \theta} \right) + \left[\frac{Ra_L^{1/3}}{18} - 1 \right] \quad (29)$$

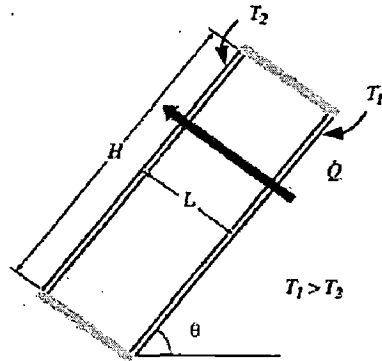


Figure 31: An inclined rectangular enclosure with isothermal surfaces.

7.5.3. Vertical Rectangular Enclosures

For vertical enclosures (Fig. 32), Catton (1978)[32] recommends these two correlations due to Berkovsky and Polevikov (1977)[33],

$$Nu = 0.18 \left(\frac{Pr}{0.2+Pr} Ra_L \right)^{0.29} \quad 1 < \frac{H}{L} < 2 \text{ any Prandtl number } Pr \frac{Ra_L Pr}{0.2+Pr} > 10^3 \quad (30)$$

$$Nu = 0.22 \left(\frac{Pr}{0.2+Pr} Ra_L \right)^{0.28} (H/L)^{-1/4} \quad 2 < \frac{H}{L} < 10 \text{ any Prandtl number } Ra_L < 10^{10} \quad (31)$$

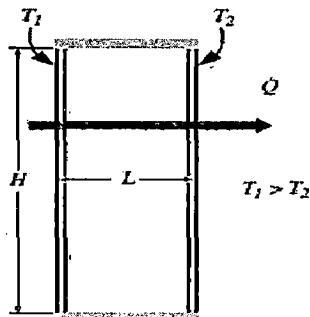


Figure 32: A vertical rectangular enclosure with isothermal surfaces.

Chapter 8. Literature Review on Natural Convection in Enclosures

A lot of articles have dealt with the natural convection problems in the rectangular or square enclosures subjected to a temperature difference in the past. Wroblewski & Joshi [34] numerically studied the laminar heat transfer and flow field arising from a heated protruding element mounted on one vertical wall of an enclosure. Heindel et al. [35, 36] theoretically and experimentally investigated the natural convection in a rectangular cavity induced by 3×3 array of discrete, flush-mounted heat sources. They found that the difference between two- and three-dimensional predictions is within 5% as the aspect ratio of heat source is greater than 3. For a liquid-filled square cavity embedded in a substrate, Sathe & Joshi [37] studied the characteristics of heat removal from a protruding heat source. Anderson & Bohn [38] presented the results of an experimental investigation of the influences of surface roughness on natural convection in a cubical enclosure. They obtained a maximum 15% increase in overall Nusselt number. Amin [39] examined the natural convection heat transfer in a two-dimensional vertical enclosure fitted with a periodic array of large rectangular elements on the bottom adiabatic wall. As compared with the results of smooth-wall enclosure, the roughness elements significantly reduce the heat transfer rate across the enclosure. In a later study, Amin [40] stated that if this enclosure with a periodic array of roughness elements is heated from the bottom wall, the heat transfer rate can be greatly enhanced.

In spite of its importance in many practical applications, natural convection in enclosures with a backward step received much less attention than that in open channels. Lin et al. [8] and Abumulaweh et al. [41] reported measurements and predictions of mixed convection characteristics for open channels with a backward-facing step. In addition, the effects of a backward-facing step on natural convection in open channels were investigated by AbuMulaweh et al. [42, 43]. Their results reveal that the step height can significantly affect the thermal and hydrodynamic behaviors.

The lack of information on the natural convective heat transfer in enclosures with a backward step motivates the present work. In this study, a numerical analysis is performed to examine the effects of a heated backward step on natural convection in enclosures. Great attention is given to

examine the difference in heat transfer characteristics of enclosures with and without the presence of a backward step.

Steady state convection heat transfer from a rotating cylinder to its surrounding enclosure is a subject of practical importance. This type of thermally driven flow is encountered in numerous applications especially in some building service situations, when a pipe carrying a hot water passes through an enclosure formed by structural components of the building, rotating-tube heat exchangers, and the drilling of oil wells. The function of the outer surface of the enclosure is to reduce the heat transfer from the inner rotating hot cylinder or to save the inner body in harsh outdoor environment. In recent years, the flow around a rotating circular cylinder is considered a fundamental fluid mechanics problem of great interest. It has potential relevance to a huge number of practical applications such as submarines, off shore structures, pipelines etc. Several numerical and experimental methods have been developed to investigate enclosures with and without rotating or stationary obstacle because these geometries have great practical engineering applications.

Chang et al. [44] made a numerical analysis for natural convective heat transfer in an irregular two-dimensional enclosure formed by an inner square cylinder and an outer circular envelope. They also performed an experimental investigation to verify some of the numerical results. Fu et al. [45] studied numerically natural convection of an enclosure by a rotating circular cylinder near a hot wall using a finite element method. They showed that the rotating cylinder direction had an important effect in enhancing natural convection heat transfer in the enclosure. Ha et al. [46, 47] considered the problem of natural convection in a square enclosure with isothermal top and bottom boundaries and adiabatic side walls. A square cylinder was placed at the center of the enclosure and different boundary conditions were considered for this internal cylinder. A wide range of Rayleigh numbers was considered extending from the steady regime to that of highly chaotic turbulence. The effect of the internal square body and its thermal boundary condition on the nature of convection and overall heat transfer was investigated.

Roychowdhury et al. [48], used a collected, non-orthogonal grid based on finite volume technique to investigate the two-dimensional natural convective flow and heat transfer around a heated cylinder kept in a square enclosure. The effects of different enclosure wall thermal boundary conditions, fluid Prandtl number and the ratio between enclosure and cylinder

dimensions were also studied. It was observed that the patterns of recirculatory flow and thermal stratification in the fluid are significantly modified, if any of the considered parameters are varied. De & Dalal [49], studied numerically natural convection around a tilted heated square cylinder kept in an enclosure in the range of $10^3 \leq Ra \leq 10^6$. Stream function–vorticity formulation of the Navier–Stokes equations was solved numerically using finite-difference method. It was found that the uniform wall temperature heating was quantitatively different from the uniform wall heat flux heating. Flow pattern and thermal stratification were modified, if aspect ratio was varied. Also, it was found that the overall heat transfer also changed for different aspect ratios. Angeli, et al. [50], investigated numerically buoyancy-induced flow regimes of a horizontal cylinder centered into along co-axial square-sectioned cavity. Substantial differences were observed in the flow and thermal fields, depending on the aspect ratio and the Rayleigh number, in the regions of either asymptotically steady or time-dependent flows. A correlating equation for the average Nusselt number on the cylinder, as a function on both the Rayleigh number and the diameter-to-side ratio was derived which covering the whole steady-state region. Hwang et al. [51], studied the flow field around an infinitely long circular cylinder rotating in fluid with no outer boundary.

The governing equations were discretized by using a finite-volume method on a cylindrical grid system. Wall pressure fluctuations are found to be of much larger spatial extent than velocity fluctuation scales. Rahman et al. [52], performed a numerical investigation of laminar mixed convection in a square cavity with a heat conducting horizontal square cylinder to investigate the effect of the locations of the conducting cylinder on the fluid flow and heat transfer in the square cavity for different Richardson numbers in the range of $0 \leq Ri \leq 5$. The results indicated that, the cylinder locations had a significant effect on the flow and thermal fields and the value of average Nusselt number was the highest in the forced convection dominated area when the cylinder was located near the top wall along the mid-vertical plane and in the free convection dominated area when the cylinder moved closure to the left vertical wall along the mid-horizontal plane. Ghazanfarian & Nobari [53] presented a numerical investigation of convective heat transfer from a rotating cylinder with cross-flow oscillation. A finite element analysis using Characteristic Based Split method (CBS) was developed to solve governing equations. It was found that similar to the fixed cylinder, beyond a critical rotating speed, vortex shedding was mainly suppressed. Also by increasing the non-dimensional rotational speed of the cylinder, both the Nusselt number

and the drag coefficient decreased rapidly. Shih et al. [54], investigated numerically the periodic state of fluid flow and heat transfer due to isothermal or adiabatic rotating cylinder enclosed in a square cavity. By comparing the time averaged Nusselt numbers of the system for both adiabatic and isothermal objects, it was concluded that for high Reynolds number cases, heat transfer was independent of the shape of the object. Yoon et al. [55], presented a numerical investigation of the characteristics of the two-dimensional laminar flow around two rotating circular cylinders in side-by-side arrangements. Numerical simulations are performed for various ranges of absolute rotational speeds at Reynolds number of 100.

Quantitative information about the flow variables such as the pressure coefficient and wall vorticity distributions on the cylinders was highlighted. Paramane & Sharma [56], analyzed convection heat transfer across a circular cylinder rotating with a constant non dimensional rotation rate varying from 0 to 6 for Reynolds numbers of 20–160 and a Prandtl number of 0.7. They concluded that, the average Nusselt number decreased with increasing rotation rate and increased with increasing Reynolds number. It was also found that, the heat transfer suppression due to rotation increased with increasing Reynolds number and rotation rate. Oztop et al. [57], studied mixed convection heat transfer characteristics for a lid-driven air flow within a square enclosure having a circular body. The cavity was differentially heated and the left wall was maintained at a higher temperature than the right wall. Three different temperature boundary conditions were applied for the inner cylinder as adiabatic, isothermal or conductive. The computation was carried out for wide ranges of Richardson numbers, diameter of inner cylinder and center and location of the inner cylinder. It was found that, the thermal conductivity became insignificant for small values of diameter of the circular body and the circular body can be used as a control parameter for heat and fluid flow. Rahman et al. [52], studied numerically combined free and forced convection in a two dimensional rectangular cavity with a uniform heat source applied on the right vertical wall. A circular heat conducting horizontal cylinder was placed somewhere within the cavity. The results indicated that both the heat transfer rate from the heated wall and the dimensionless temperature in the cavity strongly depended on the governing parameters and configurations of the system studied, such as size, location, thermal conductivity of the cylinder and the location of the inflow and outflow opening. Yoon et al. [58], carried out a numerical calculations for the natural convection induced by temperature difference between a cold outer square enclosure and a hot inner circular cylinder for Rayleigh number of $Ra=10^7$.

Their study investigated the effect of the inner cylinder location on the heat transfer and fluid flow. They concluded that, at the unsteady region, the natural convection showed a single frequency and multiple frequency periodic patterns alternately according to the location of inner circular cylinder. Costa & Raimundo [59], studied mixed convection in a differentially heated square enclosure with a rotating cylinder inside it. The flow structure, the temperature field and the heat transfer process were analyzed using the dimensionless stream function, temperature and heat function. It was observed that the size of the cylinder had a strong influence on the resulting flow and heat transfer process, as it limited the space for fluid flow between the cylinder and the enclosure walls. They concluded that, for high values of the cylinder radius, the overall Nusselt number was small if the rotating velocity was low. Mohammed & Salman [60] studied experimentally laminar combined natural and forced convection heat transfer in a uniformly heated vertical circular cylinder for assisting flow with different entrance sections length under constant wall heat input.

The results clearly showed that the surface temperature values decreased as the cylinder inclination angle moved from $\theta=90^\circ$ (vertical cylinder) to $\theta=0^\circ$ (horizontal cylinder). Laskowski et al. [61] studied both experimentally and numerically heat transfer to and from a circular cylinder in a cross-flow of water at low Reynolds number. The cylinder was placed near the lower surface of a water channel. The results explained that the predicted spatially averaged Nusselt number was from 37% to 53% larger than the measured spatially averaged Nusselt number.

The air flow profiles and the cylinder wall temperatures issued from numerical calculations are analyzed and the results are compared with the experimental ones. Recently, Hussain & Hussein [62] investigated numerically the laminar steady natural convection where a uniform heat source applied on the inner circular cylinder enclosed in a square enclosure in which all boundaries are assumed to be isothermal. They concluded that with increasing Rayleigh number, the average and local Nusselt number values increased with different upward and downward locations of the inner cylinder, due to the significant influence of thermal convection.

Natural convection in differentially heated enclosures has been extensively studied, mainly following the numerical way. The problem can be enriched by adding a rotating cylinder, arbitrarily placed inside the enclosure, thus giving rise to a mixed convection problem. The

resulting flow is due both to the natural convection component, associated to buoyancy and to the differentially heated vertical walls of the enclosure, and to the forced convection associated to the cylinder rotation. This can rotate in the direction corresponding to combined or opposite natural and forced convection, thus resulting on the intensification or on the attenuation of the convective flow, and of the corresponding overall thermal performance of the enclosure, respectively. This can be the model for real situations where a rotating shaft can be used to control the natural convection taking place on an enclosure, and thus to control the overall thermal performance of the enclosure, in order to increase or to reduce its effect.

Some studies can be found in the literature concerning the convection inside an enclosure that includes a cylinder, rotating or not, and in the presence of pure forced convection, mixed convection or pure natural convection. In the work of Hayase et al. [63] it is analyzed the forced convection heat transfer between rotating coaxial cylinders with periodically embedded cavities, a problem mainly related with heat transfer inside electric machinery. The transient performance of a circular rotating cylinder placed eccentrically inside a micro-channel with a forced flow has been considered by Phutthavong & Hassan [64]. Mixed convection corresponding to a rotating circular cylinder inside a square or rectangular enclosure has been numerically studied by Fu et al. [45], Ghaddar & Thiele [65], and Ghaddar [66].

The laminar convection flow around a heated horizontal square cylinder rotating slowly within a concentric circular enclosure has been numerically examined by Yang & Farouk [67]. Natural convection situation, with a stationary non-rotating heated circular cylinder inside a cold square enclosure, can be found in the works by Shu et al. [68], Shu & Zhu [69], Peng et al. [70], Ding et al. [71], and Moukalled & Acharya [72], where emphasis is mainly placed on the used numerical method.

The study of the natural convection around a steadily rotating cylinder, subjected to periodic distribution of temperature was presented by Hasan & Sanghi [73], and some studies can be founded dealing with natural convection in rotating annuli, some of them giving emphasis to the possible multiple solutions of this kind of problems. Natural convection in cylinders immersed in porous media has been the subject of some works, mentioning only a few, but considering the cylinders without rotation.

However, so far there is no study related to transfer characteristic of the flow and thermal fields past a rotating circular cylinder with combined convection heat transfer in a heated backward facing enclosure. This problem is particularly important as an industrial problem and has several applications in rotating crucibles and also furnaces. This is the main concern of the present paper. Here, a numerical scheme is constructed using a finite volume approach to deal with a laminar steady natural convection problem in a two dimensional backward facing enclosure which contains a rotating circular cylinder enclosed inside it. The numerical calculations are performed for wide ranges of Rayleigh numbers, the fluid Prandtl numbers and inner rotating circular cylinder angular speed (α).

Chapter 9. Problem Statement, Governing Equations and Boundary Conditions

The physical system under consideration, as shown schematically in Fig. 33, is a two-dimensional enclosure with a heated backward step located at the left corner. The backward step is kept at a higher, uniform and constant temperature T_H . In the meanwhile, the right wall of the enclosure is at a lower temperature T_L . Besides, the other walls of the enclosure are thermally insulated. Circulating flow in the enclosure is induced by the buoyant force resulting from the given temperature difference between the heated backward step and the cooled plate. In this study, the natural convection flows of Newtonian fluid in enclosures of interest are considered to be steady-state, two-dimensional and laminar. To simplify the analysis, the Boussinesq approximation is employed to account for the thermal buoyancy effects. According to the stated assumptions, the basic equations in dimensionless form are as follows:

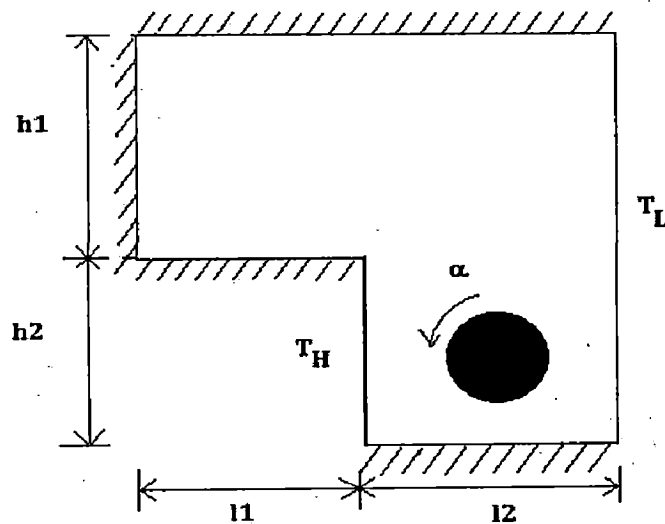


Fig. 33. Schematic diagram of physical system.

Continuity equation:

$$\frac{\partial U}{\partial X} + \frac{\partial V}{\partial Y} = 0 \quad (32)$$

X – momentum

$$\frac{\partial U}{\partial t} + \frac{\partial UV}{\partial X} + \frac{\partial VU}{\partial Y} = -\frac{\partial P}{\partial X} + Pr \left(\frac{\partial^2 U}{\partial X^2} + \frac{\partial^2 U}{\partial Y^2} \right) \quad (33)$$

Y – momentum

$$\frac{\partial V}{\partial t} + \frac{\partial UV}{\partial X} + \frac{\partial VV}{\partial Y} = -\frac{\partial P}{\partial Y} + Pr \left(\frac{\partial^2 V}{\partial X^2} + \frac{\partial^2 V}{\partial Y^2} \right) + RaPr\theta \quad (34)$$

Energy equation

$$\frac{\partial \theta}{\partial t} + \frac{\partial (U\theta)}{\partial X} + \frac{\partial (V\theta)}{\partial Y} = Pr \left(\frac{\partial^2 \theta}{\partial X^2} + \frac{\partial^2 \theta}{\partial Y^2} \right) \quad (35)$$

The corresponding boundary conditions are $\theta=0$ and 1 for the cold and hot plates, respectively. The normal temperature gradients are zero for all the other surfaces. In addition, no-slip condition is applied to all solid walls.

The local and average Nusselt numbers for the heated backward step are of interest to the thermal system design. These are defined as :

$$Nu = \frac{hh_1}{k} = \frac{h_1(-\partial T / \partial x)_{x=L_1}}{T_H - T_L} = - \left(\frac{\partial \theta}{\partial X} \right)_{X=L_1} \quad (36)$$

and

$$\overline{Nu} = \int_0^1 Nu dY. \quad (37)$$

Chapter 10. Numerical Methodology

Figs. 34 - 37 presents the computational grid structure adopted for solving the case of unobstructed backward facing flow problem (i.e., without cylinder). The grid is generated by using ANSYS FLUENT and shows the uniform orthogonal grid structure for the whole of the computational domain.

A total of 4 grids were adopted to carry out the simulations of Natural convection heat transfer in this geometry. Rayleigh Number was kept constant at 10^3 . A thorough analysis of the sensitivity of the simulation results with regard to the number of elements, mesh size and grid fineness for each case is carried out using 3 different grids of varying fineness. After the sensitivity analysis a computational grid consisting of 1,36,000 cells with the minimum grid spacing in the vicinity of the wall being $0.003S$ and the maximum grid spacing being $0.01S$ is found to be sufficiently fine to resolve the flow and heat transfer phenomena in the unobstructed backward-facing step case and is used in all subsequent calculations.

Similarly, the grid structure adopted for simulating the case of the adiabatic circular cylinder in the backward-facing step domain is shown in Figs.35 - 37.

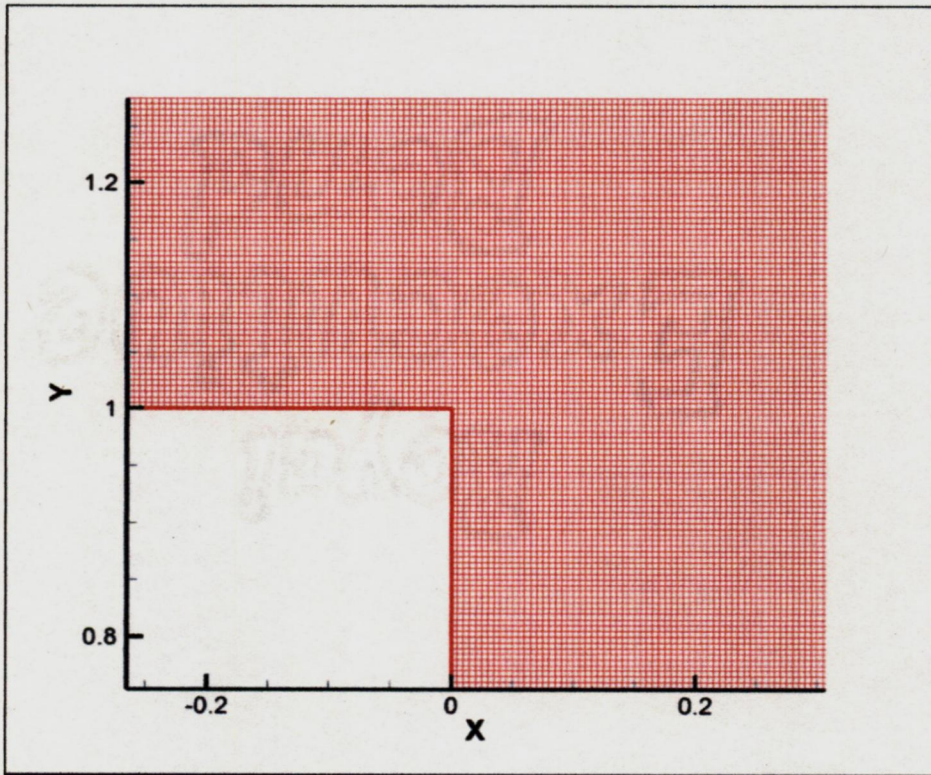


Fig. 34 .GRID 1

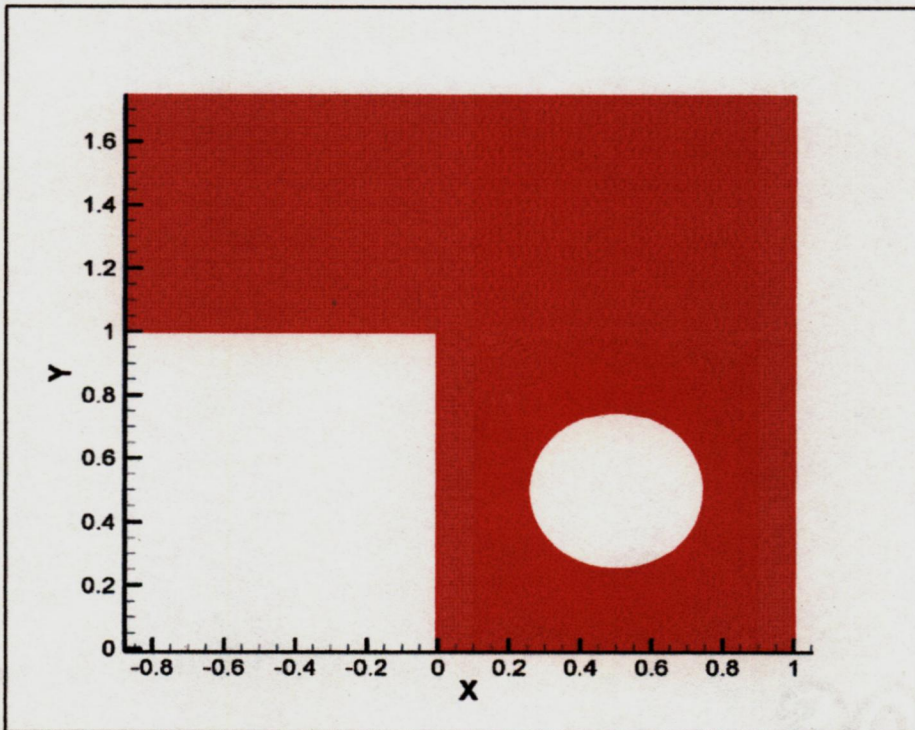


Fig. 35.GRID 2

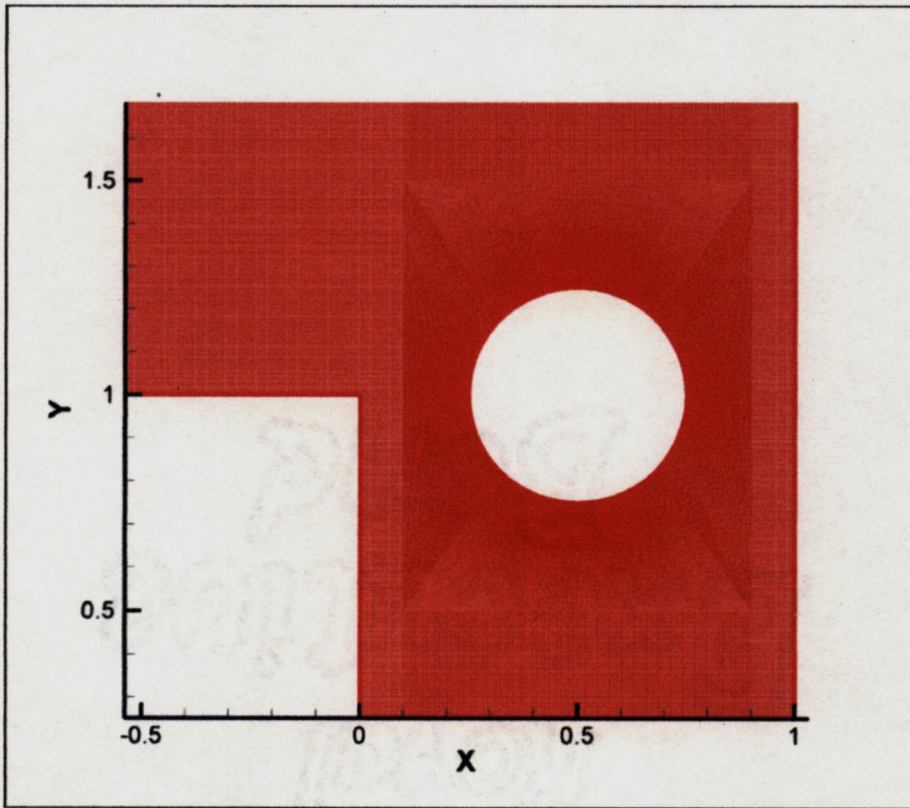


Fig. 36.GRID 3

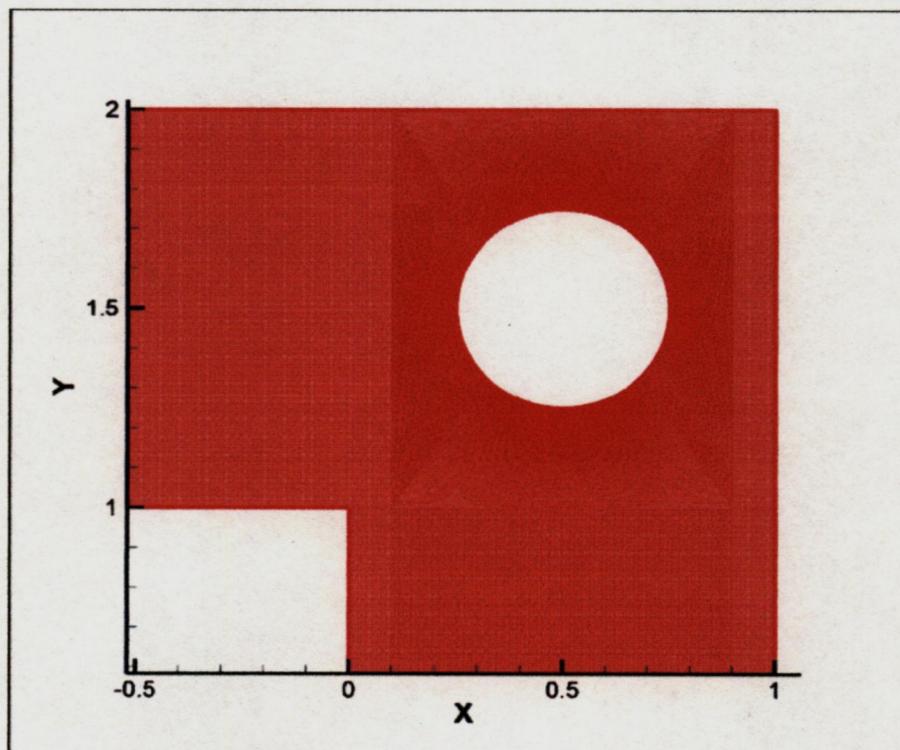


Fig. 37.GRID 4

This numerical study has been carried out using ANSYS FLUENT. The two-dimensional laminar, segregated solver is used to solve the incompressible flow on the collocated grid arrangement. The 'Boussinesq density' and 'Newtonian' viscosity models are used. The QUICK scheme has been used to discretize the convective terms in the momentum and thermal energy equations. The semi-implicit method for the pressure linked equations (SIMPLE) scheme is used for solving the pressure-velocity decoupling. FLUENT solves the system of algebraic equations using the Gauss–Siedel (G–S) point-by-point iterative method in conjunction with the algebraic multi-grid (AMG) method solver. The use of AMG scheme can greatly reduce the number of iterations (and thus, CPU time) required to obtain a converged solution, particularly when the model contains a large number of control volumes. The relative convergence criteria of 10^{-10} for the continuity and x- and y-components of the velocity and 10^{-20} for temperature is prescribed in this work.

In order to carry out a detailed study of the effect of the circular cylinder on heat transfer in this domain a preliminary study into the effect of the cylinder position and its influence on heat transfer was carried out. Figure 38 shows the streamline patterns generated in the geometry on account of natural convection for various cylinder positions and Fig. 39 is a representation of the isotherm patterns for the same. As can be clearly noted from the figure that the position of the cylinder when it lies at the bottom position just next to the heated step is the case when the isotherm lines get distorted the most. Hence this was the place that was chosen for further experimentation and studies in this work.

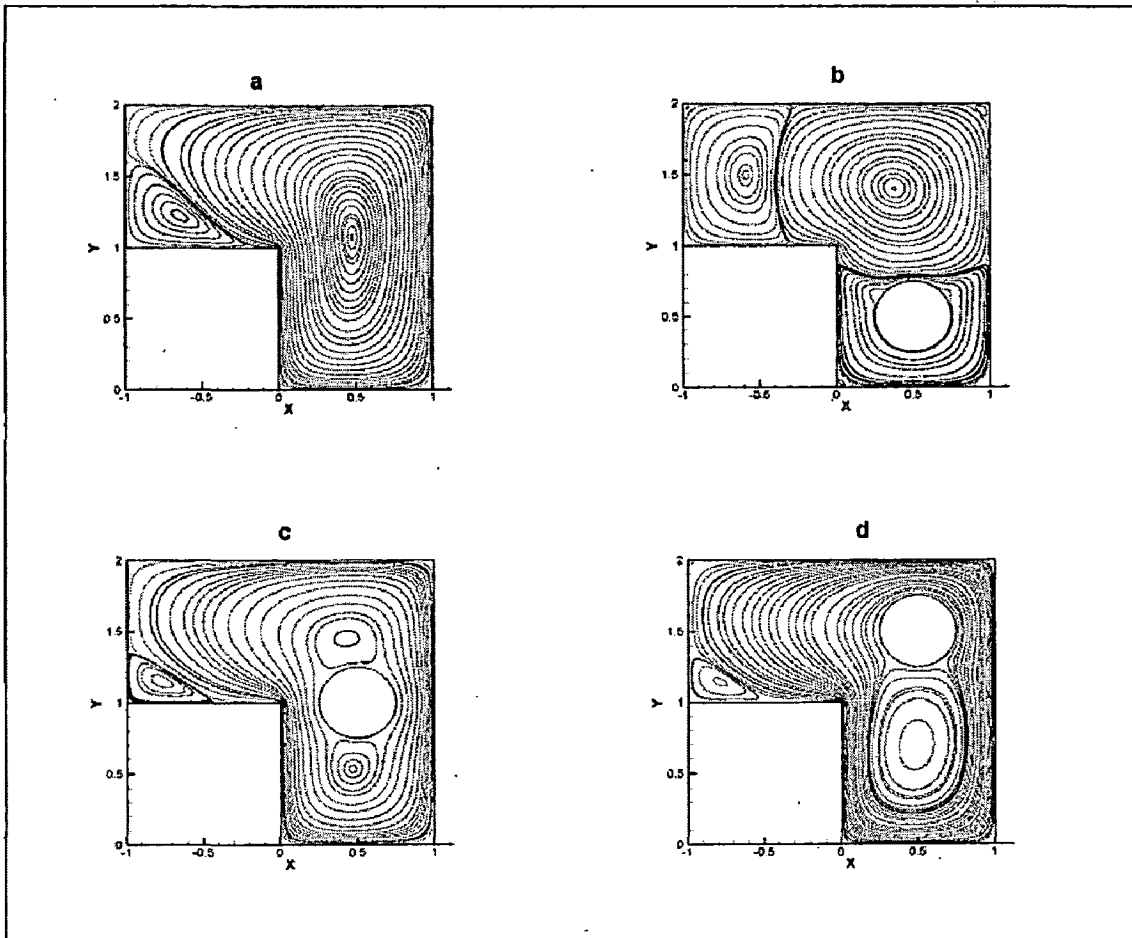


Fig. 38. Streamline patterns for different positions of the adiabatic circular cylinder.

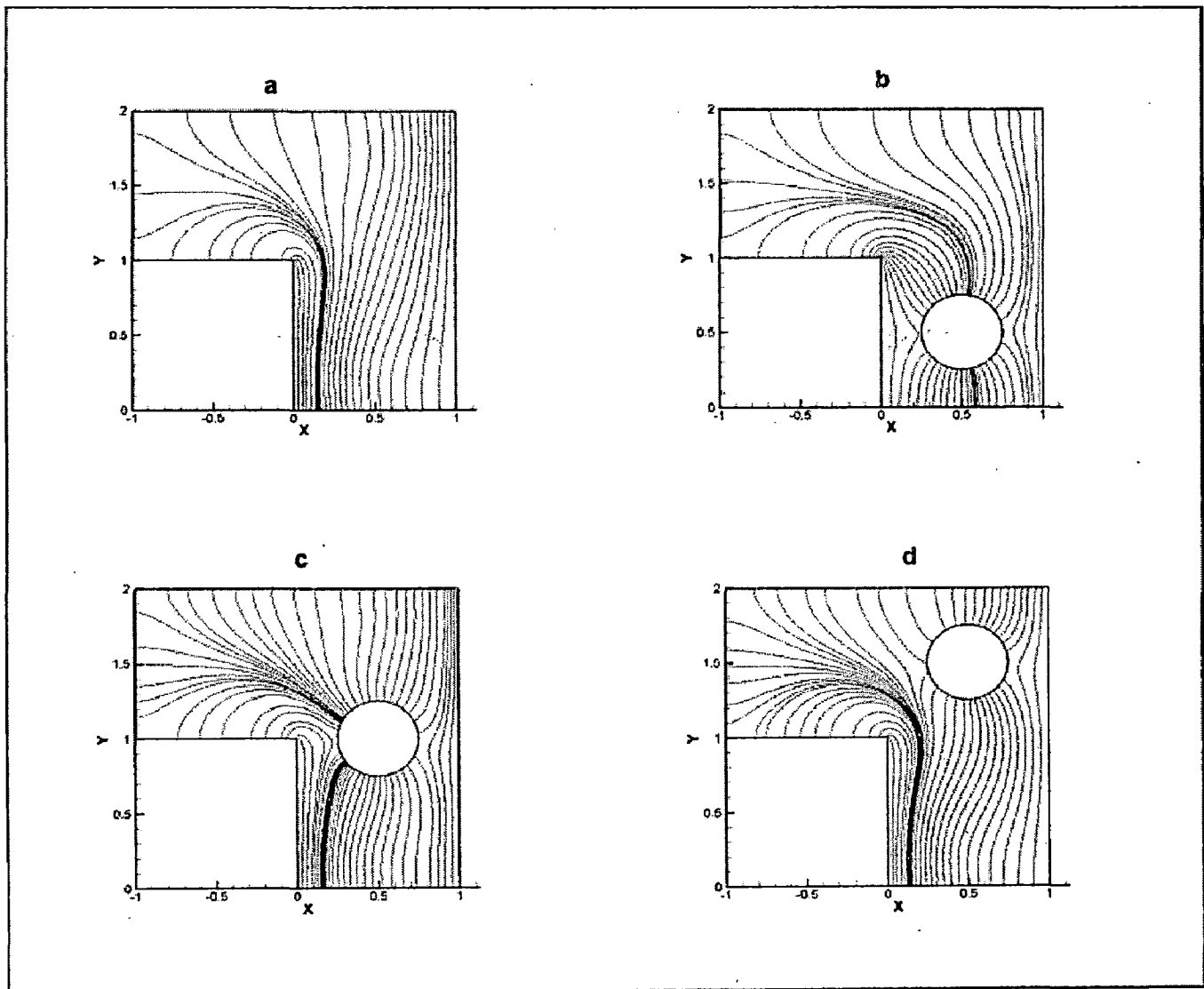


Fig. 39. Isotherm patterns for different positions of the adiabatic circular cylinder.

Inspection of the foregoing analysis discloses that the characteristics of natural convection in an enclosure induced by a heated backward step depends on six governing parameters. These are the Rayleigh number Ra , the Prandtl number Pr , the dimensionless height of the insulated vertical wall H_2 , the dimensionless distance between the insulated vertical wall and heated backward step L_1 , the dimensionless distance between heated backward step and cooled wall L_2 and the angular speed of the circular cylinder α . In the following, we present the results for:

$Pr = 1, 10, 50$

$\alpha = 0, 1, 2, 4$

$Ra = 10^3, 10^4, 10^5$

The effects of these parameters on the flow structure and thermal behavior are investigated in detail. Additionally, the differences in the results for the enclosures with or without circular cylinder will be presented.

11.1. Validation of Results

The numerical code employed for the present study was rigorously verified. First, a computation experiment was carried out to ensure that the solution is grid-independent. For a typical case with $Ra=10^3$, $Pr= 1$, and $L_1=L_2=H_2=1$, it is found that the differences in velocity, temperature and average Nusselt number for 80×80 and 110×110 grids are always less than 1.2%. To further check the adequacy of the numerical scheme, results for a limiting case of natural convection in a square enclosure were obtained. Excellent agreement was found between the present predicted results and those of de Vahl Davis [74], as shown in Table 1.

Table 4. Comparison of predicted Nusselt numbers with those of de Vahl Davis [74] under various Rayleigh numbers

| Ra | de Vahl Davis [74] | Present study |
|--------|--------------------|---------------|
| 10^3 | 1.117 | 1.116 |
| 10^4 | 2.238 | 2.244 |
| 10^5 | 4.509 | 4.515 |
| 10^6 | 8.817 | 8.803 |

11.2. Flow and Thermal Patterns

The isotherms and streamlines for various cases with $Ra=10^3 - 10^5$ and $H_2=L_1=L_2=1$ are illustrated in Figs. 40 - 43. As can be seen in Fig. 41 - 43, the isotherms horizontally distribute from the left plate to the cold plate and are parallel to each other in the bottom region. This indicates that the conduction plays the dominant role for heat transfer process. However, the isotherms are gradually distorted toward left with increasing Y . The phenomena are particularly evident in the region above backward step. Accordingly, the existence of a backward step can significantly affect the heat transfer characteristics. The streamlines plotted in Fig. 40 reveal that only a large recirculation cell is formed and slightly expands into the upper space of the backward step. This is due to the fact that the induced flow is rather weak under such a low Rayleigh number ($Ra=10^3$). On further increasing Ra , it is expected that the buoyancy-induced flow becomes stronger and the convective heat transfer becomes more important. Thermal stratification takes place in the most area between the heated and cooled plates. In addition, a rather large portion of the space above the backward step remains nearly isothermal. Further with the introduction of rotation of the circular cylinder in the domain the streamlines and corresponding isotherms get distorted so as to produce numerous characteristic features in the domain. This involves the break-up of the recirculation region into separate recirculation regions. More specifically at an angular speed of 1 rads^{-1} there seems to be a total break-up of the recirculation into three distinct zones as can be noted from Fig. 40. Further increasing the angular speed to 4 rads^{-1} results in the generation of 4 separate zones as can be again noted from the figure. An increase in the Prandtl number results in an increase in the compression of the thermal boundary layers adjacent to the heated backward facing plate thereby increasing the Nusselt values calculated at it.

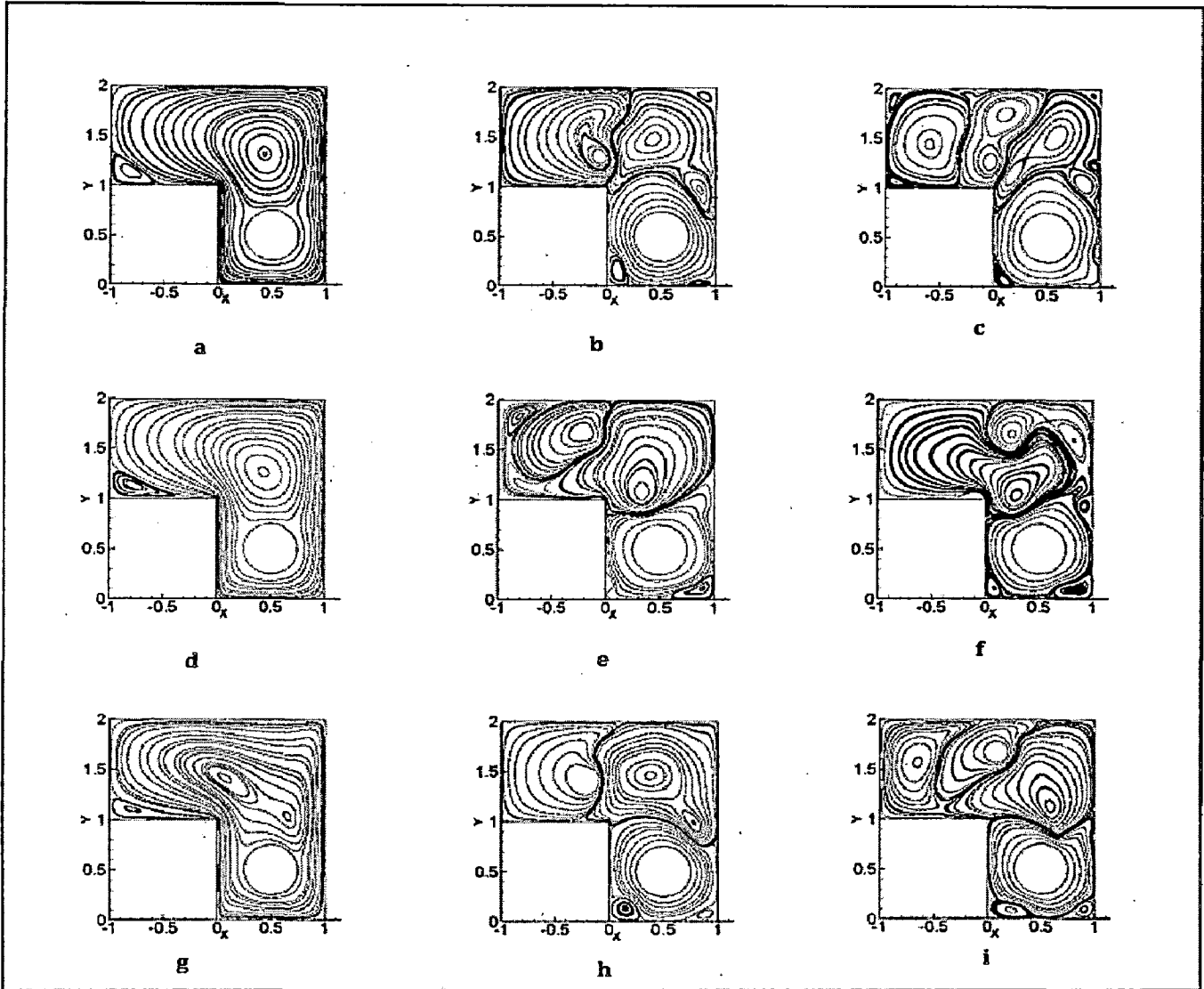


Fig. 40. Streamlines for a) $Ra = 10^3, \alpha = 0$ b) $Ra = 10^3, \alpha = 1$ c) $Ra = 10^3, \alpha = 4$ d) $Ra = 10^4, \alpha = 0$ e) $Ra = 10^4, \alpha = 1$ f) $Ra = 10^4, \alpha = 4$ g) $Ra = 10^5, \alpha = 0$ h) $Ra = 10^5, \alpha = 1$ i) $Ra = 10^5, \alpha = 4$

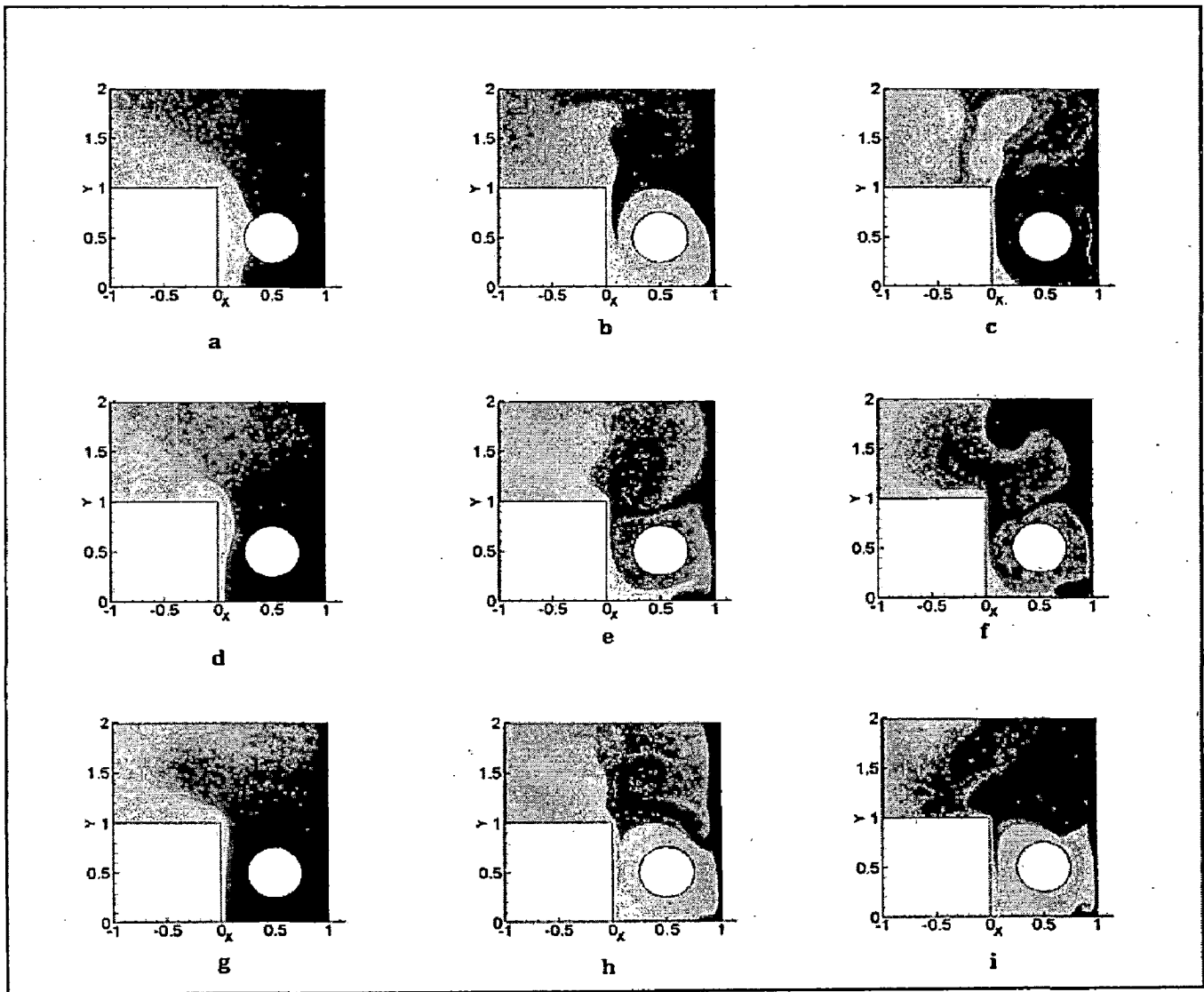


Fig. 41. Isotherm patterns for $Pr = 1$ and for a) $Ra = 10^3, \alpha = 0$ b) $Ra = 10^3, \alpha = 1$ c) $Ra = 10^3, \alpha = 4$ d) $Ra = 10^4, \alpha = 0$ e) $Ra = 10^4, \alpha = 1$ f) $Ra = 10^4, \alpha = 4$ g) $Ra = 10^5, \alpha = 0$ h) $Ra = 10^5, \alpha = 1$ i) $Ra = 10^5, \alpha = 4$

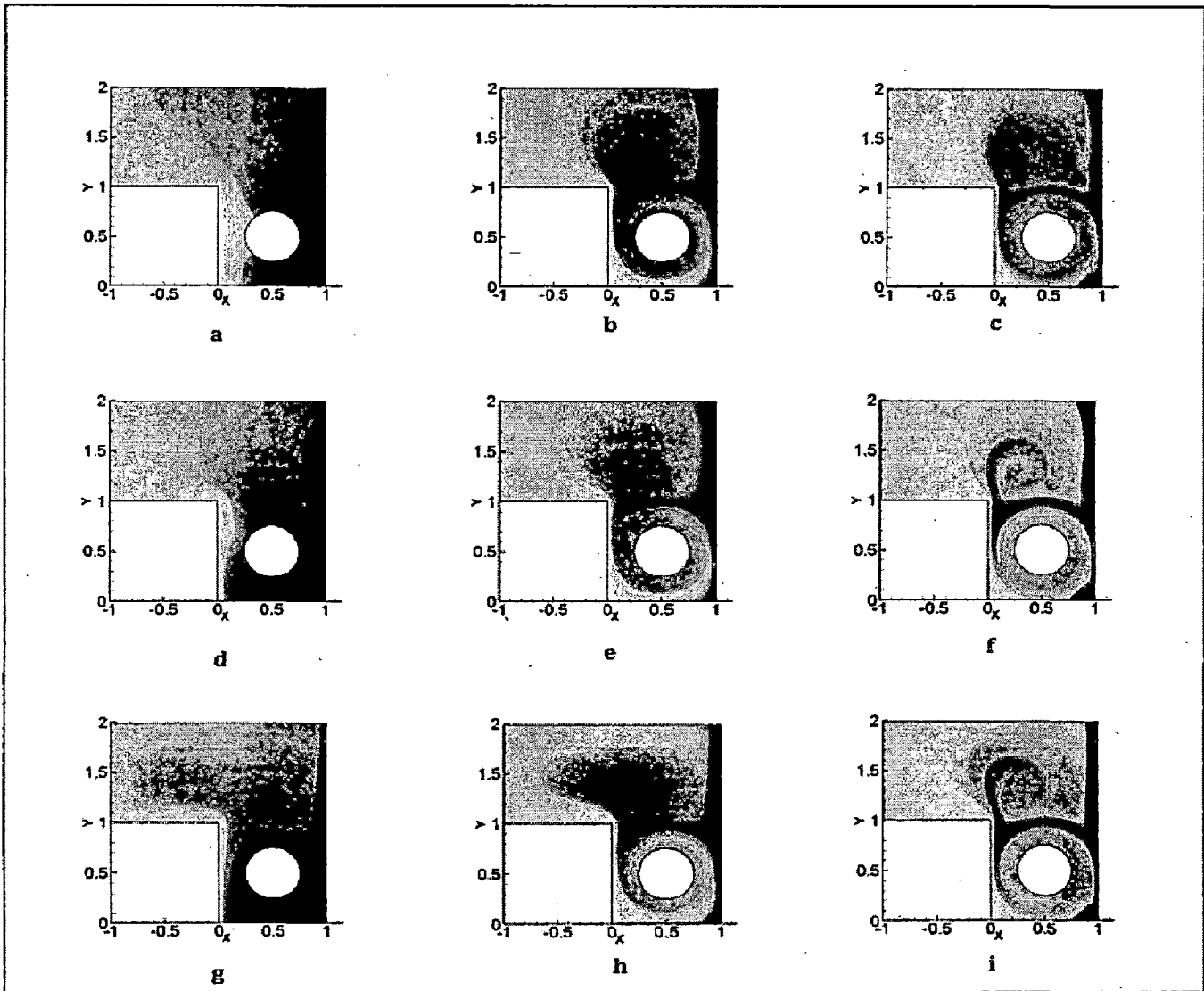


Fig. 42. Isotherm patterns for $Pr = 10$ and for a) $Ra = 10^3, \alpha = 0$ b) $Ra = 10^3, \alpha = 1$ c) $Ra = 10^3, \alpha = 4$ d) $Ra = 10^4, \alpha = 0$ e) $Ra = 10^4, \alpha = 1$ f) $Ra = 10^4, \alpha = 4$ g) $Ra = 10^5, \alpha = 0$ h) $Ra = 10^5, \alpha = 1$ i) $Ra = 10^5, \alpha = 4$

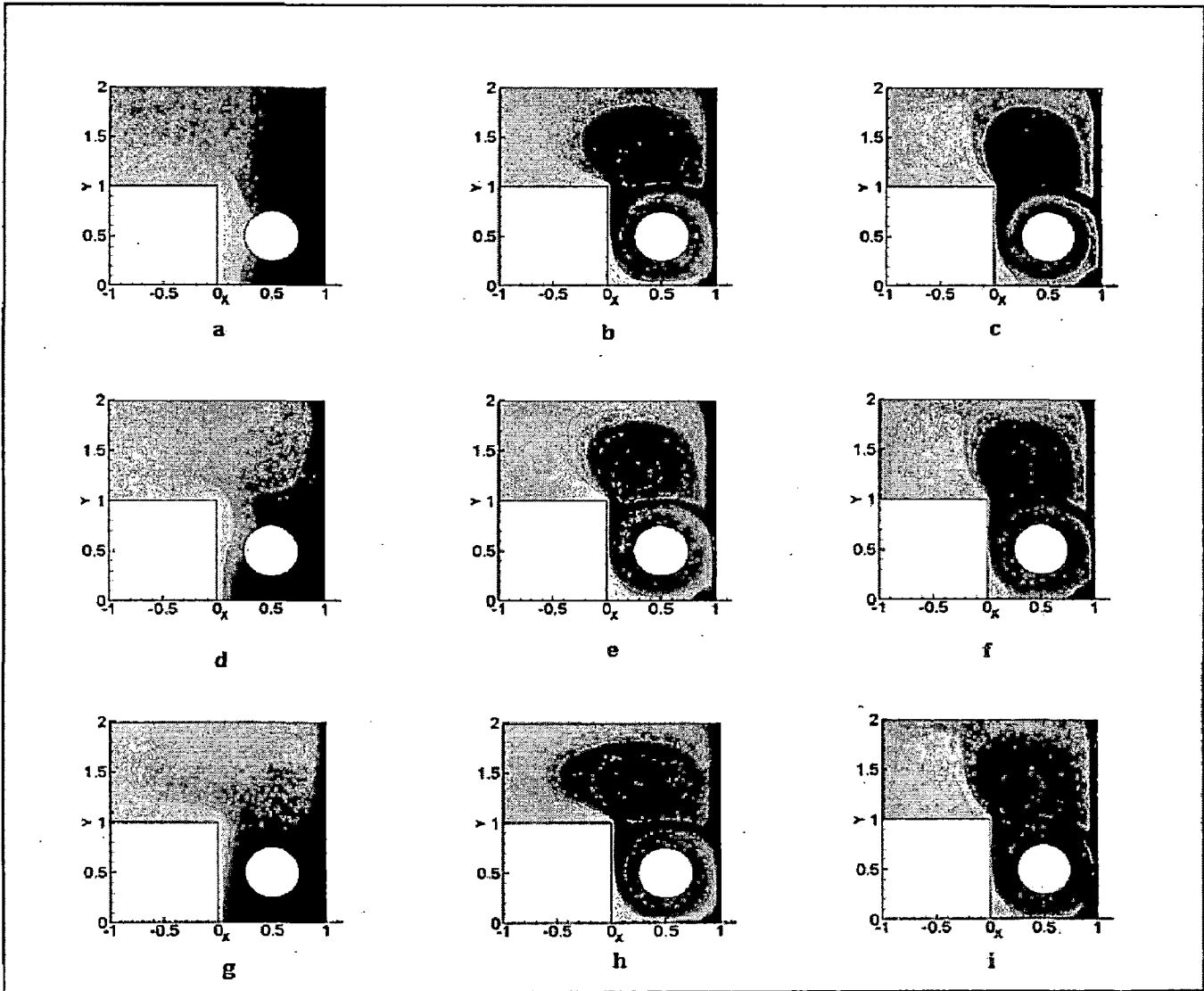


Fig. 43. Isotherm patterns for $Pr = 50$ and for a) $Ra = 10^3, \alpha = 0$ b) $Ra = 10^3, \alpha = 1$ c) $Ra = 10^3, \alpha = 4$ d) $Ra = 10^4, \alpha = 0$ e) $Ra = 10^4, \alpha = 1$ f) $Ra = 10^4, \alpha = 4$ g) $Ra = 10^5, \alpha = 0$ h) $Ra = 10^5, \alpha = 1$ i) $Ra = 10^5, \alpha = 4$

11.3. Average Nusselt Values

The variations of the average Nusselt number Nu calculated at the heated backward facing step with different Ra and Pr are plotted in Figs. 44 - 46. As can be noted from the figures that the Nusselt values increase with increasing angular rotation of the cylinder. This increase is found to be exponential in nature. Further an increase in the Prandtl number and also the Rayleigh number leads to an increase in the Nusselt number values and has been clearly depicted in these figures.

There appears to be a very high increase in the Nusselt values which is approximately 20 times the value for the case without rotation of the circular cylinder.

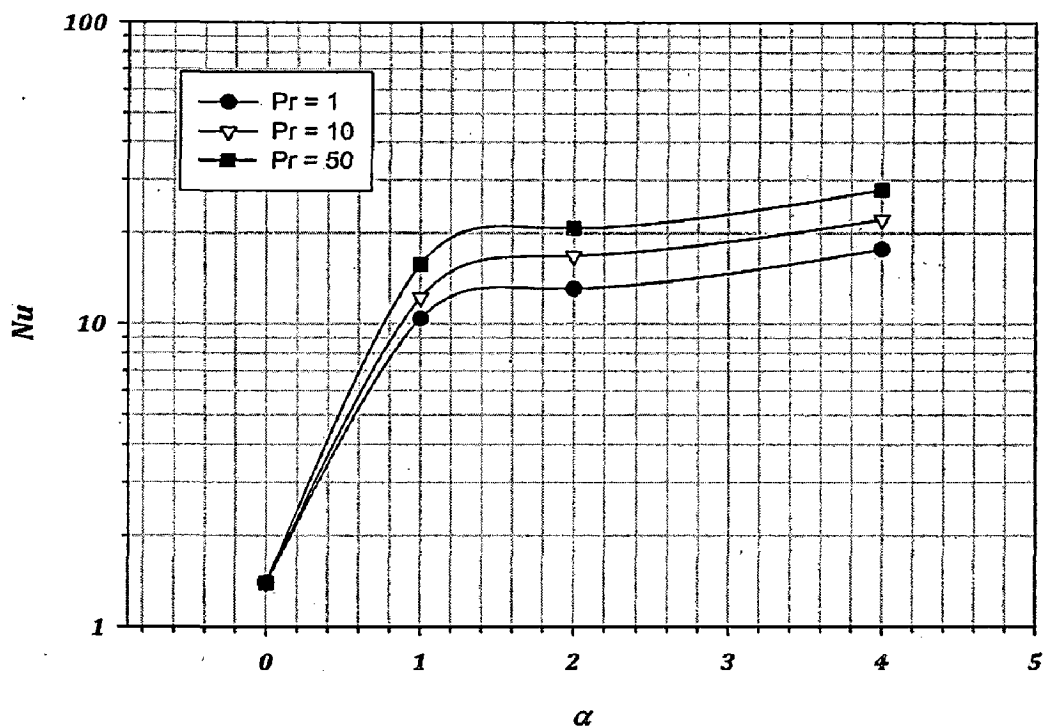


Fig. 44. Nusselt number variations with angular speed at the heated step for $Ra = 10^3$

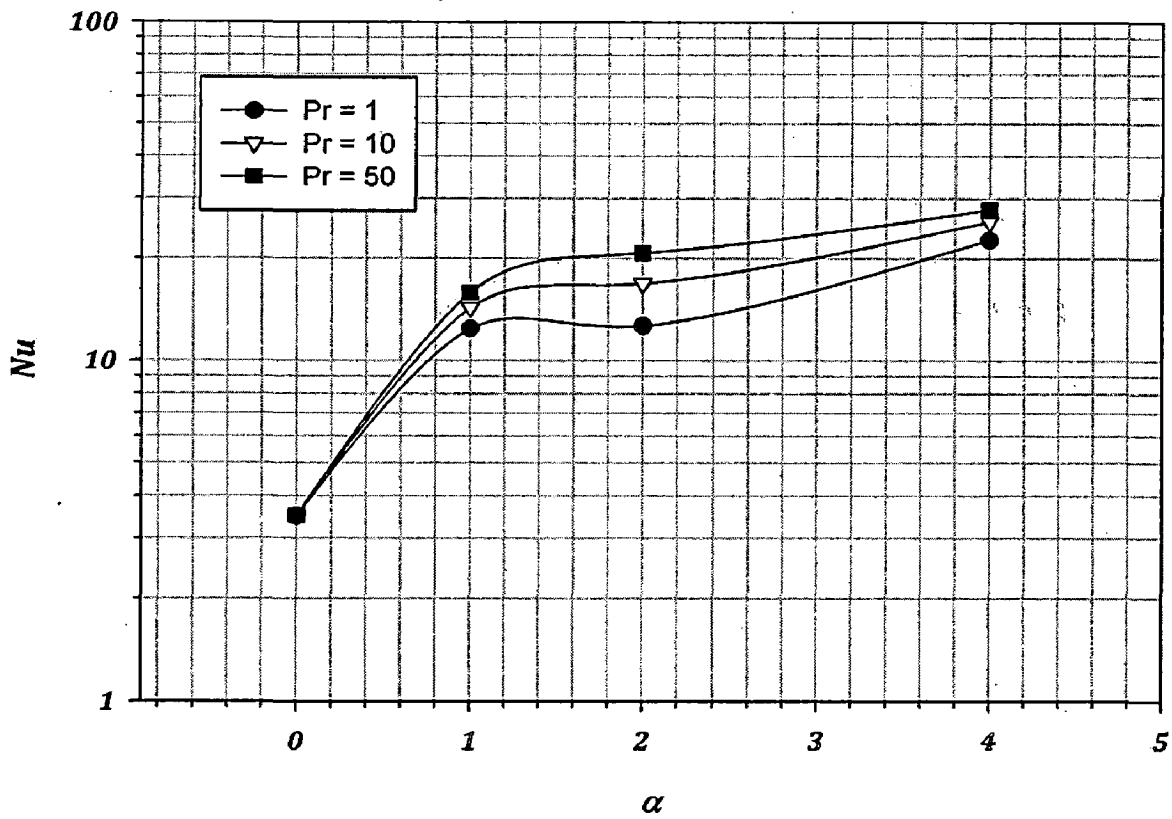


Fig. 45. Nusselt number variations with angular speed at the heated step for $Ra = 10^4$

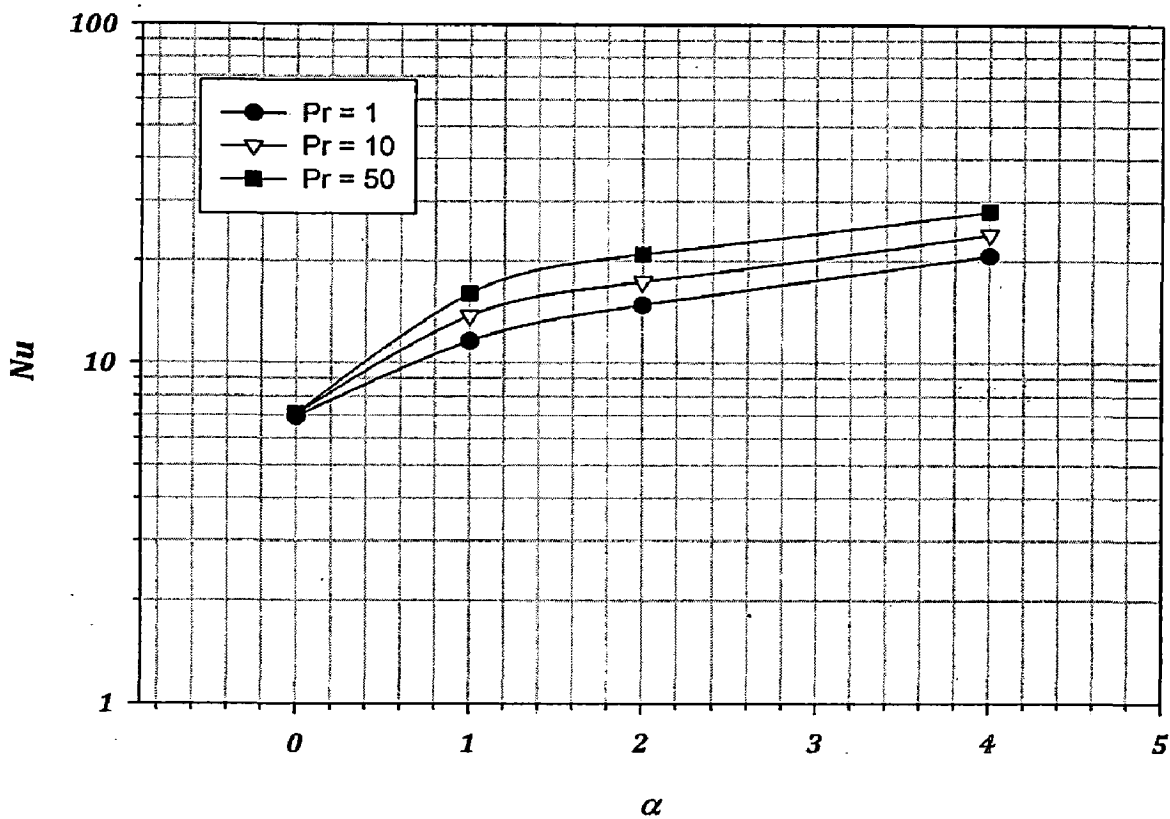


Fig. 46. Nusselt number variations with angular speed at the heated step for $Ra = 10^5$

Table 5. Enhancement factors for various cases of rotation of the circular cylinder with respect to the stationary case.

| Ra | α | 1 | 2 | 4 |
|--------------------------|-----------|----------|----------|----------|
| | Pr | | | |
| 10^3 | 1 | 7.452657 | 9.360994 | 12.64576 |
| | 10 | 8.734513 | 12.01209 | 15.85487 |
| | 50 | 11.23826 | 14.83133 | 19.91361 |
| 10^4 | 1 | 3.548821 | 3.617005 | 6.476198 |
| | 10 | 4.080631 | 4.812229 | 7.319071 |
| | 50 | 4.52212 | 5.919321 | 7.943624 |
| 10^5 | 1 | 1.663147 | 2.125829 | 2.974035 |
| | 10 | 1.939339 | 2.43866 | 3.37364 |
| | 50 | 2.249032 | 2.945917 | 3.934258 |

11.4. Drag Coefficients

Fig.47 presents the drag coefficient variation with the angular rotation of the cylinder. The figure shows the variation of both the viscous and pressure based drag coefficients and also the total drag around the circular cylinder. As can be noted from the figure that with increasing angular velocity of the cylinder the drag around the cylinder increases. A unique feature of this increase in drag is that it gives a straight line on a semi-log graph. A quadratic fit to the data showing the variation of the drag coefficient as a function of the angular rotation of the cylinder has been presented in equation 38. This predicted the calculated values to within 5% error.

$$C_D = 0.0012\alpha^2 - 0.0015\alpha + 0.0002 \quad (38)$$

For $Ra = 10^3$, $\alpha = 0 - 4$

Fitting a similar equation to the other cases of varying Rayleigh number results in significant error in the equation fit and hence has not been presented here.

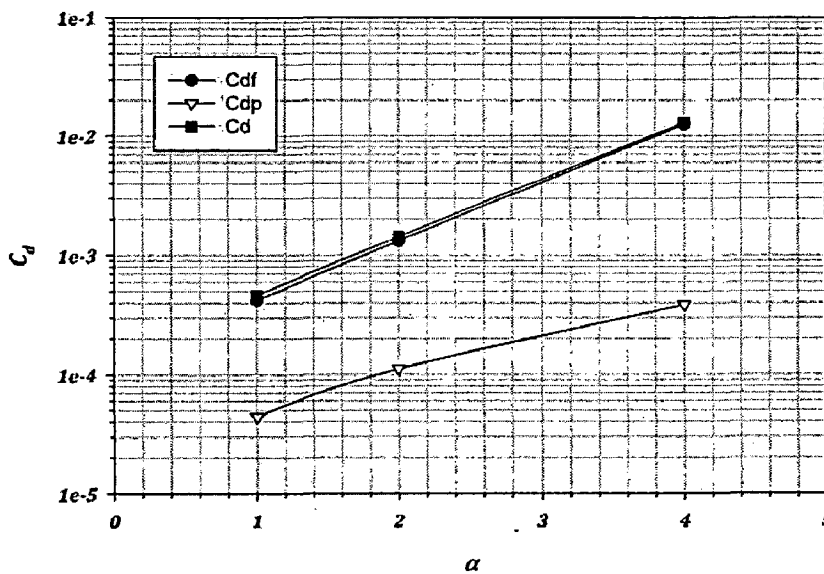


Fig.47.Drag variations with angular speed at the circular cylinder for $Ra = 10^3$

Chapter 12. Conclusions

A study into the natural convection heat transfer characteristics in backward-facing step geometry was carried out for the range of settings: $Ra = 10^3 - 10^5$, $Pr = 1 - 50$ and $\alpha = 0 - 4$. The flow is found to be steady for the range of physical parameters studied. It was found that the heat transfer can be significantly enhanced (20 times) by means of introducing an adiabatic circular cylinder at the appropriate location and by inducing rotation into it. Further, the influence of other parameters such as the Rayleigh number and also the Prandtl number was carried out and the results were presented in detail. It was found that the Nusselt number increases monotonically with an increase in both these parameters. Finally, the drag coefficient variation was explored and simple correlations for the same were obtained.

References

- [1] Armaly B.F., Durst F., Pereira J.C.F., Schonung B., Experimental and Theoretical Investigation of Backward-Facing Step Flow, *J Fluid Mech*, 127 (1983) 473-496.
- [2] Baek B.J., Armaly B.F., Chen T.S., Measurements in Buoyancy-Assisting Separated Flow Behind a Vertical Backward-Facing Step, *J Heat Trans-T Asme*, 115 (1993) 403-408.
- [3] Denham M.K., Patrick M.A., Laminar-Flow over a Downstream-Facing Step in a 2-Dimensional Flow Channel, *T I Chem Eng-Lond*, 52 (1974) 361-367.
- [4] Ichinose K., Tokunaga H., Satofuka N., Numerical simulation of two-dimensional backward-facing step flows, *Transactions of JSME*, (1991) 3715-3721.
- [5] Kaiktsis L., Karniadakis G.E., Orszag S.A., Onset of 3-Dimensionality, Equilibria, and Early Transition in Flow over a Backward-Facing Step, *J Fluid Mech*, 231 (1991) 501-528.
- [6] Kim J., Moin P., Application of a Fractional-Step Method to Incompressible Navier-Stokes Equations, *J Comput Phys*, 59 (1985) 308-323.
- [7] Lin J.T., Armaly B.F., Chen T.S., Mixed Convection in Buoyancy-Assisting, Vertical Backward-Facing Step Flows, *Int J Heat Mass Tran*, 33 (1990) 2121-2132.
- [8] Lin J.T., Armaly B.F., Chen T.S., Mixed Convection Heat-Transfer in Inclined Backward-Facing Step Flows, *Int J Heat Mass Tran*, 34 (1991) 1568-1571.
- [9] Chiang T.P., Sheu T.W.H., A numerical revisit of backward-facing step flow problem, *Phys Fluids*, 11 (1999) 862-874.
- [10] Iwai H., Nakabe K., Suzuki K., Flow and heat transfer characteristics of backward-facing step laminar flow in a rectangular duct, *Int J Heat Mass Tran*, 43 (2000) 457-471.
- [11] Biswas G., Breuer M., Durst F., Backward-facing step flows for various expansion ratios at low and moderate Reynolds numbers, *J Fluid Eng-T Asme*, 126 (2004) 362-374.
- [12] Erturk E., Numerical solutions of 2-D steady incompressible flow over a backward-facing step, Part I: High Reynolds number solutions, *Comput Fluids*, 37 (2008) 633-655.
- [13] Lan H., Armaly B.F., Drallmeier J.A., Three-dimensional simulation of turbulent forced convection in a duct with backward-facing step, *Int J Heat Mass Tran*, 52 (2009) 1690-1700.

- [14] Dyne K.M., Heinrich J.C., Flow over a backward-facing step: a benchmark problem for laminar flow with heat transfer, *Benchmark problems for heat transfer codes ASME HTD*, 222 (1992) 73-76.
- [15] Choudhury D., Woolfe A.E., Computation of laminar forced and mixed convection in a heated vertical duct with a step, *ASME HTD*, 258 (1993) 29-36.
- [16] Hong B., Armaly B.F., Chen T.S., Laminar Mixed Convection in a Duct with a Backward-Facing Step - the Effects of Inclination Angle and Prandtl Number, *Int J Heat Mass Tran*, 36 (1993) 3059-3067.
- [17] Kondoh T., Nagano Y., Tsuji T., Computational Study of Laminar Heat-Transfer Downstream of a Backward-Facing Step, *Int J Heat Mass Tran*, 36 (1993) 577-591.
- [18] AbuHijleh B., Convection heat transfer from a laminar flow over a 2-D backward facing step with asymmetric and orthotropic porous floor segments, *Numer Heat Tr a-Appl*, 31 (1997) 325-335.
- [19] Martin A.R., Saltiel C., Shyy W., Heat transfer enhancement with porous inserts in recirculating flows, *J Heat Trans-T Asme*, 120 (1998) 458-467.
- [20] Singha S., Sinhamahapatra K.P., Flow past a circular cylinder between parallel walls at low Reynolds numbers, *Ocean Eng*, 37 (2010) 757-769.
- [21] Acharya S., Dixit G., Hou Q., Laminar mixed convection in a vertical channel with a backstep: A benchmark study, *ASME HTD*, 258 (1993) 11 - 20.
- [22] Choudhury D., A numerical study of laminar flow and heat transfer in a backward-facing step using fluent: a finite-volume CFD, *Benchmark problems for heat transfer codes, ASME HTD*, 222 (1992) 53-56.
- [23] Cochran R.J., Horstman R.H., Sun Y.S., Emery A.F., Benchmark solution for a vertical buoyancy-assisted laminar backward-facing step flow using finite element, finite volume and finite difference methods, *ASME HTD*, 258 (1993) 37-47.
- [24] Hong B., Armaly B.F., Chen T.S., Mixed convection in a laminar, vertical, backward-facing step flow: Solution to a benchmark problem, *ASME HTD*, 258 (1993) 57-62.
- [25] Ghia U., Ghia K.N., Shin C.T., High-Re Solutions for Incompressible-Flow Using the Navier Stokes Equations and a Multigrid Method, *J Comput Phys*, 48 (1982) 387-411.

- [26] Yao M., Nakatani M., Suzuki K., Flow Visualization and Heat-Transfer Experiments in a Turbulent Channel Flow Obstructed with an Inserted Square Rod, *Int J Heat Fluid Fl*, 16 (1995) 389-397.
- [27] Cengel Y., *Heat Transfer – A Practical Approach*, McGrawHill (2006).
- [28] Churchill S.W., Chu H.H.S., Correlating Equations for Laminar and Turbulent Free Convection from a Horizontal Cylinder., *International Journal of Heat Mass Transfer*, 18 (1975) 1049.
- [29] Fujiii T., Imura. H., Natural Convection Heat Transfer from a Plate with Arbitrary Inclination., *International Journal of Heat Mass Transfer*, 15 (1972) 755.
- [30] Jakob M., *Heat Transfer* New York: Wiley, (1949).
- [31] Hollands K.G.T., Unny T.E., Raithy G.D., Koniek L., Free Convective Heat Transfer Across Inclined Air Layers., *Journal of Heat Transfer*, 98 (1976) 189 - 193.
- [32] Catton., *Natural Convection in Enclosures.*, *Proceedings of Sixth International Heat Transfer Conference, Toronto, Canada.*, 6 (1978) 13-31.
- [33] Berkovsky B.M., Polevikov V.K., Numerical Study of Problems on High-Intensive Free Convection., *Heat Transfer and Turbulent Buoyant Convection*, 12 (1977) 443 - 445.
- [34] Wroblewski D.E., Joshi Y., Computations of Liquid Immersion Cooling for a Protruding Heat-Source in a Cubical Enclosure, *Int J Heat Mass Tran*, 36 (1993) 1201-1218.
- [35] Heindel T.J., Ramadhyani S., Incropera F.P., Laminar natural convection in a discretely heated cavity .1. Assessment of three-dimensional effects, *J Heat Trans-T Asme*, 117 (1995) 902-909.
- [36] Heindel T.J., Incropera F.P., Ramadhyani S., Laminar natural convection in a discretely heated cavity .2. Comparisons of experimental and theoretical results, *J Heat Trans-T Asme*, 117 (1995) 910-917.
- [37] Sathe S.B., Johsi Y., Natural-Convection Arising from a Heat Generating Substrate-Mounted Protrusion in a Liquid-Filled 2-Dimensional Enclosure, *Int J Heat Mass Tran*, 34 (1991) 2149-2163.
- [38] Anderson R., Bohn M., Heat-Transfer Enhancement in Natural-Convection Enclosure Flow, *J Heat Trans-T Asme*, 108 (1986) 330-336.
- [39] Amin M.R., The Effect of Adiabatic Wall Roughness Elements on Natural-Convection Heat-Transfer in Vertical Enclosures, *Int J Heat Mass Tran*, 34 (1991) 2691-2701.

- [40] Amin M.R., Natural-Convection Heat-Transfer in Enclosures Fitted with a Periodic Array of Hot Roughness Elements at the Bottom, *Int J Heat Mass Tran*, 36 (1993) 755-763.
- [41] Abumulaweh H.I., Armaly B.F., Chen T.S., Measurements in Buoyancy-Opposing Laminar-Flow over a Vertical Backward-Facing Step, *J Heat Trans-T Asme*, 116 (1994) 247-250.
- [42] AbuMulaweh H.I., Armaly B.F., Chen T.S., Laminar natural convection flow over a vertical backward-facing step, *J Heat Trans-T Asme*, 117 (1995) 895-901.
- [43] AbuMulaweh H.I., Armaly B.F., Chen T.S., Laminar natural convection flow over a vertical forward-facing step, *J Thermophys Heat Tr*, 10 (1996) 517-523.
- [44] Chang K.S., Won Y.H., Cho C.H., Patterns of Natural-Convection around a Square Cylinder Placed Concentrically in a Horizontal Circular-Cylinder, *J Heat Trans-T Asme*, 105 (1983) 273-280.
- [45] Fu W.S., Cheng C.S., Shieh W.J., Enhancement of Natural-Convection Heat-Transfer of an Enclosure by a Rotating Circular-Cylinder, *Int J Heat Mass Tran*, 37 (1994) 1885-1897.
- [46] Ha M.Y., Kim I.K., Yoon H.S., Yoon K.S., Lee J.R., Balachandar S., Chun H.H., Two-dimensional and unsteady natural convection in a horizontal enclosure with a square body, *Numer Heat Tr a-Appl*, 41 (2002) 183-210.
- [47] Ha M.Y., Kim I.K., Yoon H.S., Lee S., Unsteady fluid flow and temperature fields in a horizontal enclosure with an adiabatic body, *Phys Fluids*, 14 (2002) 3189-3202.
- [48] Roychowdhury D.G., Das S.K., Sundararajan T., Numerical simulation of natural convective heat transfer and fluid flow around a heated cylinder inside an enclosure, *Heat Mass Transfer*, 38 (2002) 565-576.
- [49] De A.K., Dalal A., A numerical study of natural convection around a square, horizontal, heated cylinder placed in an enclosure, *Int J Heat Mass Tran*, 49 (2006) 4608-4623.
- [50] Angeli D., Levoni P., Barozzi G.S., Numerical predictions for stable buoyant regimes within a square cavity containing a heated horizontal cylinder, *Int J Heat Mass Tran*, 51 (2008) 553-565.
- [51] Hwang J.Y., Yang K.S., Yoon D.H., Bremhorst K., Flow field characterization of a rotating cylinder, *Int J Heat Fluid Fl*, 29 (2008) 1268-1278.

- [52] Rahman M.M., Alim M.A., Mamun M.A.H., Finite Element Analysis of Mixed Convection in a Rectangular Cavity with a Heat-Conducting Horizontal Circular Cylinder, *Nonlinear Anal-Model*, 14 (2009) 217-247.
- [53] Ghazanfarian J., Nobari M.R.H., A numerical study of convective heat transfer from a rotating cylinder with cross-flow oscillation, *Int J Heat Mass Tran*, 52 (2009) 5402-5411.
- [54] Shih Y.C., Khodadadi J.M., Weng K.H., Ahmed A., Periodic Fluid Flow and Heat Transfer in a Square Cavity Due to an Insulated or Isothermal Rotating Cylinder, *J Heat Trans-T Asme*, 131 (2009).
- [55] Yoon H.S., Chun H.H., Kim J.H., Park I.L.R., Flow characteristics of two rotating side-by-side circular cylinder, *Comput Fluids*, 38 (2009) 466-474.
- [56] Paramane S.B., Sharma A., Numerical investigation of heat and fluid flow across a rotating circular cylinder maintained at constant temperature in 2-D laminar flow regime, *Int J Heat Mass Tran*, 52 (2009) 3205-3216.
- [57] Oztop H.F., Zhao Z., Yu B., Fluid flow due to combined convection in lid-driven enclosure having a circular body, *Int J Heat Fluid Fl*, 30 (2009) 886-901.
- [58] Yoon H.S., Ha M.Y., Kim B.S., Yu D.H., Effect of the position of a circular cylinder in a square enclosure on natural convection at Rayleigh number of 10(7), *Phys Fluids*, 21 (2009).
- [59] Costa V.A.F., Raimundo A.M., Steady mixed convection in a differentially heated square enclosure with an active rotating circular cylinder, *Int J Heat Mass Tran*, 53 (2010) 1208-1219.
- [60] Mohammed H.A., Salman Y.K., Combined natural and forced convection heat transfer for assisting thermally developing flow in a uniformly heated vertical circular cylinder, *Int Commun Heat Mass*, 34 (2007) 474-491.
- [61] Laskowski G.M., Kearney S.P., Evans G., Greif R., Mixed convection heat transfer to and from a horizontal cylinder in cross-flow with heating from below, *Int J Heat Fluid Fl*, 28 (2007) 454-468.
- [62] Hussain S.H., Hussein A.K., Numerical investigation of natural convection phenomena in a uniformly heated circular cylinder immersed in square enclosure filled with air at different vertical locations, *Int Commun Heat Mass*, 37 (2010) 1115-1126.

- [63] Hayase T., Humphrey J.A.C., Greif R., Numerical-Calculation of Convective Heat-Transfer between Rotating Coaxial Cylinders with Periodically Embedded Cavities, *J Heat Trans-T Asme*, 114 (1992) 589-597.
- [64] Phutthavong P., Hassan I., Transient performance of flow over a rotating object placed eccentrically inside a microchannel-numerical study, *Microfluid Nanofluid*, 1 (2004) 71-85.
- [65] Ghaddar N.K., Thiele F., Natural-Convection over a Rotating Cylindrical Heat-Source in a Rectangular Enclosure, *Numer Heat Tr a-Appl*, 26 (1994) 701-717.
- [66] Ghaddar N.K., Natural convection over rotating cylindrical heat source in an enclosure, *J Thermophys Heat Tr*, 10 (1996) 303-311.
- [67] Yang L., Farouk B., Mixed Convection around a Heated Rotating Horizontal Square Cylinder in a Circular Enclosure, *Numer Heat Tr a-Appl*, 28 (1995) 1-18.
- [68] Shu C., Xue H., Zhu Y.D., Numerical study of natural convection in an eccentric annulus between a square outer cylinder and a circular inner cylinder using DQ method, *Int J Heat Mass Tran*, 44 (2001) 3321-3333.
- [69] Shu C., Zhu Y.D., Efficient computation of natural convection in a concentric annulus between an outer square cylinder and an inner circular cylinder, *Int J Numer Meth Fl*, 38 (2002) 429-445.
- [70] Peng Y., Chew Y.T., Shu C., Numerical simulation of natural convection in a concentric annulus between a square outer cylinder and a circular inner cylinder using the Taylor-series-expansion and least-squares-based lattice Boltzmann method, *Phys Rev E*, 67 (2003).
- [71] Ding H., Shu C., Yeo K.S., Lu Z.L., Simulation of natural convection in eccentric annuli between a square outer cylinder and a circular inner cylinder using local MQ-DQ method, *Numer Heat Tr a-Appl*, 47 (2005) 291-313.
- [72] Moukalled F., Acharya S., Natural convection in the annulus between concentric horizontal circular and square cylinders, *J Thermophys Heat Tr*, 10 (1996) 524-531.
- [73] Hasan N., Sanghi S., The dynamics of two-dimensional buoyancy driven convection in a horizontal rotating cylinder, *J Heat Trans-T Asme*, 126 (2004) 963-984.
- [74] De Vahl Davis G., Laminar Natural Convection in an Enclosed Rectangular Cavity, *Int J Heat Mass Tran*, 11 (1968) 1675 - 1693.